Influence of Dusts on Premixed Methane-Air Flames

by

Sreenivasan Ranganathan

A Dissertation

Submitted to the Faculty

of

Worcester Polytechnic Institute

in partial fulfillment of the requirements for the

Degree of Doctor of Philosophy

in

Fire Protection Engineering

March 2018

Approved:

Dr. Ali S. Rangwala, Worcester Polytechnic Institute, USA, Advisor.

Dr. Tahar El-Korchi, Worcester Polytechnic Institute, USA, Committee Member.

Dr. Scott R. Rockwell, University of North Carolina at Charlotte, USA, Committee Member.

Dr. Raghavan Vasudevan, Indian Institute of Technology Madras, India, Committee Member.

Dr. Forman A. Williams, University of California San Diego, USA, Committee Member.

……page intentionally left blank……

Preface

This dissertation was submitted for the degree of Doctor of Philosophy at the Worcester Polytechnic Institute (WPI). The Ph.D. study was conducted between January 2012 and March 2018 at the Department of Fire Protection Engineering, under the supervision of **Ali S. Rangwala**, Professor, Dept. of Fire Protection Engineering, WPI, USA. The following articles have been published or under review as part of this Ph.D. study. The thesis author is the primary investigator in all these publications.

- **S. Ranganathan**, D. Petrow, S. R. Rockwell, A. S. Rangwala. ***Turbulent burning velocity of methane–air–dust premixed flames***, Combustion and Flame. 188, 367-375, 2018. (Presented in Chapter 4).
- **S. Ranganathan**, S. R. Rockwell, D. Petrow, R. Zalosh, A. S. Rangwala. ***Radiative fraction of dust entrained turbulent premixed flames***, Journal of Loss Prevention in the Process Industries. 51, 65-71, 2018. (Presented in Chapter 5).
- **S. Ranganathan**, D. Petrow, S. R. Rockwell, A. S. Rangwala. ***Experimental Investigation of Laminar Premixed Methane-Air Flame Extinction with Sand and Sodium Bicarbonate Particles***, Proceedings of 10th U. S. National Combustion Meeting. April 2017, Maryland, USA. (Presented in Chapter 3).
- **S. Ranganathan**, M. Lee, V. Akkerman, A. S. Rangwala. ***Suppression of premixed flames with inert particles***, Journal of Loss Prevention in the Process Industries. 35, 46-51, 2015. (Presented in Chapter 3).

……page intentionally left blank……

To my teachers.....

"अज्ञानतिमिरान्धस्य, ज्ञानाञ्जनशालाकया, चक्षुरुन्मीलितं येन, तस्मै श्रीगुरवे नमः"

"ajñāna-timirāndhasya, jñānāñjana-śalākayā, cakṣur unmīlitaṁ yena, tasmai śrī-gurave namaḥ"

"I offer my respectful obeisance unto my gurus, who with the torchlight of knowledge has opened my eyes, which were blinded by the darkness of ignorance".

……page intentionally left blank……

Acknowledgements

There are numerous individuals, teachers, colleagues, friends and family, whom I need to thank for inspiring me to complete this work. Firstly, I would like to express my sincere thanks and gratitude to my advisor, Dr. Ali Rangwala, for the guidance and constant support throughout the course of this research work. I take this opportunity to thank him for the productive technical discussions, advices and care during the entire period of my Ph.D.

I sincerely thank my thesis committee members for the suggestions and feedback they gave me all along the course of this dissertation, especially Dr. Forman Williams for feedback on the experimental results; Dr. Scott Rockwell for his guidance on experimental methodology; Dr. Raghavan Vasudevan and Dr. Tahar El-Korchi for their expert comments. I am indebted to Dr. T. Sundararajan and Dr. P. R. Suresh for introducing me to research. I am also grateful to all the dedicated faculties and office staffs of Dept. of Fire Protection Engineering at WPI. There are many teachers who have inspired me to learn and also made the process of learning enjoyable through their well written books and lectures, my salutations to all of them.

I am grateful to National Science Foundation (NSF), Alpha Foundation for Mine Safety, and Worcester Polytechnic Institute that have funded my assignment in graduate school.

I extend my sincere thanks to my colleagues at the Fire Protection Research Foundation: Amanda Kimball, Casey Grant, Daniel Gorham, Eric Peterson, Kathleen Almand, Victoria Hutchison and many others at the National Fire Protection Association for their constant encouragement and offering flexibility to complete my dissertation while working at FPRF. My experience at the Research Foundation have helped me to understand the importance of applying the fundamental research to the needs of real world.

My thanks are due to the lab staff and other research scholars of Combustion lab at WPI: David Petrow, Hamed Farahani, Minkyu Lee and Trevor Borth for their kind cooperation and help while conducting experiments.

I owe my heartfelt gratitude to Rohit, Amruta and their family for their love and care; Ava has been my joy; Gopal, Sudha and family for their deep concern in my well-being; Chirantan and Moumita for being there always. I have made a lot of friends through this journey at WPI and I am grateful to all of them, especially my supportive roommates for giving wonderful memories for rest of my life. The overseas calls were tough, but thanks to Vani for pushing me to see through the finishing line.

Finally, most importantly, I wish to express my heartfelt thanks to my Appa and Amma for instilling the importance of education. Their love and support has always been there in all my endeavors. They are my biggest driving force. Their blessing and presence gives me the courage and strength to move forward in life.

Sreenivasan Ranganathan

Table of Contents

List of Figures

List of Tables

Nomenclature

A_f	Surface area of flame
B	Frequency factor characterizing rate of gas phase oxidation of gaseous fuel
C_p	Heat capacity of air
C_s	Heat capacity of solid particle
Da	Turbulent Damköhler number
Da_v	Vaporization Damköhler number
D_f	Average flame diameter
D^*	Thermal diffusivity
d_p	Particle diameter
E	Activation energy characterizing the gas phase reaction
F	Geometric view factor
g	Boundary velocity gradient
G	Group combustion number
$H_{c,p}$	Heat of combustion of particle
Ka	Karlovitz number
K	Deflagration index
K_g	Deflagration index of gas
K_{st}	Deflagration index of dust
k	Thermal conductivity
l_o	Integral length scale of turbulence
$n_{product}$	Number of moles of products

n_s	Number of particles
$\dot{n}_s$	Number of particles per unit volume per unit time passing through the flame
n_{air}	Number of moles of air per unit time
$\dot{Q}$	Heat release rate
$\dot{q}''$	Heat flux absorbed by particles
$\dot{q_r}''$	Radiative heat flux
$\dot{q}_r$	Radiative heat release rate
P_{max}	Maximum pressure
R	Universal gas constant
Re	Reynolds number
Re_T	Turbulent Reynolds number
S_L	Laminar burning velocity
S_T	Turbulent burning velocity
St	Stokes number
T_b	Flame temperature based on gaseous mixture and unburnt gas temperature
T_f	Flame temperature
T_f''	Reduced flame temperature due to heat sink effect of particles
T_u	Temperature of unburned gas
$\bar{u}$	Average flow velocity
u'	Fluctuating component of velocity
u'_{rms}	Turbulent intensity
U	Average flow velocity at burner nozzle
$\dot{V}_{air}$	Volumetric flow rate of air

$\dot{V}_{CH_4}$	Volumetric flow rate of methane
V	Volume
$V_{p,total}$	Total volume occupied by particles
V_f	Volume of fluid
X_r	Radiative fraction of heat
Z_e	Zeldovich number

Greek Symbols

α	Flame half cone angle
$\bar{\alpha}$	Average flame half cone angle
ε	= $1/Z_e$, expansion parameter
ρ	Density of the gas mixture
ρ_s	Density of the particle
ϕ_g	Gaseous mixture equivalence ratio
ϕ_v	Volumetric loading of particles
λ_p	Particle concentration
ν	Kinematic viscosity
τ	Transmissivity
τ_e	Eddy turn over time
τ_v	Particle vaporization time
T_k	Kolmogorov time
τ_p	Particle response time

τ_c	Diffusion time in particle cloud
$\hat{o}_L$	Laminar flame thickness

Subscripts

a	Ambient condition
f	Flame
g	Gas phase
s	Solid particle in mathematical model
u	Conditions in the controlled reactant temperature condition.
p	Particle
L	Laminar
T	Turbulent

Abstract

Keywords: Premixed flame, Dust, Turbulence, Turbulent intensity, Laminar, Concentration, Coal, Inert, Sodium Bicarbonate, Burning Velocity, Radiation, Heat Flux.

Influence of dust particles on the characteristics of premixed methane-air flames has been studied in this dissertation. Experiments are performed in a Bunsen burner type experimental set-up called Hybrid Flame Analyzer (HFA), which can be used to measure the burning velocity of gas, dust, and hybrid (gas and dust) premixed flames at constant pressure operating conditions. In the current study, analysis of particle–gas–air system of different types of dust particles (at particle size, d_p = 75–90 μm) in premixed methane–air (ϕ_g = 0.8, 1.0 and 1.2) flames. Coal, sand, and sodium bicarbonate particles are fed along with a premixed methane-air mixture at different concentrations (λ_p = 0-75 g/m^3) in both laminar and turbulent conditions. First, the variation of laminar burning velocity with respect to the concentration of dust particles, and type of dusts are investigated for different equivalence ratios. Second, the laminar premixed flame extinction with inert and chemical suppressant particles are studied. Third, the variation of turbulent burning velocity of these hybrid mixtures are investigated against different turbulent intensities apart from the different concentrations and types of dusts. Fourth, the radiative fraction of heat released from turbulent gas-dust premixed flames are also presented against the operating parameters considered.

Combustible dust deflagration hazard is normally quantified using the deflagration index (K_{st}) measured using a constant volume explosion sphere, which typically is a sealed 20-liter metal sphere where a premixed mixture is ignited at the center and the progression of the resulting deflagration wave is recorded using the pressure measured at the vessel wall. It has been verified from prior studies that the quantification of the turbulence by this method is questionable and there

is a need to analyze the controlling parameters of particle-gas-air premixed system accurately through a near constant pressure operated experimental platform. Thus, the main objective of this study is to analyze the influence of dust particles on premixed methane-air flames at near constant pressure conditions. The turbulent burning velocity is calculated by averaging the measured flame heights and the laminar burning velocity is calculated through the premixed cone angle measurements from several high-speed shadowgraph images obtained from the experiments. The turbulent intensity and length scale of turbulence generated by a perforated plate in the burner is quantified from the hot-wire anemometer measurements. Radiative heat flux is also measured for each of the turbulent test conditions. The outcomes from these experiments are:

1. An understanding of the variation of turbulent burning velocity of gas-dust premixed flames as a function of dust type, turbulent intensity, integral length scale, dust concentration and gas phase mixture ratio.
2. An understanding of the flame extinction characteristics and variation of laminar burning velocity of gas-dust premixed flames as a function of dust concentration and gas phase mixture ratio.
3. Quantify the radiative heat flux and radiative fraction of heat released from gas-dust turbulent premixed flames as a function of dust type, turbulent intensity, dust concentration and gas phase mixture ratio.

Dust type and concentration play an important role in deciding the trend in the variation of both laminar (S_L) and turbulent burning velocity (S_T). Coal particles, with the release of volatile (methane), tend to increase burning velocities except for fuel rich conditions and at higher coal concentrations at larger turbulent intensities. At a higher turbulent intensity and larger concentrations, higher S_T values are observed with the addition of sand. Sodium bicarbonate

addition, with the release of CO_2 and H_2O, decreased the burning velocity at all the concentrations, turbulent intensities and equivalence ratios. Laminar flame extinction was observed with the addition of sand and sodium bicarbonate particles at conditions exceeding certain critical dust concentrations. These critical concentrations varied with the equivalence ratios of gaseous premixed flames.

The turbulence modulation exhibited by particles and particle concentration is evident in these observations. The independent characteristic time scale analysis performed using the experimental data provided further insights to the results. The chemical and convective times in gas phase confirm the broadened preheat thin reaction zone regime in the current test cases, which has an effect of attenuating turbulence and thereby the resulting turbulent burning velocity. The particle time scale analysis (Stokes number) show that the effect of particles and particle concentration is to slightly enhance the turbulence and increase the turbulent burning velocity at lower concentrations. However, the time scale analysis of particle vaporization (vaporization Damköhler number) indicate an increase in the vaporization rate for particles (coal and sodium bicarbonate) resulting in a decrease in their turbulent burning velocities at higher concentrations and turbulent intensities. Sodium bicarbonate has higher evaporation rate than coal at same level of turbulence and the absence of this effect for inert (sand) results in higher turbulent burning velocities at higher concentrations. An increase in the turbulent intensity increases the vaporization rate of particles. The investigation on radiative fraction of heat released by methane-air-dust turbulent premixed flames identified that, the addition of dust particles increases the radiative fraction irrespective of the dust type due to the radial and axial extension of flame. A unified approach to couple this multiple complex phenomenon of turbulence, particle interaction, particle vaporization and combustion in particle laden premixed gaseous flames is the direction for future research.

1 Introduction

1.1 Background and motivation

Accidental gas and dust deflagrations represent a hazard to both personnel and equipment in industries that make, transport or use flammable gases and combustible dusts. There are numerous studies related to turbulent flame propagation in gases and gas explosion, however, the problem is still not completely understood and studied with combustible dusts. The U.S. Chemical Safety Board (CSB) has identified around 281 combustible dust incidents between 1980 and 2005, causing 119 deaths and 718 injuries [1]. During the period of 2005-2011, there have been approximately 75 combustible dust incidents reported in the USA [2]. These explosions are caused by a variety of hybrid mixtures (combustible dust-gas pre-mixtures), dusts including grains, metals, coal, textile, rubber, resins, and others [3]. The recent, ever advancing and expanding chemical, metallurgical, and pharmaceutical industries have given birth to steadily increasing number of new finely divided flammable materials. The enormous number of accidents occurring due to the dust explosions indicate a lack of fundamental knowledge about gaseous and particle-air combustion in a turbulent environment.

Flames in premixed hybrid mixtures are generally propagating through mixtures containing fuels of two different phases, typically a solid phase fuel and a gaseous or liquid fuel. This type of flame propagation often occurs in coal mine explosions which start with a methane-air explosion and entrain coal dust as the flame propagates down the mine gallery. Explosion in coal mines

usually involve a mixture of solid coal and methane gas in air. National Fire Protection Association (NFPA) 68: Standard on explosion protection by deflagration venting defines a hybrid mixture as a heterogeneous mixture, comprising gas with suspended solid or liquid particulates [4]. NFPA 654: Standard for the prevention of fire and dust explosions from the manufacturing, processing, and handling of combustible particulate solids, defines combustible dust as any finely divided combustible particulate solid that presents a flash fire hazard or explosion hazard when suspended in air or the process-specific oxidizing medium over a range of concentrations [5]. Traditionally, dusts were defined as materials, 420 µm or smaller that is capable of passing through a U.S. No. 40 standard sieve. Typically, the particles which are larger than 500 µm in size, have too small surface-to-volume ratio to pose deflagration hazard [5]. Earliest documented dust explosion occurred in 1785 in Italy in a bakery store room where the ignition of flour dust was caused by a lamp [6]. Following which there have been many historical dust explosions and they still continue to occur. Some of the recent dust explosion incidents from across the world are tabulated in Table 1.1.

Table 1.1: Recent explosion incidents involving dusts.

Industry Type	Fuel	Location	Year	Fatalities
Coal mine	Methane & coal dust	Cucunuba, Colombia	2017	11
Gold mine	Methane gas	Welkom, South Africa	2017	40
Coal mine	Methane & coal dust	Badong, China	2016	11
Coal mine	Methane & coal dust	Chifeng, China	2016	32
Chemical company	Cement production	Qinghai Province, China	2016	6
Wood flour mill	Wood dust	Cheshire, UK	2015	4

Color play	Starch dust	New Taipei, Taiwan	2015	15
Car parts	Metal dust	Jiangsu Province, China	2014	75
Coal mine	Methane & coal dust	Donetsk, Ukraine	2013	7
Saw mill	Wood dust	Lakeland Mills sawmill in Prince George, Canada	2012	2
Saw mill	Wood dust	Babine Forest Products in Burns Lake, Canada	2012	2
Coal mine	Methane & coal dust	Sardinata, Colombia	2011	21
Powder Manufacturer	Iron dust	Hoeganaes Corporation, TN, USA	2011	5 (3 incidents)
Coal mine	Methane & coal dust	Upper Branch mine, West Virginia, USA	2010	29
Coal mine	Methane & coal dust	Pike River, New Zealand	2010	29

Burning velocity is one of the most important and fundamental characteristics of a premixed flame. A premixed flame is a self-sustaining propagation of localized combustion zone at subsonic velocity. Burning velocity is defined as the velocity at which the unburned mixture enters the flame zone in a direction normal to the flame sheet or it is the rate of flame propagation relative to the velocity of unburned reactants that is ahead of it. Whereas the flame speed is defined as the speed of a flame front relative to a fixed reference point [4]. Although several experimental test methods [7] (e.g., Bunsen burner, flat-flame burner, outwardly expanding spherical flame, stagnation flame burner and flame propagation in tube) and experimental data are available for flammable gas-air mixtures, there exists no standardized experimental apparatus to measure the fundamental properties like burning velocity for dust and hybrid (dust-air-gas) flames. Similarly, for any

numerical model to predict the flame propagation in dust-air environment accurately, it requires the input as well as results for validating parameters, which are obtained from experiments. Currently, there are very less numerical models and experimental platforms which generate model input parameters for turbulent dust explosions. This scientific problem involves new fundamental questions about the interaction of particles with a turbulent flow field as well as chemical reactions in multiphase flows. This study is unique since the physical understanding of the controlling mechanisms associated with particle-air flames have not been explored in depth. An extensive experimental data of laminar and turbulent burning velocity for hybrid and particle-air flames as a function of influencing parameters such as particle type, particle size, particle concentration, turbulent intensity and turbulent length scale are absent. Producing these data can be further used to develop or extend existing correlations for turbulent premixed flames mixed with particles.

Traditionally, the reactivity of explosive gas-air mixtures, flammable vapors, mists, and dust clouds has been characterized by the rate of pressure rise and maximum pressure (P_{max}) determined in constant volume explosion vessels (NFPA 68 [4] and NFPA 69 [8]). These are typically tested in approximately spherical calibrated test vessels of at least 20 L capacity as per ASTM E 1226: Standard test method for explosibility of dust clouds [9] or ISO 6184/1: Explosion Protection Systems - Part 1: Determination of explosion indices of combustible dusts in air [10]. The explosion mitigating measures such as explosion vents, suppression systems etc., have relied on empirical correlations involving parameters called deflagration indices (K_g for gas and K_{st} for dusts) and maximum pressure, P_{max}. The deflagration index (K), defined as $K = \left(\frac{dP}{dt}\right)_{max} V^{1/3}$, is estimated from the maximum rate of pressure rise in a closed vessel with volume, V.

The calculation method (per NFPA 68) for the venting of deflagration of gaseous mixtures was revised based primarily on the fundamental burning velocity of gas mixture and can be

expressed in general as $A_v = f(S_L, P_{max}, \lambda)$, where A_v is the min required venting area, S_L is laminar burning velocity of gas-air mixture, P_{max} is the pressure developed in constant volume vessel and λ is the ratio of gas-air mixture burning velocity accounting for turbulence in vented deflagration to the fundamental laminar burning velocity. This revision was possible because of the extensive research done on laminar and turbulent burning velocity and the availability of these data for gaseous mixtures. However, the venting design of dust-air and hybrid mixtures still rely on K_{st} and P_{max}. These methods do not provide acceptable levels of risk in many situations due to the inconsistency in the dependent parameter values determined from different spherical vessels and they are revised constantly with the development of additional research outcomes. Thus, the studies similar to the current research on fundamental burning velocity of dust-gas mixtures and hybrid mixtures are important for the future development of deflagration protection design and calculations.

Majority of the combustion experiments in dust clouds performed in constant volume combustion bombs measure the pressure variations. The deflagration indices (K_g or K_{st}), which are estimated from the rate of pressure rise, changes with the size of the explosion sphere used [11]. The problem arises mainly due to the increase in turbulent intensity caused by the expanding combustion products in a constant volume vessel [11] and the initial turbulence from the dispersal of dusts. Benedetto et al. [12] showed that the turbulence generated by the expanding products of combustion needs to be quantified in order to determine the correct turbulent burning velocity estimated from constant volume vessels. The non-isobaric conditions make it difficult to obtain the fundamental parameters. It is seen that less number of studies are available with isobaric conditions on dust and hybrid flames. Bunsen burner is proved to be one of the simplest method to do these tests in isobaric conditions.

Rockwell [13] provided an excellent review of literature involving premixed dust experiments. Cassel et al. [14] found that the burning velocity of dust clouds is a function of burner diameter. Lee et al. [15] also studied this dependency of experimental conditions on the burning velocity measurements using cone angle method from Bunsen burner. Their results indicated a decrease in the burning velocity with the increase in the nozzle diameter. Goroshin et al. [3] reported that the molecular heat conduction resulting in the heating of dust mixtures beyond the preheat zone lead to a reduction in the flame speed. Liu et al. [16] found that hybrid mixtures of coal dust-methane–air flames show a lower flammability limit than coal dust-flames. The importance of turbulent intensity was highlighted. However, accurate measurement of turbulence was not achieved because of constant volume explosion sphere experiments. Laminar hybrid flames of methane-coal and air mixtures were successfully studied by Xie et al. [17] using a hybrid Bunsen burner, similar to the one used for laminar flames in this study. In fuel lean mixtures, because of coal dust addition, particle volatilization causes the mixture to become richer locally around the flame. The volatilization of coal particles also extracts energy from the flame. The influence of these competing effects on the experimentally determined laminar burning velocity was analyzed for several equivalence ratios less than 0.85 [17]. Lee et al. [18] followed similar methodology to investigate laminar hybrid flames with coal dust over a range of fuel lean, stoichiometric and fuel rich pre-mixtures of methane and air. They also investigated the effects of unburnt mixture temperature on the burning velocity of the hybrid flames. Rockwell and Rangwala [19] designed an experimental platform to study the hybrid flames and called it Hybrid Flame Analyzer (HFA). This experimental platform has been used in the current study. They investigated the influence of coal particles of different sizes on turbulent methane-air flames. Their results indicated an increase in the turbulent burning velocity with the addition of coal particles. They

also concluded that the smaller particle sizes and larger concentrations (> 50 g/m^3) increase turbulent burning velocity compared with larger particle sizes and lower concentration ranges.

Majority of the inorganic combustible dusts are metals [20]. The machining operations involving metals that produce fine dust particles of varied sizes and concentrations. Metals are also good energy carriers and used along with propellants, explosives etc. as additives. Sun et al. [21] reported that the metal particles hardly vaporize and hence they hardly change the composition and equivalence ratio of the gas phase mixture. Iron is a refractory metal and does not evaporate, whereas metals like aluminum or magnesium are more volatile. When mixed with a reacting stream, metals being a good thermal conductor can reach thermal equilibrium with the gas stream in a shorter time period. Metals undergo phase changes at its boiling point, but do not exhibit chemical decomposition like organic dusts do. Addition of iron also results in surface reactions [22]. The laminar experiments conducted by Poletaev et al. [23] confirms that particle size of combustion products of metals increases substantially. Joulin et al. [24] observed that the addition of inert particles to a gaseous fuel-oxidizer mixture will promote flame propagation and that the flames may be more resistant to quenching.

Prevention of explosions by using inert gases such as nitrogen is well known and is one of the most commonly used methods. The usage of chemically inert dusts such as sand, rock dust, limestone is another way to protect against explosions [25], [26] and the practice of rock-dusting in coal mines has been adopted since very old days [27]. It is important to scrutinize the influence of particle interaction on the rate at which a flame propagates to evaluate the hazardousness of any explosion. Fundamentally, this requires an investigation of the impact of both inert and reacting particles on the laminar burning velocity of a gas-air pre-mixture. Prior studies on suppression of flames using dust particles are divided into using inert and chemically reacting particles. The

suppression mechanisms involved in the two types of particles are quite different [28]–[30]. Specifically, inert particles in a reacting gas flow can suppress the flame through cooling, and chemically reacting particles produce inert gasses, which locally dilute the fuel or oxidizer levels thereby suppressing the flame. For example, chemically reacting particles such as sodium bicarbonate, potassium chromate and metal salts are found to decompose and produce CO_2 to extinguish the flame [31]–[34]. Whereas the thermal inhibitors like silica, alumina etc. reduce the flame temperature significantly [35]–[37]. As explained in Amyotte [35], the chemical inhibitors terminate the chain branching reactions by capturing the free radicals thereby inhibiting the chain reactions. The current study also focuses on suppression mechanisms using inert (sand) and chemically reacting particle like ($NaHCO_3$) and their effect on the burning velocity of a premixed flame.

Fundamentally, when a particle enters the flame zone, it absorbs some energy from the flame, thereby acting like a heat sink. Based on the nature of the particle, mass transfer from the particle can occur, and this could result in modification of local equivalence ratio, thereby acting as a local source. The extinction mechanism is thus, controlled mainly by thermal energy balance, where the particle size, concentration and thermal properties such as thermal conductivity (k), density (ρ), specific heat (C_p) are the important controlling parameters. On a large scale, the ability of the inert particles to suppress an explosion was investigated, experimentally and computationally, by Dong et al. [38]. An increase in the particle cloud density and a decrease in the particle size facilitates explosion suppression because of an increase in the inhibition surface area of contact with the gaseous flame front.

The current study will focus on investigating three types of particles, coal, sand, and sodium bicarbonate at mean particle size ranging between 75-90 μm (Figure 1.1). Coal, and sodium

bicarbonate are chemically reacting dusts with contrasting characteristics. Coal is a combustible dust whereas sodium bicarbonate is typically used as chemical fire suppressant. Sand is used in the study as an inert. Hence, the dusts selected for this study present a wide variety of chemical and thermal characteristics, and it is important to understand its fundamental effect on the burning velocity of premixed flame.

Figure 1.1: Different 75-90 µm dust types used a) coal; b) sand; c) sodium bicarbonate

The present study will be a step towards generating the turbulent burning velocity and radiative heat flux experimental data for the hybrid mixtures with different particle types, concentrations, turbulent intensity, and gas phase mixture ratios. It also aims to improve the understanding of suppression of flames by inert and reacting particles, using an experimental platform that inherits a simple flow geometry, which can be conveniently reproduced in the laboratory as well as modelled by CFD. The mathematical model developed for laminar hybrid

mixtures can be used to generalize the experimental results and make them applicable to a wide range of parameters and to predict the flame extinction concentrations.

1.2 Objectives of the current study

The main objective of this study is to analyze the influence of dust particles (coal, sand and sodium bicarbonate) on premixed methane-air flames using a Bunsen burner experimental set-up at constant pressure conditions. The turbulent burning velocity is calculated by averaging the measured flame heights for several images and the laminar burning velocity is calculated by the premixed cone angle measurements from several high-speed Shadowgraph images obtained from the experiments. A *MATLAB* image-processing program is used to process the turbulent images whereas *ImageJ* [39] software is used for processing laminar images. The turbulent intensity and length scale generated by a perforated plate in the burner is estimated directly from the hot-wire anemometer measurements. Radiative heat flux is also measured for each of the turbulent test conditions. The proposed outcomes from these experiments are:

1. An understanding of the variation of turbulent burning velocity of gas-dust premixed flames as a function of dust type, turbulent intensity, integral length scale, dust concentration and gas phase mixture ratio.
2. An understanding of the flame extinction characteristics and variation of laminar burning velocity of gas-dust premixed flames as a function of dust concentration and gas phase mixture ratio.
3. Quantify the radiative heat flux and radiative fraction of heat released from gas-dust turbulent premixed flames as a function of dust type, turbulent intensity, dust concentration and gas phase mixture ratio.

Ultimately, the experimental data from this study will form as reference basis for different hybrid mixtures studied and can be used to validate and improve the modeling correlations (e.g., Computational Fluid Dynamics simulation codes) to obtain the burning velocity for particle-air flame systems.

1.3 Organization of the thesis

This thesis is organized into six chapters and an appendix.

- Chapter 1, introduces the general problem of gaseous premixed combustion and the influence of turbulence on the burning velocity and discusses the influence of dust addition and addresses the knowledge gap related to the need for data on the burning velocity using constant pressure experiments.
- Chapter 2 reviews the experimental setup, procedure and uncertainties in measurements.
- Chapter 3 presents the results of laminar burning velocity of dust entrained methane-air premixed flames and the effect of suppression of sand and sodium bicarbonate particles.
- Chapter 4 focuses on studying the turbulent burning velocity of dust entrained methane-air premixed flames.
- Chapter 5 reports the radiative fraction of heat transferred by the dust entrained methane-air premixed flames.
- Chapter 6 summarizes the current study and presents the need for possible future research.

The appendices consist of additional material such as dust feeder calibration charts, experimental matrices, measured data points, uncertainty in measurements, additional photographs and plots.

2 Experimental set-up and procedure

2.1 Introduction

This chapter explains the experimental platform used in this study, Hybrid Flame Analyzer (HFA) designed and assembled by Rockwell [13]. This platform allows the systematic variation of the parameters which influence the problem such as particle size, dust type, turbulent intensity, integral length scale, dust concentration, and gas phase equivalence ratio. A detailed description of the apparatus and its construction details are presented in Rockwell [13] thesis, hence only the explanations relevant to the current study is presented here.

2.2 Hybrid Flame Analyzer (HFA)

Although, vast amounts of testing of dust explosions have been conducted with explosion spheres, an anchored Bunsen burner experimental design has been chosen for the reasons of being the simplest to use and analyze. This type of experiment also allows a continuous turbulent flame which can be studied for an extended period. It is important because turbulent flames are inherently not in a steady state therefore average quantities determined about the flame should come from continuous measurements taken over large time period. This temporal averaging is not possible in explosions spheres and other methods, such as open tubes, where transitioning flames result.

The experimental set-up used in this study, referred as the Hybrid Flame Analyzer (HFA) is same as the one developed by Rockwell [13]. HFA, as shown in Figure 2.1 and Figure 2.2, was

designed to measure the burning velocity of gaseous, dust, and hybrid (methane-air) flames by independently controlling the: turbulent intensity (u'_{rms}), turbulent integral length scale (l_0), particle size (d_p), and particle concentration (λ_p).

The main components of the HFA consist of: (1) a combustion chamber with a burner nozzle, (2) dust feeder, (3) shadowgraph optical system, and (4) an exhaust hood. Methane-air premixed flames are considered in this study. Mass flow controllers are used to control the gaseous flow rates of methane and air independently. Methane-air equivalence ratios (ϕ_g) of ϕ_g= 0.8, 1.0, and 1.2 are used to replicate fuel lean, stoichiometric, and fuel rich premixed gaseous flames. Methane-air total flow rates of 10, 30, 35 and 40 liters per minute (lpm) are used for different laminar and turbulent test conditions. A particle screw feeder then injects the dust into the methane-air flow creating the hybrid mixture of particle-methane-air at the burner exit. The dust feeder screw speed calibration is determined by collecting unburned dust at the end of the nozzle, weighing it and then developing a calibration curve. The shadowgraph optical system to capture the flame images consist of three components, a point source of light, biconvex lens, and a reflective lens high speed camera with a macro lens. A point source of light, which is a 480 W fan cooled projector bulb covered with a pin hole, is used. It is placed at the focal point of a 100 mm diameter biconvex lens (focal length 200 mm) mounted on the side of combustion chamber. When powered on, this creates a 100 mm diameter section of parallel light that travels through the flame in the combustion chamber to a second identical biconvex lens. This second biconvex lens reduces the diameter of the image making it narrow enough to fit on the sensor of the high speed digital camera. At the focal point of the second lens a Photron FASTCAM SA1.1 Digital High-Speed Camera System attached with a Zeiss Macro-Planar 100 mm lens set to infinity was placed. A high-speed camera was chosen due to the ability to view the image in real time and take videos as opposed to still

images. Images were recorded at 1,000 frames per second with a shutter speed between 1/104,000 and 1/593,000. This frame rate was chosen as it was the camera's highest setting available while still outputting a high resolution image. The shutter speed was adjusted depending on the light released from the dust being tested at that time. The flame images are then processed by extracting frames from the high speed video.

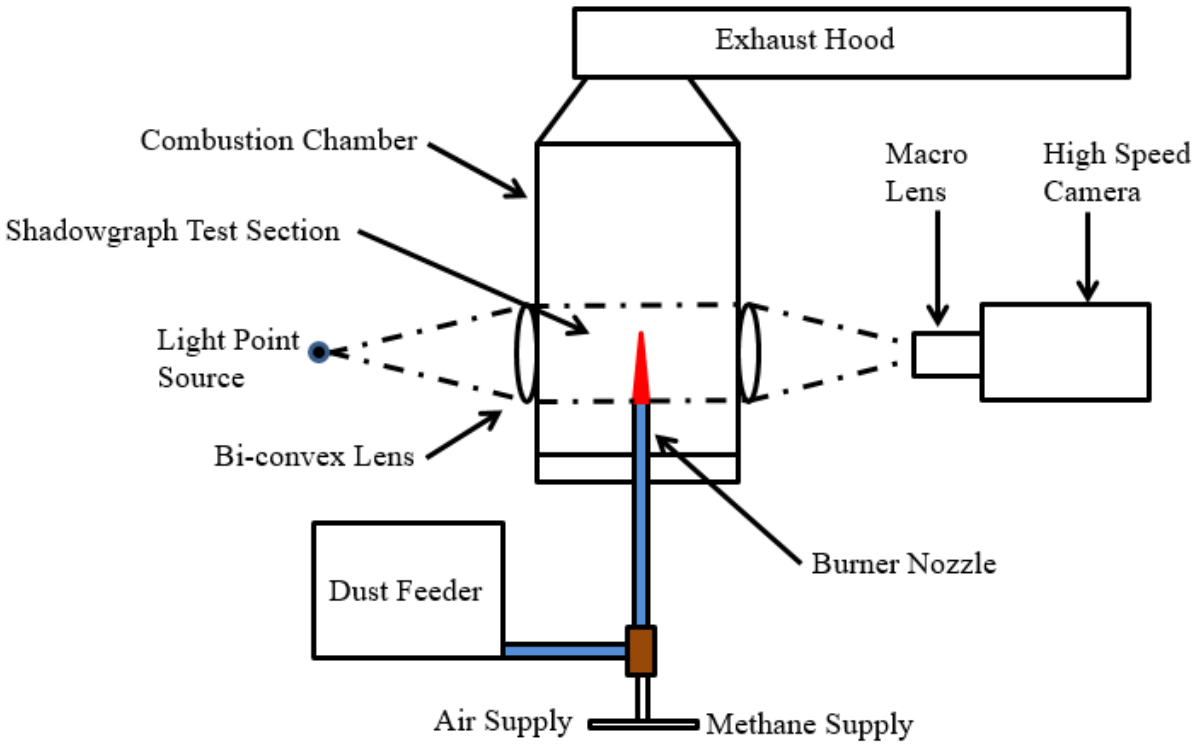

Figure 2.1: Experimental setup layout.

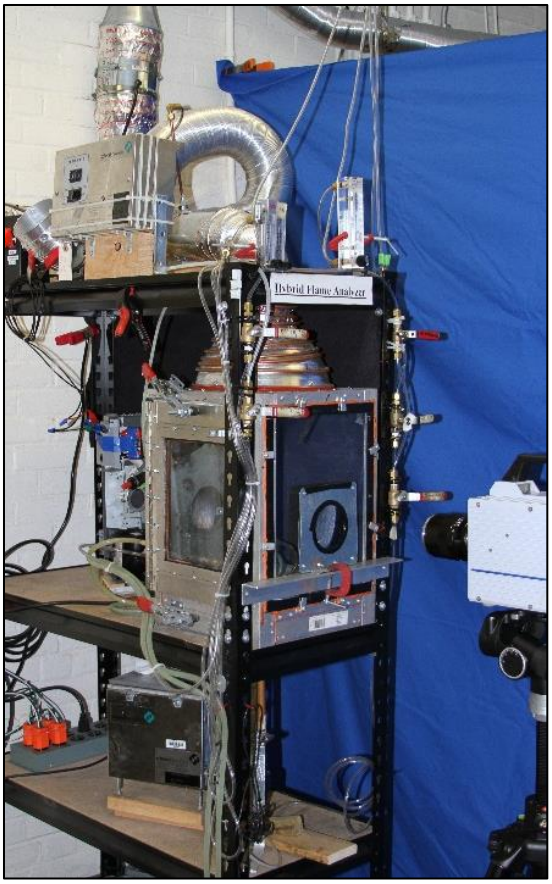

Figure 2.2: Experimental setup: Hybrid Flame Analyzer

The HFA utilizes two separate burner nozzles for burning velocity measurement, one for laminar flames and a second for turbulent flames (Figure 2.3). The laminar burner nozzle is a straight copper tube with an inner diameter of 14.5 mm. In addition, the turbulent burner nozzle consists of a perforated plate (3 mm diameter holes) to create turbulence, a premixed annular methane-oxygen pilot to anchor the flame, and the water cooling lines. The perforated plate used to create turbulence is similar to the work by Kobyashi et al. [40] and Liu et al. [41]. The study by Rockwell [13] indicated that different perforated hole sizes can create different ranges of turbulence intensities and length scales. A 3 mm diameter perforated plate has been used in this study, which has a blockage ratio (area of holes/total area) of 36% (Figure 2.4).

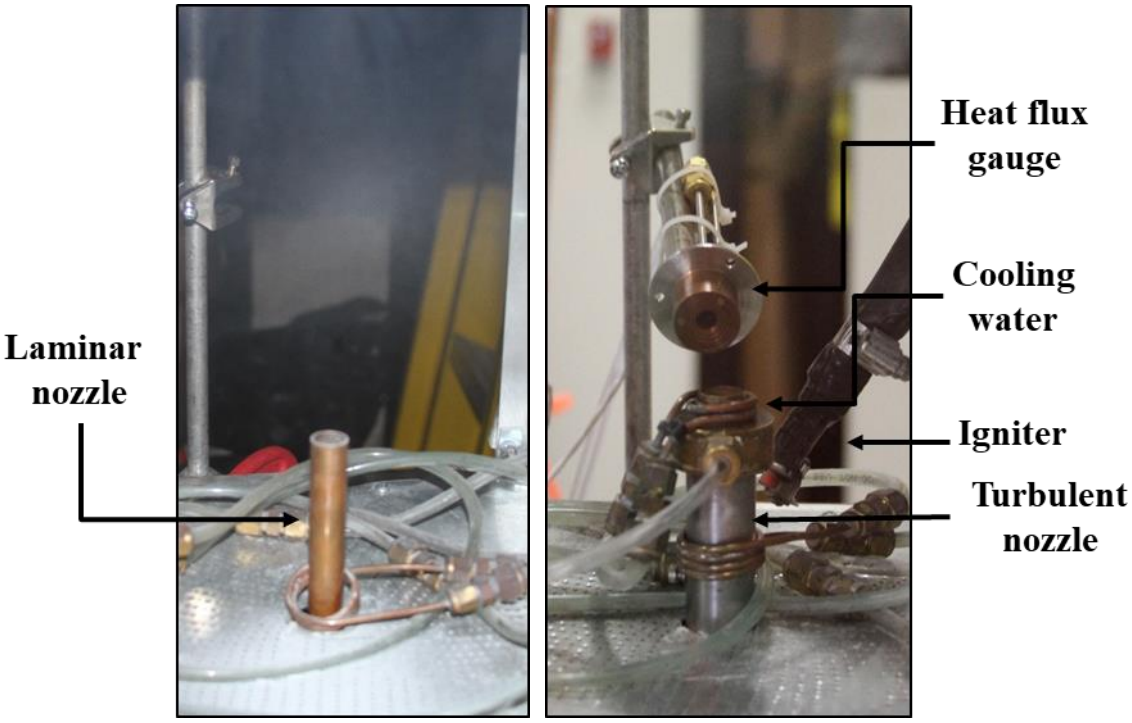

Figure 2.3: (a) Laminar and (b) Turbulent nozzle.

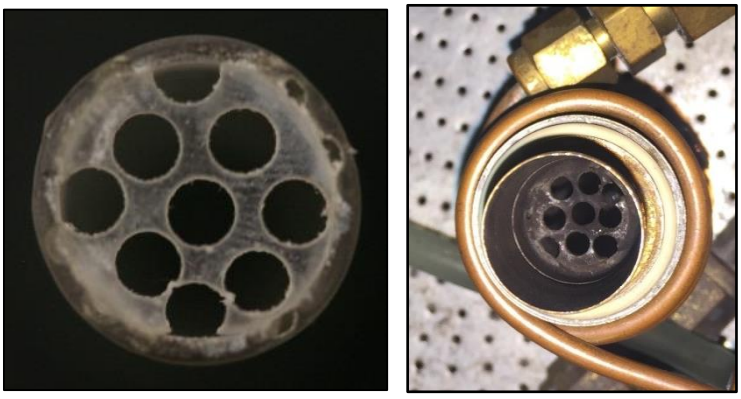

Figure 2.4: 3 mm diameter perforated plate and top view inside the burner nozzle at 30 mm from the nozzle exit.

A stoichiometric premixed methane-oxygen flame (ϕ_g = 1.0) as an annular pilot flame is used to anchor the turbulent flame. The annular pilot flame, shown in Figure 2.5, follows Kobayashi et al. [40] which was adopted while designing HFA by Rockwell [13]. The circumferential inserts around the main burner nozzle allows for the flow of stoichiometric mixture of methane (200 cc/min) and oxygen (700 cc/min). The burner nozzle has water cooling (with flow rate of 10 liters per hour controlled by a flowmeter) made of copper tubing wound around the burner diameter. This prevents the burner from overheating.

Figure 2.5: Premixed methane-oxygen pilot flame.

Turbulence measurements are conducted with a hot-wire anemometer (Dantec MiniCTA 54T42) in a cold flow at a sampling rate of 100 kHz (Figure 2.6). A sample hotwire anemometry measurement output for 1 second at100 kHz for 30 lpm flow rate with 3 mm perforated plate is shown in Figure 2.7. The velocity measurements in the experiments described below are done in cold flow without a flame. Pope [42] describes how the presence of flame could have an effect on the turbulent velocity field due to the large temperature gradients in the flame. Not many literatures provide a thorough description of the effects of a flame on the turbulent flow field. Recent studies

of Wabel et al. [43], [44] investigate these scenarios in detail. Many prior studies in literature have used the cold flow measurements of turbulence to characterize turbulence experienced by a flame and same procedure has been followed in this work.

Figure 2.6: Hot wire anemometry.

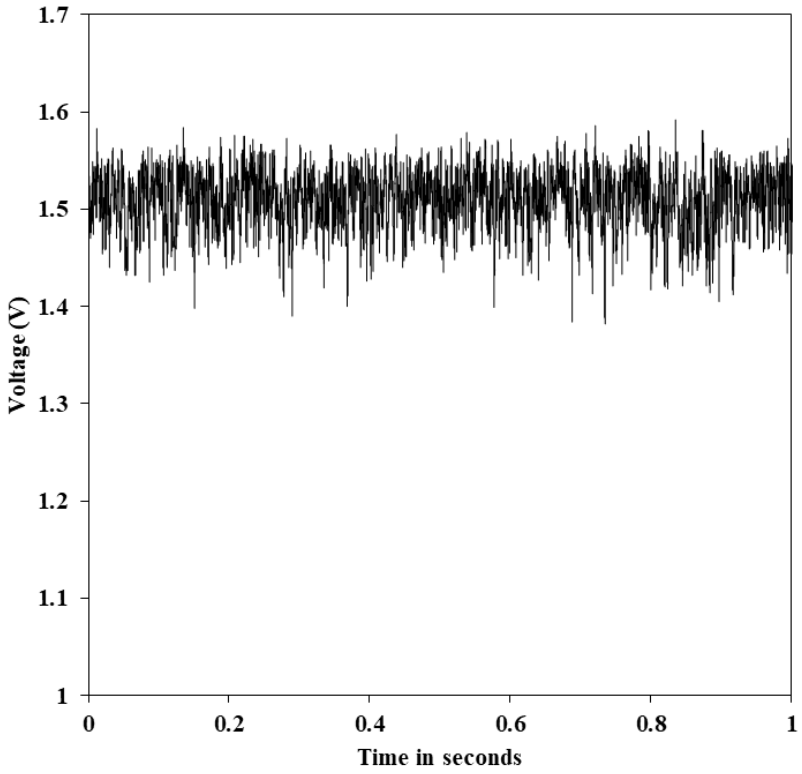

Figure 2.7: Hotwire anemometry sample output.

The platinum-plated tungsten wire sensor has a diameter of 5 µm and is 1.25 mm long. The hot-wire anemometer is calibrated using the average bulk flow velocity through the burner based on the mass flow controller flow rates. A calibration curve for the hot wire anemometer is developed with a third order polynomial fit as shown below in Figure 2.8.

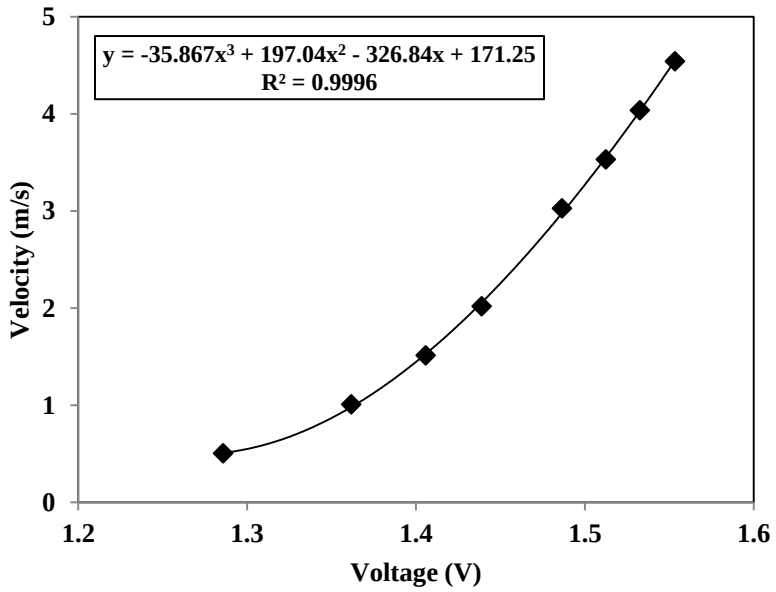

Figure 2.8: Hot-wire anemometry calibration curve

Turbulent flow can be described as $u = \bar{u} + u'$, where *u* is the axial flow velocity component, $\bar{u}$ is the average flow velocity and, u' is the fluctuating component of the flow velocity. The turbulent intensity is defined as Root Mean Square (RMS) of the fluctuating component of flow velocity.

$$u'_{rms} = \sqrt{\frac{u'^2_1 + u'^2_2 + u'^2_3 \ldots\ldots + u'^2_n}{n}}$$

The integral length scale (l_0) of turbulence is calculated as presented in Brunn [45].

$$l_0 = \bar{u} \int_0^\infty \rho_u(\tau)\, d\tau$$

Where, $\bar{u}$ is the average flow velocity and $\rho_u(\tau)$ is the autocorrelation of the velocity fluctuation. The calculated value of integral length scale of turbulence, l_0 = 2.7 mm - 2.9 mm is comparable to the perforated plate hole diameter of 3 mm. The total methane-air flow rates of 30, 35, and 40 liters per minute create a range of turbulent intensities of 0.65 to 0.88 m/s (Table 2.1).

Table 2.1: Turbulent intensity and integral length scale

Flow regime	Flow rate (lpm)	Flow velocity (m/s)	u'_{rms} (m/s)	% u'_{rms}	l_0 (mm)	*Re*
Laminar	10	1.01	-	-	-	926
Turbulent	30	3.03	0.646	21.3	2.9	2802
	35	3.53	0.718	20.3	2.8	3264
	40	4.04	0.882*	21.8	2.7	3736

* *For Sodium Bicarbonate and Iron dust experiments, the turbulent intensity measured at 40 lpm was u'_{rms} = 0.82 m/s. This is due to the use of a different perforated plate for these test conditions.*

Turbulent intensity can be altered by changing the perforated plate hole diameter, and/or by adjusting the distance of the location of perforated plate 10 to 30 mm from the nozzle exit and/or by adjusting the flow velocity or through a combination of all the above. Figure 2.9 shows the effect of using a 2 mm hole diameter perforated plate versus a 3 mm hole diameter perforated plate at three different distances (20 mm, 25 mm, 30 mm) of perforated plate location from the burner exit. As mentioned before, in the current study 3 mm hole diameter perforated plate has been used and the location has been kept constant at 30 mm from the nozzle exit and the flow velocities are varied (10, 30, 35, 40 lpm) in order to generate different levels of turbulence.

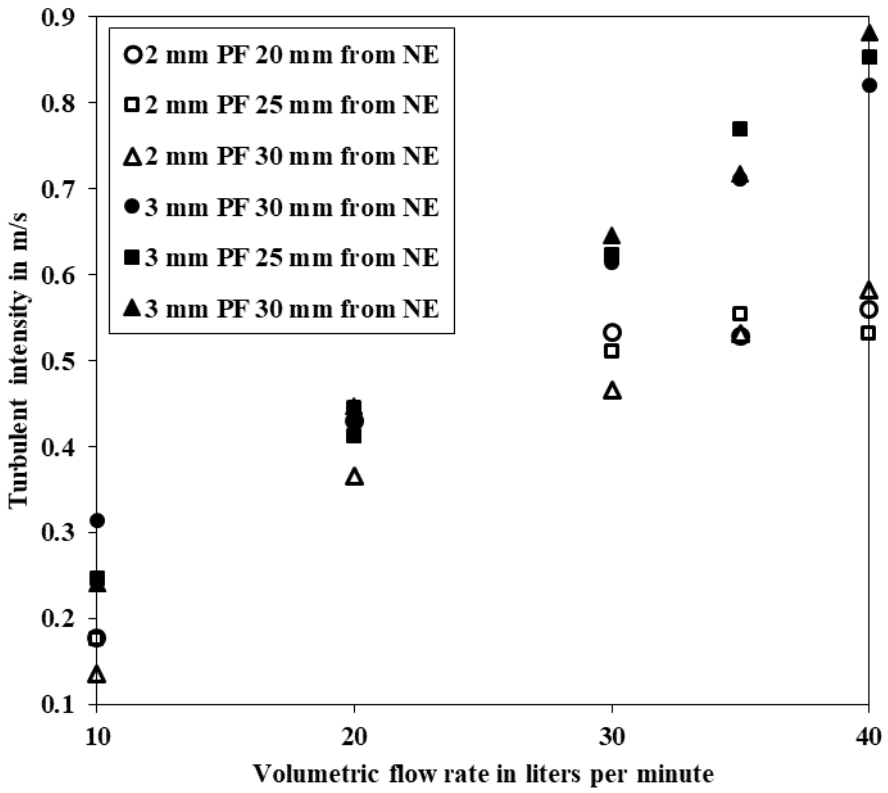

Figure 2.9: Effect of perforated plate diameter and distance of perforated plate location. PF: perforated plate; NE: nozzle exit.

To find out the combustion regime in which the current experiments exist a preliminary analysis with plot of u'_{rms}/S_L vs. l_0/δ_L commonly referred to as the Borghi diagram (as presented and explained by Peters [46]) is shown in Figure 2.10. The regime of the current experiments is within the rectangular red shaded region, which falls into the broadened preheat thin reaction zone. For the purpose of comparison with the work by Rockwell [13], the regime studied by Rockwell has also been indicated as gray shaded region in the Figure 2.10. Further details of the Borghi diagram and the combustion regimes are discussed in chapter 4.

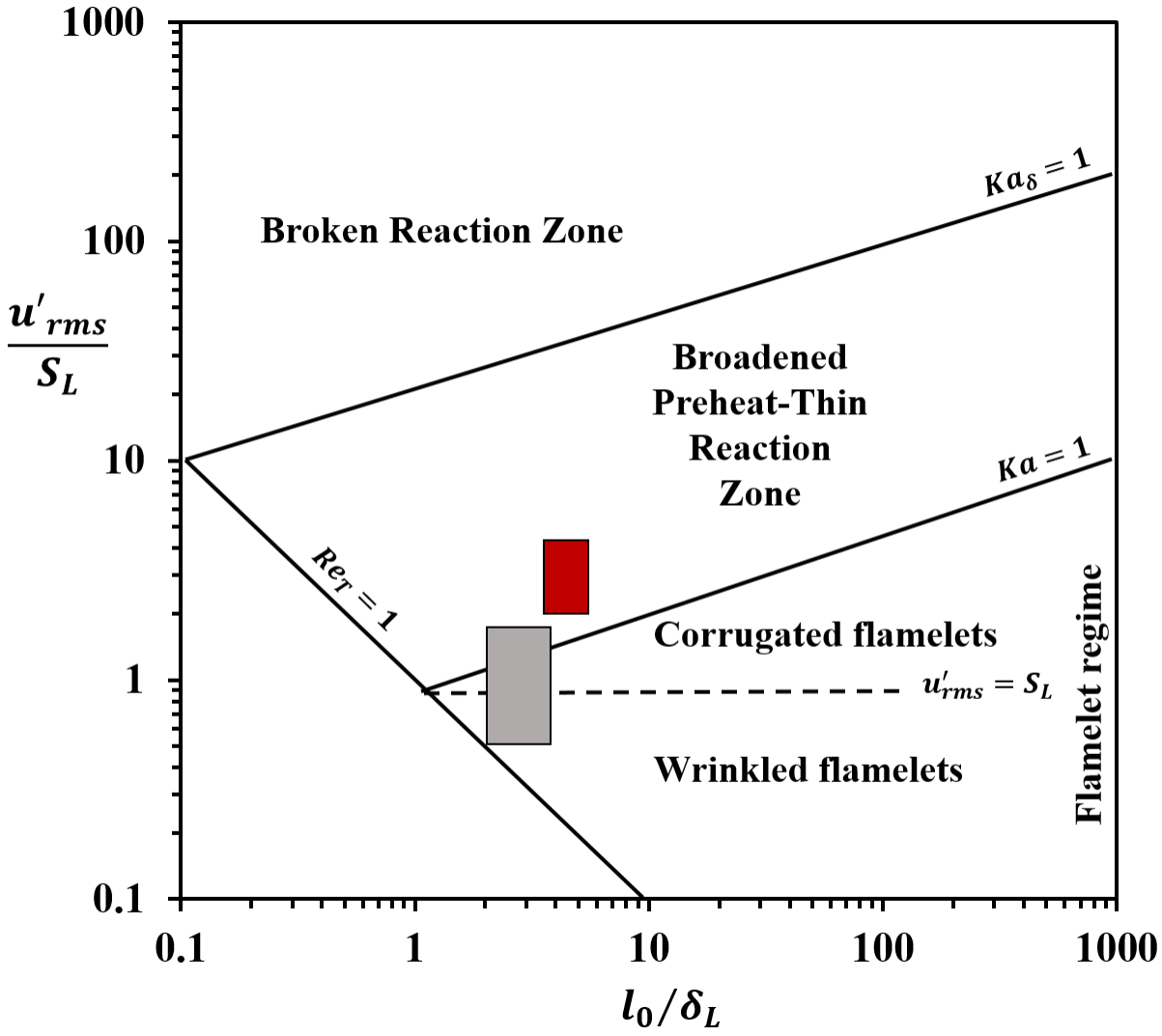

Figure 2.10: Turbulent combustion regime, Borghi Diagram. Gray region indicate study by Rockwell et al. [19] **and red region indicate the current study.**

A water cooled heat flux gauge was fixed at vertical and radial locations of 25 mm and 33 mm measured from the burner exit and center of the burner, respectively, in order to capture the heat flux measurements (Figure 2.11). The Medtherm 64 series [http://medtherm.com/]: 64P-2-24 Schmidt-Boelter type heat flux gauge with full scale output range of 0-20 kW/m^2, at responsivity of 1.284 kW/m^2 per mV has been used in this study. The responsivity of the gauge has an expanded

uncertainty of $\pm 3\%$ during the calibration conditions. Heat flux is absorbed at the sensor surface and transferred to an integral heat sink that remains at a different temperature than the sensor surface. For the heat sink surface to remain at the same temperature and not get heated, water cooling has been provided. The difference in temperature between sensor surface and sink is a function of the net absorbed heat flux. The heat flux gauge produces a linear output with $\pm 0.5\%$ non-linearity for full scale measurements. Zero correction was done for all the measurements using the voltage outputs from no flame conditions. Radiative heat flux measurements were significant only in turbulent flames and hence no measurements were made with laminar flames in this study.

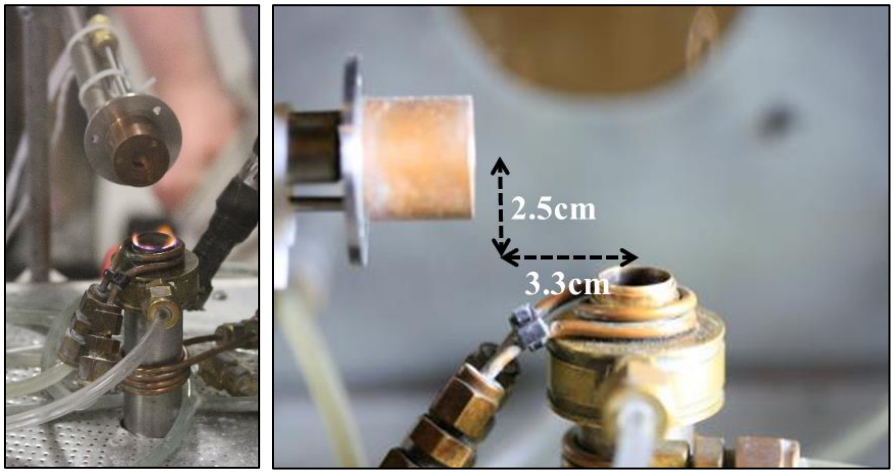

Figure 2.11: Heat flux gauge location from nozzle exit.

2.3 Experimental matrix

This section narrates the different test conditions studied for this thesis. As mentioned before, the study by Rockwell has been kept as the benchmark study for this research, with conditions tested being expanded into different types of dust, different turbulent conditions and with the addition of radiative heat flux measurements. Table 2.2 explains the difference in the test

conditions studied by Rockwell [13] and the current work, both using the HFA. It can be verified that the prior study by Rockwell [13] focused on reflecting the influence of particle size of coal on turbulent premixed flame in a turbulent intensity range of 0.18 m/s – 0.532 m/s, along with the establishment of constant pressure Bunsen burner experimental platform. The important observations made by Rockwell [13] were that smaller particle size and larger dust concentration results in an increase in the overall turbulent burning velocity. Hence the current study has chosen the smallest dust size out of the two dust sizes studied by Rockwell [13].

Table 2.2: Comparison of experimental matrices of current study and Rockwell [13]**.**

Work completed	**Rockwell** [13]	**Current study**
Laminar	Experiments with coal. d_p = 75-90 µm & 106-125 µm λ_p = 0-75 g/m^3	Experiments with sand, sodium bicarbonate. d_p = 75-90 µm λ_p = 0-75 g/m^3 & extinction studies for sand & sodium bicarbonate
Turbulent	Experiments with coal. d_p = 75-90 µm & 106-125 µm λ_p = 0-75 g/m^3 u'_{rms} = 0.18 – 0.53 m/s l_0 = 1.1 – 1.6 mm	Experiments with sand, sodium bicarbonate. d_p = 75-90 µm λ_p = 0-75 g/m^3 u'_{rms} = 0.65 – 0.88 m/s l_0 = 2.7 – 2.9 mm
Radiative heat flux measurements	No	Yes, for all the turbulent cases studied.

The following Table 2.3 shows the total number of experimental cases studied for the current research. A total of over 150 turbulent test cases and more than 50 laminar test cases are studied by varying different parameters.

Table 2.3: Experimental test conditions for the current study.

Mixture type	**Laminar**	**Turbulent**
Hybrid: CH_4+air+Coal (chemically reacting, release CH_4) d_p = 75-90 µm	Lee et al. [47] (Not part of current study) λ_p = 25, 50, 60, 75 g/m^3 ϕ_g = 0.9, 1.0, 1.2	u'_{rms} = 0.65, 0.72, 0.88 m/s λ_p = 25, 50, 60, 75 g/m^3 ϕ_g = 0.8, 1.0, 1.2
Hybrid: CH_4+air+Sand (chemically inert) d_p = 75-90 µm	λ_p = 25, 50, 60, 75 g/m^3 ϕ_g = 0.8, 1.0, 1.2	u'_{rms} = 0.65, 0.72, 0.88 m/s λ_p = 25, 50, 60, 75, 100, 125 g/m^3 ϕ_g = 0.8, 1.0, 1.2
Hybrid: CH_4+air+ Sodium Bicarbonate (chemically reacting, release CO_2+H_2O) d_p = 75-90 µm	λ_p = 25, 50, 60, 75 g/m^3 ϕ_g = 0.8, 1.0, 1.2	u'_{rms} = 0.65, 0.72, 0.82 m/s λ_p = 25, 50, 60, 75 g/m^3 ϕ_g = 0.8, 1.0, 1.2
Gaseous: CH_4+air (no particles)	ϕ_g = 0.8, 1.0, 1.2	u'_{rms} = 0.65, 0.72, 0.88 m/s ϕ_g = 0.8, 1.0, 1.2

The dust screw feeder (Figure 2.12) is calibrated by collecting the dust coming out of the nozzle over the range of settings for each dust used. For each calibration point dictated by the rotational speed of the screw feeder, the dust feeder is operated for one minute and the collected dust in the hopper (see Figure 2.13) is weighed on a scale to plot Figure 2.14. The mixing between the dust and the flammable gas is not ensured if the dust is injected in the tube where the mixture gas-air is already present. In order to improve such measurements, the dust-flammable gas must be co-fed through simultaneous injection from the reservoir, thus ensuring mixing of the fuels. Current study follows this approach. All the dust feeder calibration curves for this study are presented in appendix 8.1 for further reference.

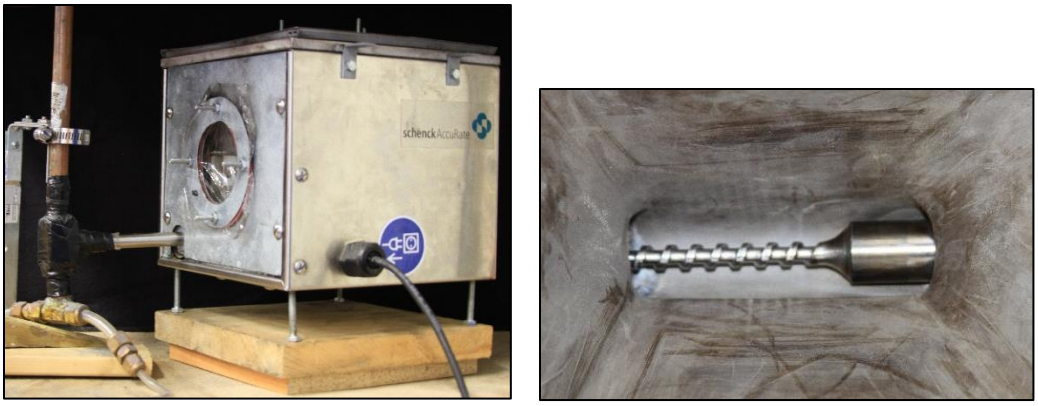

Figure 2.12: Dust screw feeder.

Figure 2.13: Dust hopper for dust calibration.

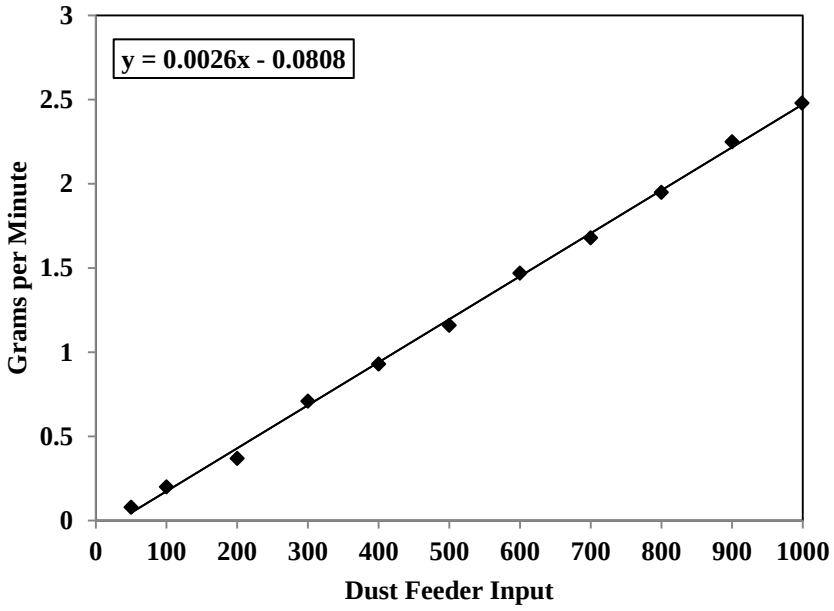

Figure 2.14: Sample calibration curve for dust feeder.

Further, the limitation of the screw feeder rotational speed need to be emphasized here, because that resulted in limiting the concentration of the dusts studied mostly with in the range of mass concentrations of 0 – 100 g/m^3 for turbulent flows and 0 – 585 g/m^3 for laminar flow. The dust concentration described throughout this study is the mass concentration of dust (a comparison of mass loading of different types of dusts, not the volumetric loading of dust) and hence it is also a function of the dust particle density. Based on the dust feeder calibration and the gaseous pre-mixture equivalence ratio and flow rate, test matrices are created as shown in the Table 2.4, show a sample test matrix of experiments conducted in this study. All other matrices are shown in appendix 8.2. The numbers highlighted in grey are the dust feeder settings for the prescribed coal dust concentration based on the feeder calibration curve.

Table 2.4: Sample experimental test matrix for coal.

Experimental matrix for Coal 75-90 µm and 30 lpm total flow rate (u'_{rms} = 0.65 m/s)							
	Oxidizer	Fuel	Particle concentration and corresponding feeder value				
ϕ_g	Air (lpm)	CH_4 (lpm)	0 (g/m^3)	25 (g/m^3)	50 (g/m^3)	60 (g/m^3)	75 (g/m^3)
0.8	27.68	2.325	0	320	608	723	896
1	27.15	2.851	0	320	608	723	896
1.2	26.64	3.357	0	320	608	723	896

The particle size of the dusts was determined using a *Retsch* AS300 Sieve Shaker (appendix Figure 8.8). This sieve shaker works with an electromagnetic drive which produces three dimensional throwing motion of the dust and allows for the dust to be sieved equally over the surface. *Retsch* UR 1 Ultrasonic Cleaner was used to clean the sieve. The coal dust used in the study is Pittsburgh seam coal, bituminous, with approximately 30% volatiles. The sand used in the study is play sand (silica) and the sodium bicarbonate used being medical grade $NaHCO_3$.

2.4 Experimental uncertainties

Certain level of uncertainties are involved in different components of measurements explained in the earlier sections. The two mass flow controllers used to control methane-air flow rates into the main burner have an uncertainty of 1% of its full scale measurements (i.e., 0.5 lpm for air and 0.05 lpm for methane). The dust feeder screw speed calibration is determined by collecting unburned dust at the end of the nozzle, weighing it and then developing a calibration curve. The instantaneous fluctuations in the feed rate of the dust feeder were not quantified. However long duration of sampling (60 seconds) and usage of average value from multiple measurements of dust collected minimizes this uncertainty. The standard deviation of volumetric feed rate of dust feeder

is ±2% from mean value. The makeup air was controlled using a rotameter with an uncertainty of 5% of full scale. This could lead to slight variations in the ambient flow speed inside the combustion chamber.

Turbulence measurements are captured with a hot-wire anemometer in a cold flow at a sampling rate of 100 kHz. The uncertainty of hotwire measurements is a combination of the uncertainties of the individually acquired voltages converted to velocities and the uncertainty of the statistical analysis of the velocities. The standard deviation of the 300,000 samples of voltage measurements is around $\pm$2% of the mean values. The uncertainty of velocity sample acquired the calibration conditions is typically 1% with a confidence interval of 95%. When uncertainty of mass flow controller itself is included, total uncertainty may increase to about 3%.

A high-speed digital camera was chosen for video acquisition that were recorded at 1,000 frames per second with a shutter speed between 1/104,000 and 1/593,000. This frame rate was chosen as it was the camera's highest setting available while still outputting a high resolution videos. The shutter speed was adjusted depending on the light released from the dust being tested at that time and was mainly dependent on the type of dust. The turbulent flame can move some amount during this exposure time depending on the level of turbulent intensity. The flame edges were selected manually using a *MATLAB* program. The uncertainty associated with manual selection of edges from images is not quantified. However, 25 flame images are used for the estimation of burning velocity based on the prior work by Rockwell [13]. Since the uncertainty of the experiment could not be quantitatively measured error bars are calculated as the standard deviation of the burning velocity. These are presented in appendix 8.5 for further reference.

The radiative heat flux measurements were taken at 50 Hz sampling rate for a period of minimum 5 seconds. For all the radiative flux measurements, uncertainty analysis was conducted.

The standard deviation of heat flux measurements for experiments with coal dust varied between 5.6% - 13.1%; for experiments with sand varied between 11.7% - 22.9%; for experiments with $NaHCO_3$ dust varied between 11.1% - 26.7%.

The uncertainty associated with the derived quantities of laminar and turbulent burning velocities are discussed in the respective chapters and tabulated in detail for each of the experimental test cases studied in the appendix section (8.3, 8.4 and 8.5) of this thesis. Further, the individual values of laminar burning velocity, turbulent burning velocity and radiative heat flux measurements and their standard deviation values are also presented in the appendix 8.6 and 8.7 for future reference.

3 Laminar burning velocity and extinction of premixed methane-air-dust flames

3.1 Chapter abstract

This chapter discusses the influence of 75-90 μm sized sand and sodium bicarbonate particles at different concentrations (λ_p = 0 to 585 g/m^3) on the laminar burning velocity and flame extinction of methane-air mixtures (ϕ_g = 0.8, 1.0 and 1.2) using the Bunsen-burner type experimental set-up. Addition of sand and sodium bicarbonate always decreases the laminar burning velocity. At ϕ_g = 0.8, flame extinction occurred at 350 g/m^3 and 75 g/m^3 with sand and sodium bicarbonate, respectively, whereas at ϕ_g = 1.2 flame extinction occurred at 585 g/m^3 and 125 g/m^3 with sand and sodium bicarbonate, respectively. Sodium bicarbonate reacts by absorbing heat from the flame zone to release CO_2 and H_2O gases. As a result, the flame extinction occurs at a lower particle concentration as compared to that with sand, which is inert. At ϕ_g = 1.0, flash back scenarios with tilted flames were observed with sand in the concentration range of 50 to 585 g/m^3. Variation in the burning velocity for different particle concentration and equivalence ratios are discussed. Further, this chapter explains the mathematical model developed to generalize the applicability of flame extinction results and validate the model results against the current experiments. Mathematical model predicted that for sand particle size in the range of 75-90 μm, concentrations of 340, 660 and 590 g/m^3 are necessary for extinction of a methane-air flames of lean,

stoichiometric and rich equivalence ratios, respectively at ambient temperature feed. Model is able to predict the critical concentration of inert required of flame extinction.

3.2 Introduction and related literature

Laminar burning velocity is the most important and fundamental characteristic of premixed flames. This chapter is a continuation of Lee's [47] study with laminar premixed flames. This is specifically focused on the effects of sand and sodium bicarbonate injected to gas mixture on decreasing the laminar burning velocity of methane-air flames and further to understand how flame extinction occurs. Prior research work by Xie [48] and Lee [47] have investigated in detail about the effect of adding coal dust on the laminar premixed methane-air flames, both at atmospheric and at preheated reactant temperatures. Figure 3.1 is recreated from Lee [47], where the effect of coal addition is presented. Equivalence ratio promotion effect due to the release of methane is clearly visible, especially at fuel lean conditions with the addition of coal. This results in an increase in the S_L at smaller concentrations and a further decrease in S_L at higher concentrations of coal. Further, Lee's study [47] also presented the effect of sand in reducing the laminar burning velocity of methane-air flame.

Flame extinction is important from the perspective of fire and explosion protection. Prevention of explosions by using inert gases such as nitrogen is well known and is one of the most commonly used methods. Dispersal of chemically inert dusts such as sand, rock dust, limestone on a flame front is another way to protect against explosions and the practice of rock-dusting in coal mines has been adopted since very old days (Haswell Colliery explosion and Faraday and Lyell report in 1845 [27]).

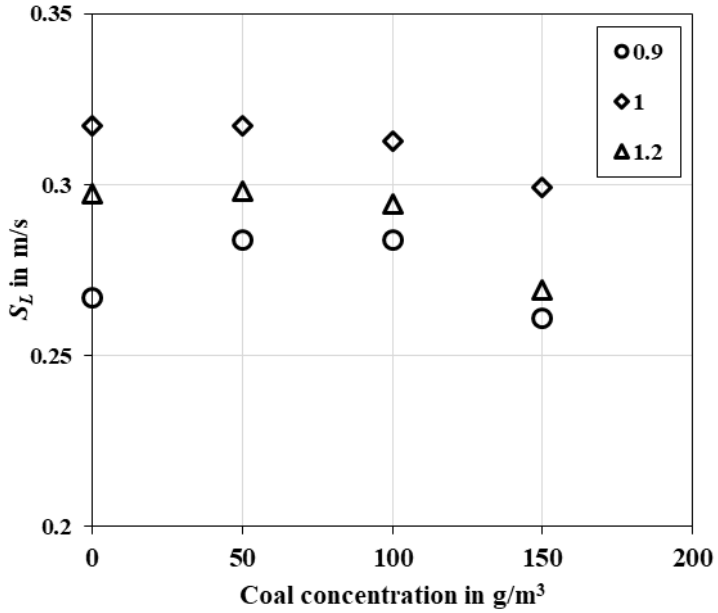

Figure 3.1: Laminar burning velocity of methane-air-coal premixed flames, reproduced from Lee [47]**.**

Flame inhibition and extinction using dust particles, in general, is divided into two types, thermal and chemical inhibitions. Sand, inert particles in general, like inert gases, act as heat sink causing a reduction of flame temperature thereby behave as thermal inhibitor. Dry inorganic salts or chemicals like Sodium Bicarbonate ($NaHCO_3$) chemically interfere in the combustion process by locally diluting the fuel-air mixture levels in addition to being heat sink. Combustion inhibition and flame extinction by using dry chemicals and inert particles have been studied for a long time [26], [49]. The inorganic salts of sodium and potassium (such as sodium bicarbonate, potassium chromate and metal salts) have been vastly used in fire extinguishers as they decompose at high temperature and produce CO_2 to extinguish the flame. A detailed literature review on the dry chemical fire extinguishing agents was conducted by Thorne [49] and the mechanism of flame inhibition by different metal salts was discussed extensively by Birchall [31]. As explained by Amyotte [35], the chemical inhibitors terminate the chain branching reactions by capturing the

free radicals, thereby inhibiting the chain reactions. An extensive literature review about the influence of solid inert-particles in mitigating and preventing explosions can be found in Amyotte [35], Kosinski [50], Qiao et al. [51]. Further studies with chemically reacting particles reporting decomposition and producing CO_2 to extinguish the flame are found in the reports of Birchall [52], Linteris et al. [32], Mitani and Niioka [33], Rosser et al. [53], Trees and Seshadri [34].

The effectiveness of $NaHCO_3$ on laminar diffusion flame extinction was studied by Trees and Seshadri [34] with a counter flow configuration. They studied the minimum amount of $NaHCO_3$ (10-30 µm) required for flame extinguishment and identified that the inhibition was predominantly chemical, based on temperature estimations close to flame extinction conditions. It needs to be emphasized that the particle size plays an important role in determining the inhibition mechanism by dusts, as it is directly related to the particle surface area in contact with the flame sheet [54]. Below a critical particle diameter of 16 µm, $NaHCO_3$ completely vaporizes [6]. Beda et al. [6] studied the decomposition and conversion rate of bicarbonates to carbonates above this critical diameter by calculating the particle mass loss after passing through flame. They concluded that usage of bicarbonate particles above 25 µm results in heterogeneous inhibition mechanisms. Flame extinction measurements of $NaHCO_3$ using cup burner was conducted by Hamins [55] on non-premixed flames and identified that only half of extinction characteristics of $NaHCO_3$ is due to kinetics.

The premixed flame extinction studies using dust particles are relatively less understood as compared to the diffusion flame extinction. In one of the earliest studies, Levy and Friedman [56] examined the effect of aluminum chloride on the burning velocity of premixed methane-air flames stabilized on burners. This was first of a few research studies, which investigated the influence of dry chemicals on the burning velocity of premixed flames. It was observed that the burning

velocity decreased with an increase in particle concentration, but reached a constant value at higher particle concentrations [56]. Rosser et al. [53] provided the variation of flame propagation velocity of stoichiometric methane-air mixtures with different metal salts. The mechanism of heterogeneous inhibition in premixed flames as a surface phenomenon was explained by Dewitte et al. [25]. Experiments were also performed in 20-L sphere by injecting the inhibitors, to study the variation of laminar burning velocity of premixed propane-air flames [57]. It should be noted that the combustion inside 20-L sphere by the injection of particles results in a turbulent condition. Chellaiah et al. [58] presented a comparison between the extinction effectiveness of silica and $NaHCO_3$ (10-40 μm) in a Bunsen type stoichiometric premixed methane-air flames and they observed almost negligible effect of inert particles on laminar burning velocity. It is critical to scrutinize the influence of particle interaction on the rate at which a flame propagates to evaluate the hazardousness of any explosion. Fundamentally, this requires an investigation of the impact of inert particles on the laminar burning velocity of a gas-air pre-mixture. A mathematical model to predict the laminar burning velocity [59] has been now extended to predict the flame extinction concentration of inert particles [60] along with experimental results on the decrease of laminar burning velocity with increase in the sand concentrations of 75-90 μm particle size.

It is also important to understand the controlling parameters related to the suppression of flames using inert particles. In general, when a particle enters the flame zone, it absorbs some energy from the flame, thereby acts like a heat sink. The extinction mechanism is controlled mainly by thermal energy balance, where in the particle size, concentration and thermal properties such as k, ρ, C_p are important controlling parameters. Dewitte et al. [25] conducted one of the earliest experimental studies on the inhibition and extinction of premixed flames by different dust particles. Their study was based on the variation of the mean flame temperature with different

concentration of dust particles and relating the mean flame temperature to flame propagation velocity. Specifically, a limiting value of the mean kinetic flame temperature (1500-1600 K), below which the flame cannot self-sustain, was identified and subsequently used to predict the critical dust concentration for the thermal inhibitors (Dewitte et al. [25]). Mitani [37] developed a flame inhibition theory for 'thermal' inhibitors alone, based on two non-dimensional parameters, one related to the heat capacity of the particle; and the other related to the rate of heat of absorption by dust particle. On a large scale, the ability of the inert particles to suppress an explosion was investigated, experimentally and computationally, by Dong et al. [38]. An increase in the particle cloud density and a decrease in the particle size, facilitates explosion suppression because of an increase in the inhibition surface area of contact with the gaseous flame front (Dong et al. [38]).

There are limited existing literature, which explores the flame extinction concentration of dust particles on burner stabilized premixed flames. This chapter aims to improve our understanding of suppression of flames by inert and dry chemical particles, using an experimental platform with a simple flow geometry, which can be conveniently reproduced in laboratory. The chapter presents the effects of injection of sand and sodium bicarbonate particles on the laminar burning velocity of burner stabilized methane-air flames at three equivalence ratios. A mathematical model is also discussed for inert particles to generalize the experimental results and make them applicable to a wide range of parameters. The concentrations at which sand and sodium bicarbonate particles of 75-90 μm mean diameter size are injected, that result in flame extinction of lean, stoichiometric and rich methane-air flames, are also presented.

3.3 Experimental set-up and procedure

The Bunsen-burner type experimental set-up, called HFA, using a cylindrical copper tube of 14.5 mm inner diameter (Figure 2.2) for laminar studies. To this, quantified amounts of methane, air and particles have been supplied. The particles used in this study are in the mean diameter size range of 75-90 µm. The particles are pre-calibrated for different feed rates and gaseous mixture flow velocities similar to the previous studies [17], [59], [60]. Methane-air gaseous mixture, at a desired total flowrate of 10 lpm and at required respective flow rates have been controlled using mass flow controllers. The fuel-air equivalence ratios of ϕ_g = 0.8, 1.0 and 1.2 are considered. The experiments are carried out at atmospheric temperature and pressure. Videos of burner stabilized hybrid flame zone are captured using a shadowgraph technique. The shadowgraph images are then processed after extracting frames from the high speed video.

Figure 3.2: Flame images, a) Direct image of gaseous premixed flame; b) Direct image of gas-dust premixed flame; c) Shadowgraph image of gas-dust premixed flame.

The processed shadowgraph image (Figure 3.2) of flame zone is used to estimate the full and half ('α') cone angle measurements using *ImageJ* [39]. The average half cone angle, $\bar{\alpha}$, estimated from 20 images, is used to calculate the laminar burning velocity as,

$$S_L = u \ \sin \bar{\alpha} \qquad (3.1)$$

where, u is the velocity of unburned gas mixture at the burner exit, which is estimated as 1.01 m/s for the current study.

3.4 Results and discussion

The laminar burning velocity, S_{Lg}, of gaseous premixed methane-air flames, estimated using the above method, is validated against identical cases from Law, 2006 [61]. Figure 3.3 indicates a good agreement between two experiments, for the three mixture ratios considered. Same procedure has been adopted while estimating the S_L for hybrid methane-air-particle flames in this study.

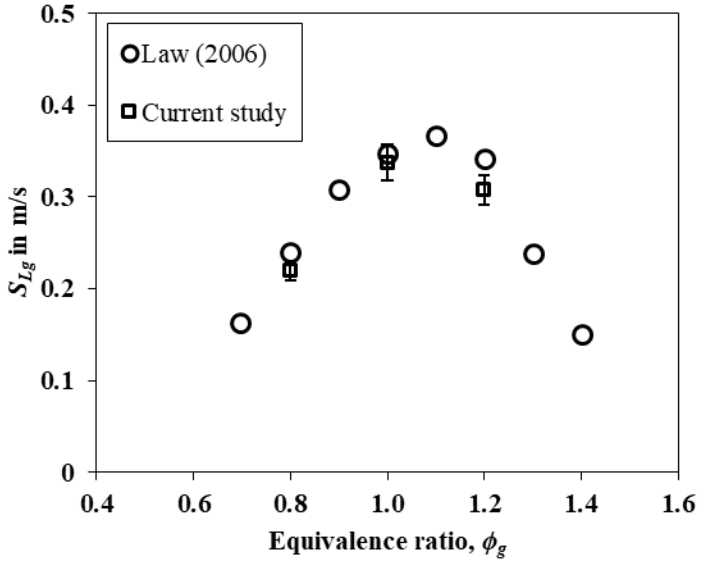

Figure 3.3: Validation of laminar burning velocity of gaseous methane-air Flames.

3.4.1 Addition of sodium bicarbonate

Figure 3.4 shows the effect of adding sodium bicarbonate particles to the laminar burning velocity of methane-air mixtures. A continuous decrease in the laminar burning velocity is observed with the addition of $NaHCO_3$. The flame images with increasing concentration of

$NaHCO_3$ are shown in Figure 3.5, Figure 3.6, and Figure 3.7, for gas equivalence ratios of 0.8, 1.0, and 1.2, respectively. The rate of decrease of S_L at 25 g/m^3 addition of $NaHCO_3$ to gaseous methane-air is found to be higher for ϕ_g = 1.2 as compared to other two equivalence ratios. Flame instability due to blow-off and extinction are observed at $NaHCO_3$ concentrations of 75 g/m^3 at ϕ_g = 0.8 and 125 g/m^3 at ϕ_g = 1.2. The higher concentration requirement for flame extinction in ϕ_g = 1.2 as compared to ϕ_g = 0.8 can be explained based on two reasons. One, the higher flame temperature and two, the presence of excess fuel at ϕ_g = 1.2 resulting in diffusion shroud covering the premixed flame zone. For stoichiometric methane-air mixture, a complete flame extinction was not observed till $NaHCO_3$ concentration of 175 g/m^3 tested in the current study. But very close to flame extinction due to blow-off was observed around 200 g/m^3. The flame tip starts to open (Figure 3.6) at a concentration of 175 g/m^3. This is due to the thermal-diffusive imbalance in the tip of flame. It is known that higher burning velocity at the burner tip is attributed to the flame curvature and flow divergence effect. At the flame tip there is an enhanced conduction of heat to the reactants typically resulting in the increase of burning velocity. Whereas the radial diffusion of the reactants also increases at the tip of the burner which has a tendency to decrease the burning velocity. At higher concentrations, with the presence of $NaHCO_3$ particles releasing CO_2 and H_2O, depletion of reactants is occurring and resulting in the local flame extinction and fading of the flame at the tip.

As the concentration of $NaHCO_3$ was increased in each of the test conditions, the S_L values decreased considerably and approached lower flammability limit S_L value (0.13 m/s with 15% volume of methane) of methane-air mixture before flame extinction. The lowest S_L value recorded with $NaHCO_3$ hybrid methane-air flames was approximately 0.156 m/s (indicated as red dotted line in Figure 3.4). This was obtained at 50 g/m^3, 175 g/m^3 and 100 g/m^3 for ϕ_g = 0.8, 1.0, and 1.2

respectively. The test results indicate that the concentration of $NaHCO_3$ required for flame extinction increases in the order ϕ_g = 1.0 > 1.2 > 0.8, which is related to the flame temperature.

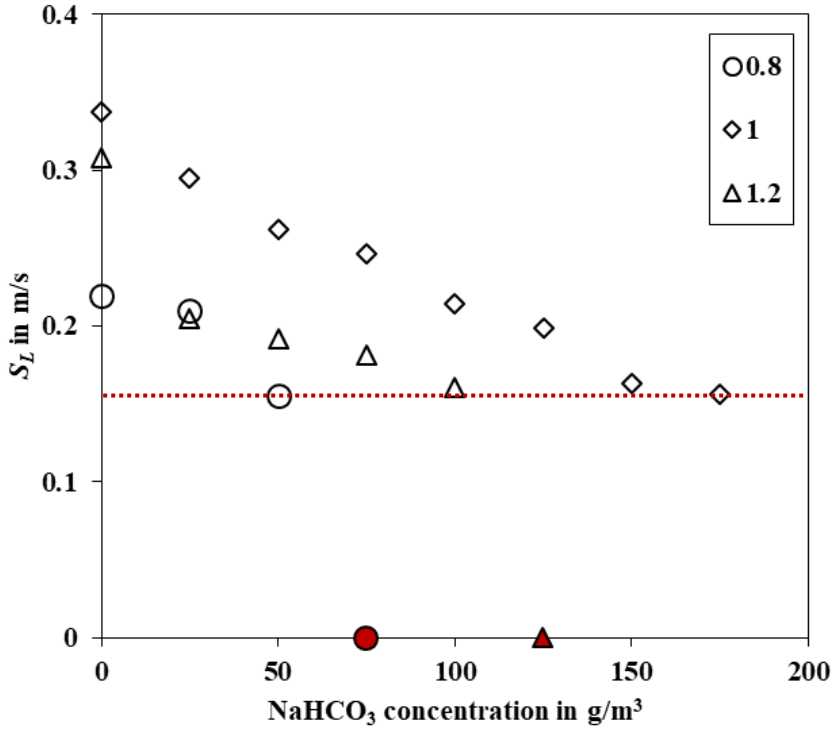

Figure 3.4: Laminar burning velocity of methane-air-$NaHCO_3$ premixed flames.

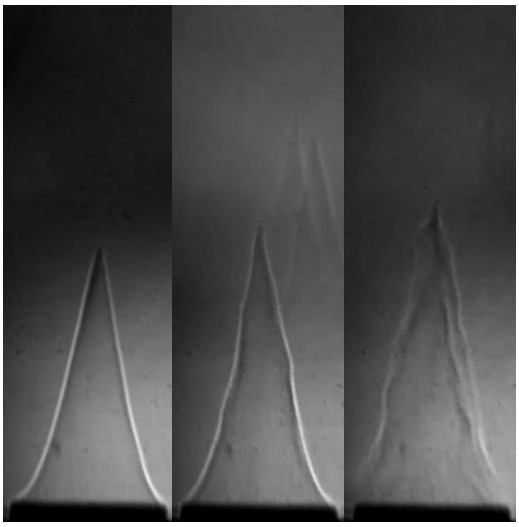

25 g/m^3 50 g/m^3 75 g/m^3

Figure 3.5: Laminar flame images at ϕ_g = 0.8 and different concentrations of $NaHCO_3$.

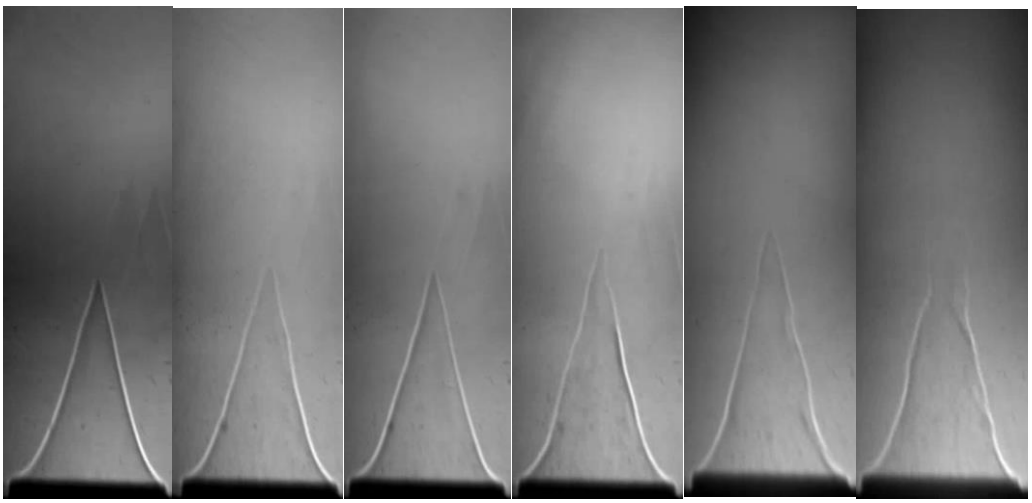

25 g/m^3 50 g/m^3 75 g/m^3 100 g/m^3 125 g/m^3 175 g/m^3

Figure 3.6: Laminar flame images at ϕ_g = 1.0 and different concentrations of $NaHCO_3$.

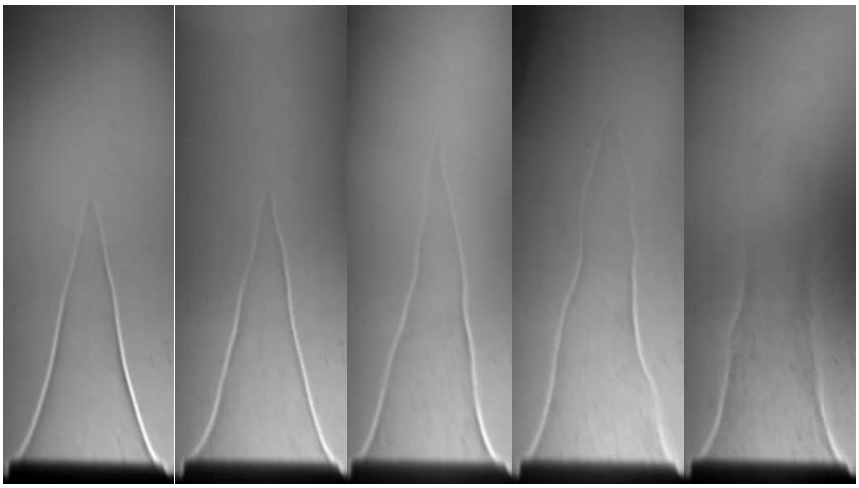

25 g/m^3 50 g/m^3 75 g/m^3 100 g/m^3 125 g/m^3

Figure 3.7: Laminar flame images at ϕ_g = 1.2 and different concentrations of $NaHCO_3$.

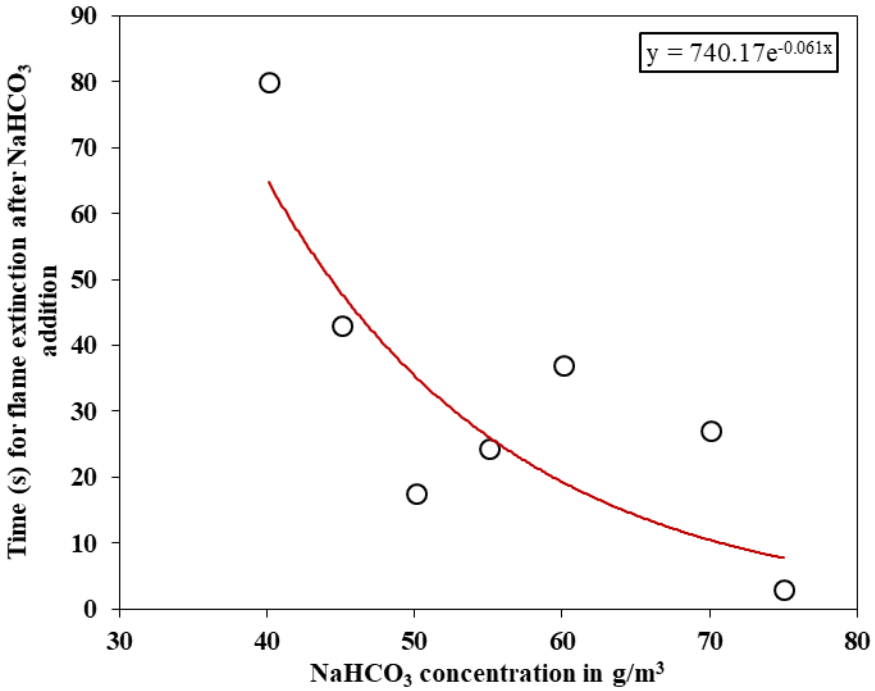

Figure 3.8: Time taken for flame extinction after $NaHCO_3$ addition.

Sodium Bicarbonate is a dry chemical typically used in Class B firefighting scenarios. The flame extinguishment is due to the chemical effect as a result $NaHCO_3$ melting, releasing CO_2 and H_2O. The sodium bicarbonate decomposition at high temperature can be explained as follows: $NaHCO_3$ reacts at a temperature of 270^oC.

$$2\ NaHCO_3 \rightarrow Na_2CO_3 + CO_2 + H_2O. \qquad (3.2)$$

The sodium carbonate formed as a result of this decomposition, is a relatively stable salt. But at a higher temperature of around 851^oC, Na_2CO_3 also reacts to release more CO_2.

$$Na_2CO_3 \rightarrow Na_2O + CO_2 \qquad (3.3)$$

Further, as observed from previous studies [62] that the $NaHCO_3$ decomposition reaction is an endothermic reaction, which results in a reduction in the flame enthalpy. This indicates that, though $NaHCO_3$ vaporization dilutes flame zone locally, it also acts as a heat sink like inert

particles. The time taken for extinction after introducing $NaHCO_3$ to the premixed methane-air flame is measured for ϕ_g = 0.8 and plotted in Figure 3.8. The data points of time are an average of three experimental trials. When the concentration of $NaHCO_3$ is increased from 40 g/m^3 to 50 g/m^3, a steep decrease in the time required for flame extinction is observed. Further addition of particle up to a concentration of 60 g/m^3 resulted in a slight increase in time for flame extinction followed by an immediate flame extinction after $NaHCO_3$ addition at 75 g/m^3. Assuming that the particle velocity is equivalent to the flow velocity, this trend indicates that at higher concentration, thermal inhibition due to the presence of more particles also comes into effect along with the chemical inhibition. In general, this is also indicative that chemical inhibitors are far more effective than thermal inhibitors due to the dual inhibition mechanism.

3.4.2 Addition of sand

Figure 3.9 shows the variation of S_L at different concentrations of sand. A higher rate of decrease of S_L is observed at lower concentrations of sand, whereas the addition of sand at concentrations above 50-75 g/m^3 does not significantly reduce the burning velocity. This could be due to the less inter-particle spaces at higher concentrations of sand preventing the heat conduction to the sand particles thereby reducing its heat sink effect. For a lean methane-air (ϕ_g = 0.8) mixture, the flame extinction is observed at a concentration of 350 g/m^3 and for rich mixture of ϕ_g = 1.2, close to flame extinction scenarios are observed at 585 g/m^3. When compared to the flame extinction concentrations of $NaHCO_3$ for ϕ_g = 0.8 & 1.2 (at 75 g/m^3 and 125 g/m^3 respectively), the flame extinction concentrations of sand are approximately 4.67 times higher than the $NaHCO_3$ concentrations. This clearly indicates the heterogeneous effect of dry chemical.

It is understood from Figure 3.12 that as the concentration of sand is increased in a fuel rich flame, the flame sheet elongates resulting in a smaller cone angle and thus reducing the burning velocity. The flame extinction observed at fuel lean and fuel rich conditions were that of blow-off, however an interesting observation is made at stoichiometric equivalence ratio, flame (partial) flashback was observed starting from 50 g/m^3 of sand until 585 g/m^3 when flame re-stabilized at the burner exit (Figure 3.11). The flame images captured just before the flashback indicated a laminar burning velocity of 0.241 m/s at 50 g/m^3 and 0.249 m/s, a slightly increasing trend at 75 g/m^3. When the flame re-stabilized at 585 g/m^3 the laminar burning velocity was estimated to be around 0.20 m/s. Flame flashback could have occurred due to the reduction of the local flow velocity lower than the laminar burning velocity near the burner wall as a result of the boundary layer velocity gradient effect. This observation of flame instability at ϕ_g = 1.0 cannot be generalized as there are various other factors like burner geometry which would influence flashback [63]. This is further discussed in the next section.

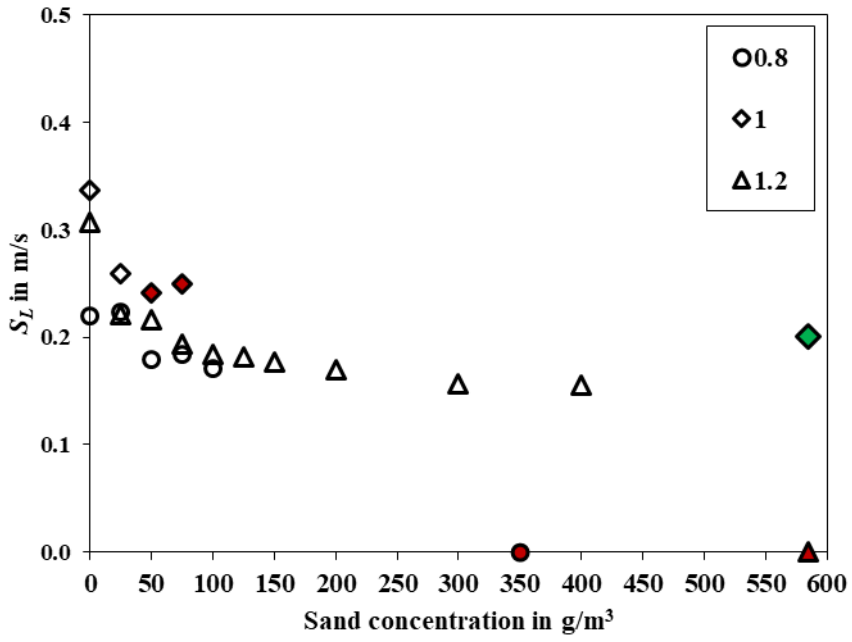

Figure 3.9: Laminar burning velocity of methane-air-sand premixed flames.

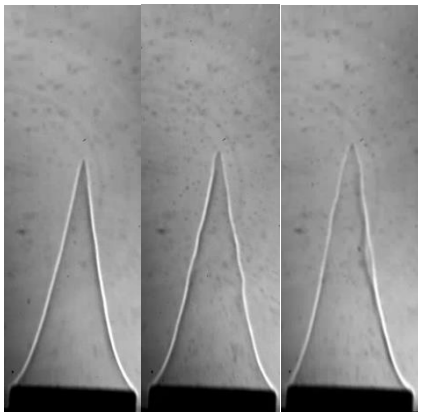

25 g/m^3 50 g/m^3 75 g/m^3

Figure 3.10: Effect of sand concentration on lean (ϕ_g = 0.8) methane-air flame.

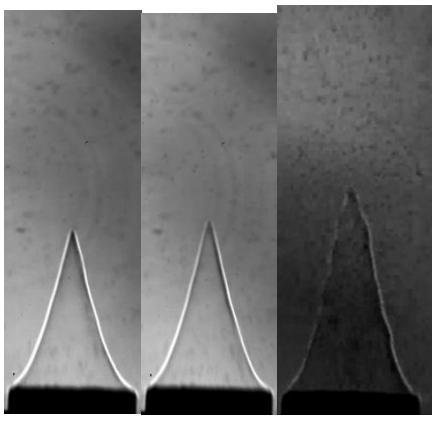

a. 25 g/m^3 50 g/m^3 585 g/m^3

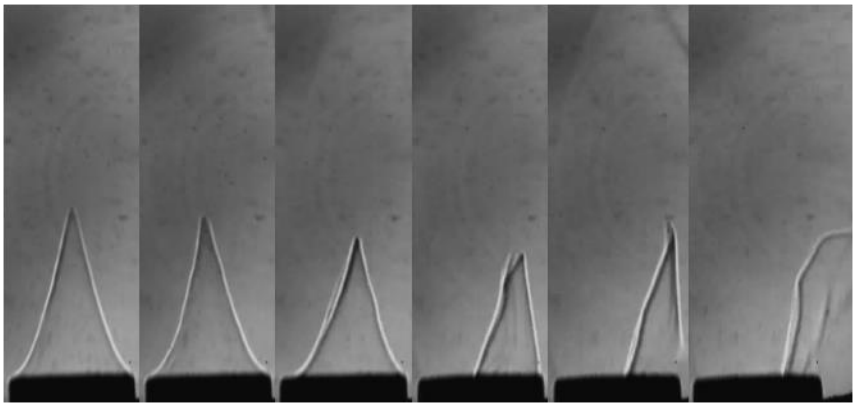

b. Flame flashback at 50 g/m^3.

Figure 3.11: Effect of sand concentration on stoichiometric (ϕ_g = 1.0) methane-air flame.

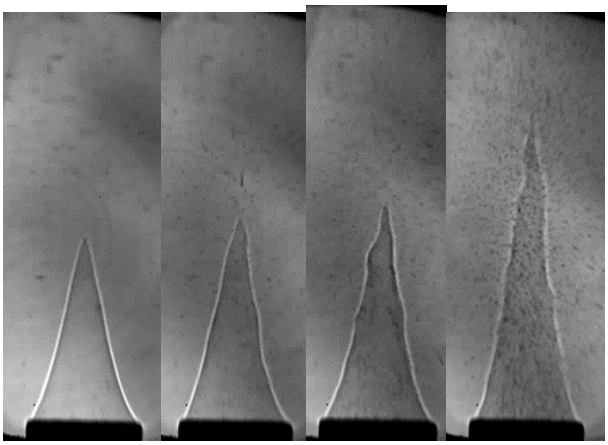

25 g/m^3 200 g/m^3 400 g/m^3 585 g/m^3

Figure 3.12: Effect of sand concentration on rich (ϕ_g = 1.2) methane-air flame.

3.4.2.1 Flashback Scenarios

The flame instabilities observed in most conditions with sand and sodium bicarbonate were that of blow-off. But, for stoichiometric mixture of methane-air and sand concentration between 50 g/m^3 and 585 g/m^3 partial flashback scenarios were observed. On further investigating these, a similarity to the "tilted flame" phenomena described by Lewis and von Elbe [64] [65]and von Elbe and Mentser [66], at flows just above the flashback limit. It is well known that a condition of equality of gas velocity and burning velocity is required for the stabilization of flame above a burner. Flashback limit is typically identified by reducing the gas flow velocity and when the burning velocity becomes larger than the gas velocity. Presumably flashback will not occur if the flame diameter is small enough or if the flow velocity is high enough. In the current study, the gas flow rate is kept constant at 10 lpm and the burner diameter is fixed at 14.5 mm. Hence the boundary gas velocity gradient near the wall defined as $g = \frac{4\,V}{\pi\,R^3}$, is supposed to be constant. But with the addition of dust and at different concentrations of dust, this may be altered.

As explained by Lewis and von Elbe [65], the combustion zone exerts a pressure on the unburned gas and this pressure is low at the base of the flame (near the burner rim) as the burning velocity is low there. Consequently there is a pressure drop in the unburned gas from center of the burner to the burner rim. The back pressure of the flame produces an asymmetric distortion of the velocity distribution near the burner outlet. This causes a localized decrease in the boundary velocity gradient and allowing the flame near the burner rim to locally enter the burner. The critical velocity gradient for flashback solely depends on the burning velocity near the burner wall and the mixture composition [64]. If some point near the burner rim is overheated (which may occur due to small irregularity), the burning velocity at this point will be greater than the local gas velocity at the boundary layer. This results in the partial entry of the flame inside the burner or the so called "tongue shaped" flashback region (Figure 3.13). If the temperature inside the tube and the unburned gas is large enough, then the flame continue to travel down the burner resulting in flashback. This kind of flashback happens with a delay time where the flame lingers at the rim. A similar flame behavior is observed in the current study with the addition of sand (between λ_p = 50 to 585 g/m^3) at stoichiometric methane-air mixture. The Figure 3.14 indicates the flame stability diagram for natural gas-air mixture against the critical boundary velocity gradient [65]. It also presents the boundary velocity gradient of present study (maroon dash line) and three equivalence ratios (blue stars) used in the current study. A comparison of this limit using natural gas-air stability diagram is reasonable as the current study uses methane-air mixture.

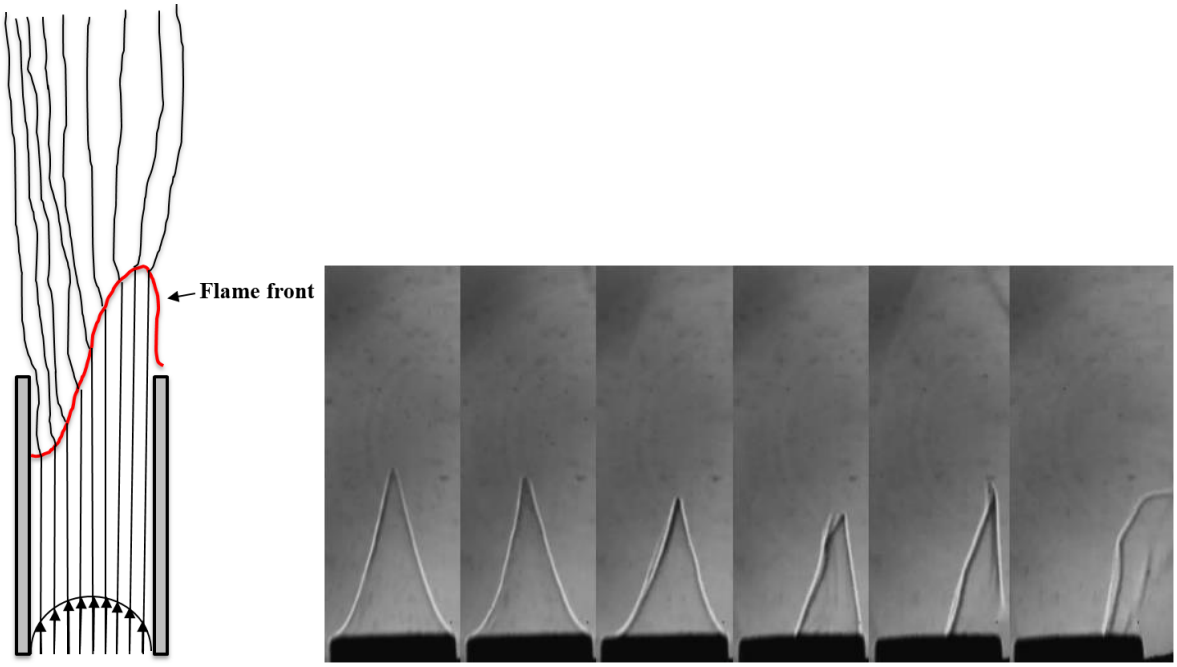

Figure 3.13: Formation of tilted flames, after Lewis and von Elbe [64].

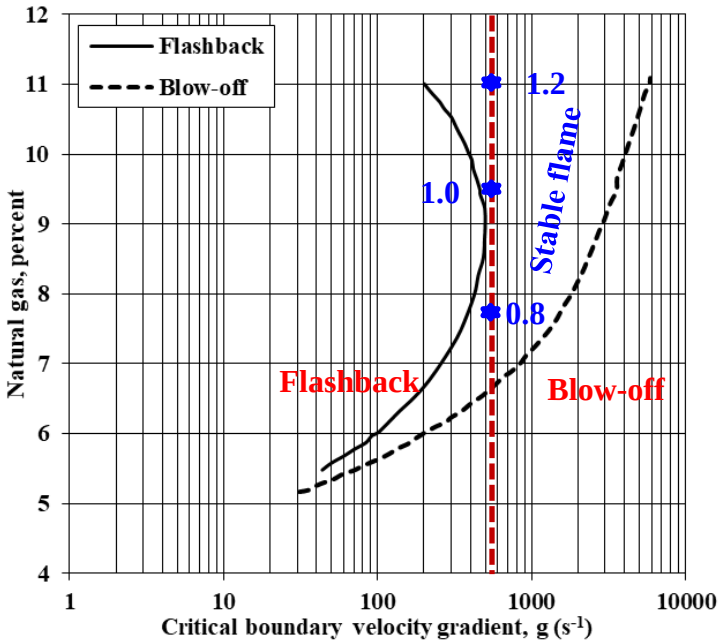

Figure 3.14: Flame stability diagram, reproduced from Lewis and von Elbe [65]**. Maroon dash line indicate the critical boundary velocity gradient of current study. Three blue stars represent the three equivalence ratio studied.**

von Elbe and Mentser [66], investigated this further and established that tilted flames are formed only below some critical flow which is a function of tube diameter. They derived a semi-theoretical condition to find the limit of tilted flame range as follows:

$$\frac{g}{\left(1-\frac{4\,S_L}{g\,R}\right)^{1/2}} = K \text{ (Constant)}$$

where, boundary velocity gradient, $g = \frac{4\,V}{\pi\,R^3}$, R is the radius of the burner, S_L is the laminar burning velocity, V is the total volumetric flow rate. It should be noted that the above condition has been developed for the gaseous premixed flames. Lewis and von Elbe [64] studied tilted flame phenomena extensively with natural gas-air and the conditions for which tilted flames was observed were reported in [66]. The burner diameter used in the current experimental study is compared to the values reported. With the burner radius of 0.00725 m, total volumetric flow rate of 10 lpm (0.000167 m^3/s) and laminar burning velocity estimated equal to 0.34 m/s for stoichiometric methane-air mixture, the estimated values of g is 558 s^{-1} and K is 695 s^{-1}. These estimated values are within the range of velocity gradient and correlation constant reported by von Elbe and Mentser [66] using natural gas-air premixed flame based on the data by Lewis and von Elbe [64]. This is presented in Table 3.1.

Table 3.1: Critical boundary velocity gradient and semi-theoretical constant values for tilted flames.

Study	Burner radius, R (m)	g (s^{-1})	K (s^{-1})
Lewis and von Elbe [64]	0.00775	652	780
Lewis and von Elbe [64]	0.00709	504	670
Present study with gaseous methane-air at ϕ_g = 1.0	0.00725	558	689
Present study with sand-methane-air at ϕ_g = 1.0, λ_p = 50 g/m^3	0.00725	558	732

It is interesting to note that even though the above values estimated for the gaseous flow are also in the range where tilted flames are expected, they were not observed with the gaseous flames as well as with sodium bicarbonate and with other equivalence ratios of sand added conditions. Firstly with sodium bicarbonate it could be due to enhanced heat sink effect as compared to sand. Secondly, the susceptibility of flame to flashback is known to be more with stoichiometric mixture conditions due to higher burning velocity. These conditions can also present the possibility of local high temperature spot in the reaction zone, which was known as the reason for flame to partially flashback as tilted flame.

3.5 Mathematical model to study heat sink effect of inert particles

Mathematical model to predict the laminar burning velocity of sand particle entrained methane-air premixed flame has been adopted from previous studies of Xie et al. [17] and Lee et al. [59] which is now extended to predict the critical dust concentration of inert particle required for flame extinction. Figure 3.15 illustrates the interaction of a sand particle with the flame region. Particles are assumed to travel along a streamline of a mixture flow field. When a sand particle passes through the flame zone, it absorbs heat from the flame and thus behaves as a heat sink whereby reducing the flame temperature. This effect has been considered in the following section to develop an expression for such a reduced flame temperature (Lee [47]).

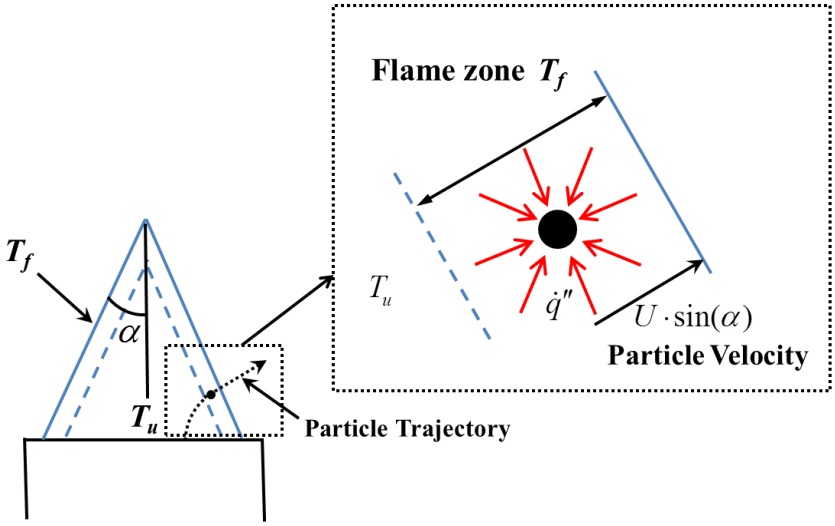

Figure 3.15: Illustration of an inert particle interacting with flame.

In order to estimate the heat absorbed by the inert particles, first, the heat released from a flame without any particles is calculated. The chemical reaction for the combustion is given by:

$$\frac{\emptyset}{2} CH_4 + (O_2 + 3.76\, N_2) \rightarrow \frac{\emptyset}{2} CO_2 + \emptyset\, H_2O + 3.76\, N_2 + 2(1 - \emptyset) O_2 \qquad (3.4)$$

The heat consumed to raise the temperature for $\frac{\emptyset}{2}$ moles of methane or 4.76 moles of air, is given by $\left[(T_b - T_u) \sum C_p . n_{product}\right]$. With the assumption that all the heat released is used to raise the temperature of the mixture, the heat release rate of the methane-air premixed flame for a given flow of air and the equivalence ratio is calculated as:

$$\dot{Q} = \left[(T_b - T_u) \sum C_p . n_{product}\right] \frac{\dot{n}_{air}}{4.76} \qquad (3.5)$$

Here $n_{product}$ is the number of moles of the products that depends on the equivalence ratio. Assuming that the flame with particles releases the same amount of heat while it is also influenced by the temperature rise of particles, a new flame temperature can be estimated using the energy conservation below:

$$\dot{Q} = \left[(T_b - T_u)\sum C_p . n_{product}\right]\frac{\dot{n}_{air}}{4.76} + \dot{n}_s C_s\left(T_f'' - T_u\right) \quad (3.6)$$

Rearranging Eq. (3.6), the new flame temperature, T_f'' is expressed in the form

$$T_f'' = \frac{\dot{Q}}{\frac{\dot{n}_{air}}{4.76}\sum C_p . n_{product} + \dot{n}_s C_s} + T_u, \quad (3.7)$$

where $\dot{n}_s$is the number of particles per unit volume per unit time passing through the flame, and it is calculated by:

$$\dot{n}_s = \left(\dot{V}_{air} + \dot{V}_{CH_4}\right) n_s \rho_s V_{particle} \quad (3.8)$$

The new flame temperature estimated after accounting for the heat sink effect is plotted in Figure 3.16, and it indicates a continous decrease in the flame temperature with the addition of sand for all the conditions tested. As expected, the stoichimetric gaseous mixture condition results in maximum flame temperature.

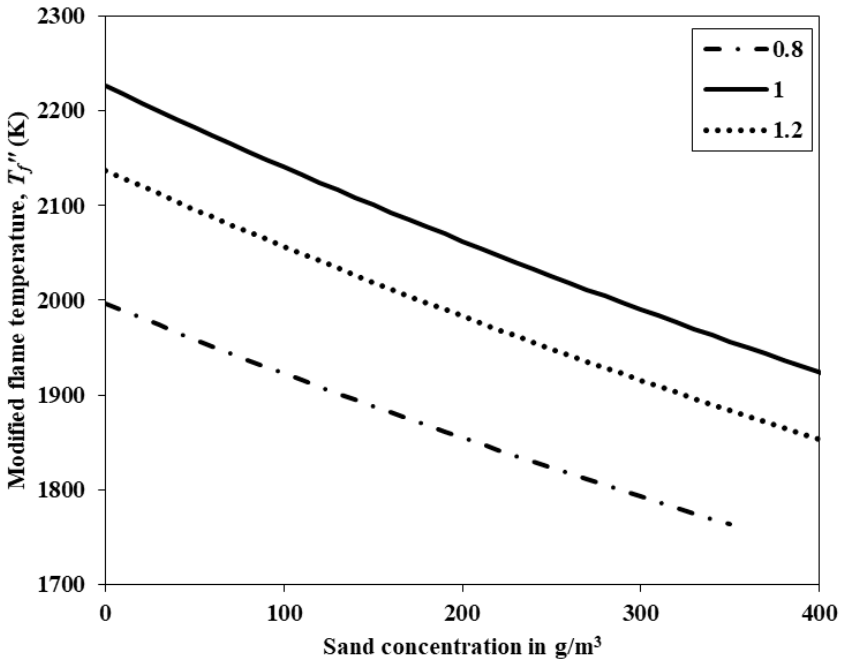

Figure 3.16: New flame temperature for different sand concentration at equivalence ratios ϕ_g = 0.8, 1.0, and 1.2.

The laminar burning velocity, S_L, is then calculated using the expression from Seshadri et al. [67]:

$$S_L = \left[\frac{2Bk_u\varepsilon^2}{\rho_g C_g} exp\left(-\frac{E}{RT_f''}\right)\right]^{1/2}, \quad (3.9)$$

where

$$\rho_g = \frac{\rho_{air}\dot{V}_{air}+\rho_{CH_4}\dot{V}_{CH_4}}{\dot{V}_{air}+\dot{V}_{CH_4}}, \varepsilon = \frac{1}{Z_e}, Z_e = \frac{E\left(T_f''-T_u\right)}{RT_f''^2} \quad (3.10)$$

B = 3.39 x 10^7 /mole.s to 3.84 x 10^7 /mole.s and E = 110.5 kJ/mole in Eq. (3.9) are chosen to match the calculated laminar burning velocity of gaseous conditions with that in experiments performed without dusts.

3.5.1 Comparison of model results with experiments

Experimentally obtained laminar burning velocities of sand-methane-air flame from the studies of Lee [47] are shown in Figure 3.17. It can be observed that irrespective of the equivalence ratio or the sand particles concentration, the laminar burning velocity increases with the reactant temperature. Indeed, an increase in the reactant temperature is accompanied by an increase in the adiabatic flame temperature, flow velocity and flame cone angle. Further, an increase in the reactant temperature reduces the density of the gas, which results in a higher flow velocity. However, since sand particle is inert, its addition in any amount only results in the decrease of the flame temperature. Therefore, a decreasing trend in laminar burning velocity is observed with increasing the sand-dust concentration.

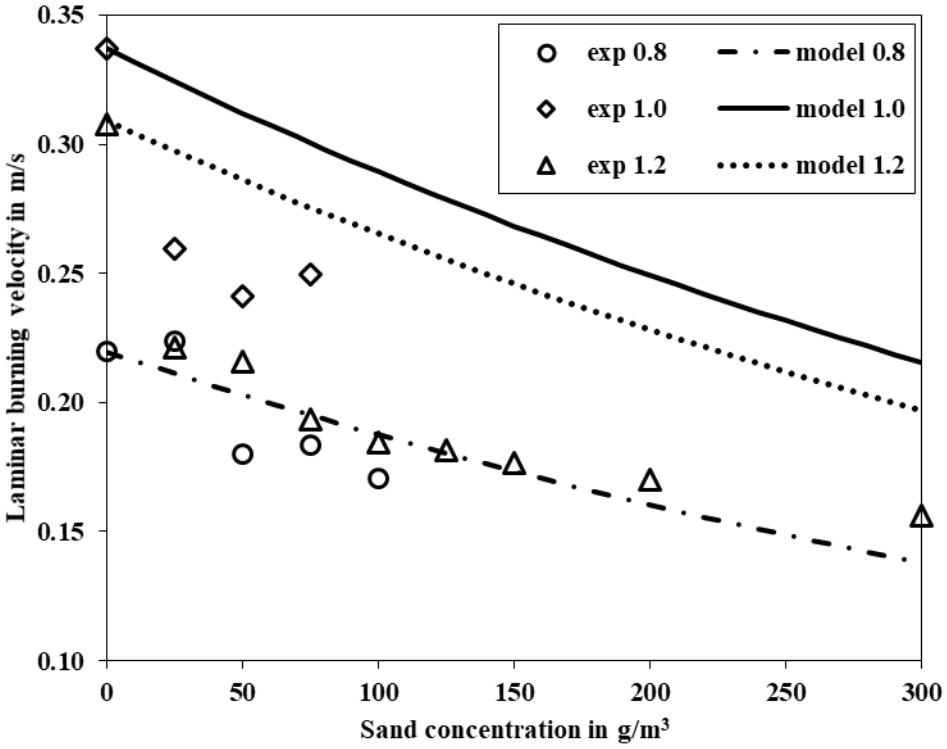

Figure 3.17: Experimental results and mathematical model of laminar burning velocity at different sand concentration for equivalence ratios.

The comparison between the experimental and mathematical model results (Figure 3.17) show a reasonable agreement only for fuel lean mixture conditions, with the model results over predicting the experimental values in other mixture ratio conditions. However, the present model predict the qualitative trend of the variation of burning velocity. As the concentration of sand particle increases, a critical value of S_L is reached whereby flame propagation is no longer possible. This value for the particle size of 75-90 μm (used in present study) can be obtained by extrapolating the mathematical model result to higher concentrations. The upper flammability limit of methane is about 15% in volume [61]. Corresponding laminar burning velocity observed from experiment is 0.13 m/s. This burning velocity is used as the limiting value in the mathematical model, and the critical sand concentrations for flame extinctions are predicted for all the conditions. Table 3.2

reports these sand concentrations for different cases considered at which the burning velocity reaches the limiting value of 0.13 m/s. The model results indicate that predicted critical concentration of sand for flame extinction is 340 g/m^3, 660 g/m^3 and 590 g/m^3 for ϕ_g = 0.8, 1.0 and 1.2 respectively. On comparing with critical sand concentration for flame extinction from current experiments, this is observed at concentration of 350 g/m^3 for ϕ_g = 0.8, and at concentration of 585 g/m^3 for ϕ_g = 1.2. As seen before, at ϕ_g = 1.0, after the partial flashback conditions, the flame re-stabilized at 585 g/m^3. This was the maximum concentration that was tested due the limitation posed by the dust feeder used in the study.

Table 3.2: Predicted critical sand concentration of sand required for flame extinction.

ϕ_g	**Predicted critical concentration of sand in g/m^3**	**Experimentally obtained critical concentration of sand in g/m^3**
0.8	340	350
1.0	660	x (experimental limitation allowed only up to 585 g/m^3)
1.2	590	585

The prior study [60], further indicates the effect of the increase in T_u, leads to an increase in the critical concentration of sand dust necessary for the flame extinction. This effect is due to two main reasons. Firstly, an increase in reactant temperature causes the flame temperature to increase thereby causing the threshold of the heat-sink effect necessary to quench the flame to increase. Secondly, for the same concentration of sand particles, at a higher reactant temperature, the residence time of the particle in the flame zone will be lower due to the higher propagation velocity. This results in a lower heat loss from the flame zone to the particles at these conditions. Hence to

produce the adequate heat sink effect to reduce the burning velocity to the critical value, at higher reactant temperatures, larger concentration of sand particles are required.

3.6 Conclusions

This chapter presents the influence of sand and sodium bicarbonate particles (75-90 µm) on the laminar burning velocity of methane-air premixed flames. The concentration of these particles required for flame extinction is also reported based on the experimental results and as predicted by the mathematical model. The experiments were conducted on a simple Bunsen burner set-up at lean, stoichiometric and rich methane-air equivalence ratios. The results indicated that $NaHCO_3$ inhibits heterogeneously and thus provides flame extinction at a lower concentration as compared to sand. The concentration of sand resulting in flame extinction of lean and rich mixture was approximately 4.67 times higher as compared to that of sodium bicarbonate. The results also indicate a flashback instability at a certain concentration range (50 to 585 g/m^3) of sand particles. A mathematical model, developed based on the heat sink effect, has been employed to predict the burning velocity values with the addition of sand. A good qualitative agreement between the predicted quantities and the experimental results were observed for fuel lean mixtures. Validation of predicted critical concentration of the sand required for flame extinction indicates that the predicted model values are comparable to the values observed from experiments.

4 Turbulent burning velocity of premixed methane-air-dust flames

4.1 Chapter abstract

This chapter covers the turbulent burning velocity (S_T) of methane-air-dust premixed flames with different dust types (coal, sand and sodium bicarbonate) and dust concentrations (λ_p = 0-75 g/m^3) added at three methane-air pre-mixture equivalence ratios (ϕ_g = 0.8, 1.0 and 1.2) and different turbulent intensities (u'_{rms} = 0.65, 0.72 and 0.88 m/s). Experiments have been conducted at constant pressure conditions to study stabilized premixed flames. The results indicate that based on the particle type, the variation of turbulent burning velocity with an increase in the particle concentration differs. In general, coal and sodium bicarbonate results in the heterogeneous effect of absorbing heat and releasing volatiles; whereas sand particles just absorbs heat from the flame zone. The detailed time scale analysis conducted shows that the presence of particles in the concentration range considered tend to slightly enhance the cold flow turbulence whereas with the presence of flame zone, an increase in the turbulent intensity results in increasing the vaporization rate of the particles. This effects in decreasing the turbulent burning velocity of methane-air mixtures with coal and sodium bicarbonate particles at higher concentrations and turbulent intensities. Out of three dusts examined, sodium bicarbonate addition results in the lowest S_T due to the release of CO_2 and H_2O. Between coal and sand, at fuel lean and stoichiometric conditions, S_T values with coal is greater than sand due to the equivalence ratio promotion with the release of

CH_4. But, as the turbulent intensity increases, for ϕ_g = 1.0 to 1.2, S_T values with sand becomes comparable to or even greater than that of coal. Model coefficients are generated from the experimental data to estimate the turbulent burning velocity in these conditions and the results show a clear distinction in the model coefficients for gaseous versus gas-dust mixtures. Further the collective effect of dust concentration, equivalence ratio and dust type resulting in having two sets of model coefficients to predict the turbulent burning velocity of gas-dust mixtures are also explained.

4.2 Introduction and related literature

Combustible gas mixtures and dust clouds, present severe threat to process industries and facilities [68]. The explosions resulting from these mixtures are mostly hybrid and turbulent in nature, especially when combustible dust particles are entrained into the gaseous flame propagations. Coal mine explosions [69] are one such case where combustible coal dust particles are entrained to methane-air flame propagation resulting in a hybrid mixture combustion. With the development of varied process industries and operations, different types of dusts (e.g., wood, plastic, metal, chemicals etc.) may entrain into the flame propagation [69]. These dusts will have different effects on the flame propagation, based on their thermo-chemical characteristics and concentration.

Burning velocity is one of the most important and fundamental characteristics of a premixed combustible mixture. Most of the dust cloud flame propagation experiments are performed in standard spherical vessels [16], [70], where the problem of an increase in turbulent intensity caused by the expanding combustion products in a constant volume vessel has been identified. Benedetto

et al. [12] showed that the turbulence generated by the expanding products of combustion needs to be quantified in order to determine the correct turbulent burning velocity. Rockwell and Rangwala [19] investigated the influence of coal particles of different sizes (75-90 µm and 106-125 µm) on turbulent methane-air flames in a Bunsen burner type experimental platform. The same experimental set-up has been used in the current study. Their results indicated that the smaller particle sizes and larger concentrations (> 50 g/m^3) increase turbulent burning velocity compared with larger particle sizes and lower concentration ranges [19].

Sand and sodium bicarbonate particles were studied extensively as flame extinction agents [26], [49]. The difference in their mechanism of inhibition and the critical concentrations for flame inhibition are studied mainly with diffusion flames. Most of the available studies [53], [56] on the interaction of inert and dry chemicals in burner stabilized premixed flame conditions are laminar. Chellaiah et al. [58] presented a comparison between the extinction effectiveness of silica and $NaHCO_3$ (10-40 µm) in a Bunsen type, stoichiometric premixed laminar methane-air flames and they observed almost negligible effect of inert particles on laminar burning velocity. A mathematical model to predict the laminar flame extinction concentration of inert particles was explained in Chapter 3 along with experimental results on the decrease of laminar burning velocity with increase in the sand concentrations of 75-90 µm particle size. Behavior of inert and sodium bicarbonate particles in turbulent premixed flame conditions are less understood, especially in burner stabilized flames. The variation of turbulent burning velocity as a function of concentration and turbulent intensity is also important for understanding their effect on flame propagation. Further, the studies [71]–[81] on the turbulence modulation due to the interaction of particles and gas in cold flow indicate both attenuation and augmentation of the turbulent intensity with the addition of particles. Factors such as particle size, particle density, particle loading, and Stokes

number, affect the modulation of turbulence. The effect of particle size [74] on turbulent intensity show that smaller particle size as compared to the turbulent length scale attenuate turbulence whereas the large particle size tend to enhance turbulence.

This chapter aims to analyze the turbulent burning velocity of methane-air-dust premixed flames. Coal, sand and sodium bicarbonate particles of 75-90 μm mean diameter size at different concentrations (0-75 g/m^3) are studied in a Bunsen burner stabilized premixed hybrid flames. A characteristic time scale analysis is done to understand the coupling of turbulence, particle interaction, particle vaporization and combustion. An analysis to develop empirical correlation coefficients from experimental results to estimate the turbulent burning velocity as a function of turbulent intensity and laminar burning velocity is also done in this chapter.

4.3 Experimental set-up and procedure

As explained in chapter 2, a Bunsen burner type experimental set-up, designed by Rockwell (2012) [13] to measure the burning velocity of gaseous, and dust entrained gaseous flames has been used in this study. A schematic of this set-up is shown in Figure 2.2. The parameters that can be independently controlled include turbulent intensity (u'_{rms}), length scale (l_0), particle size (d_p), and particle concentration (λ_p). Methane-air equivalence ratios of ϕ_g = 0.8, 1.0, and 1.2 are considered to replicate fuel lean, stoichiometric, and fuel rich premixed flame conditions. A particle screw feeder injects the dust into the methane-air flow creating a hybrid mixture. The turbulent burning velocity is calculated by extracting frames from the high-speed video.

Similar to Rockwell et al. [19] and Grover et al. [82] the turbulent burning velocity is determined by averaging the measure flame height of 25 images as shown in Figure 4.3. The comparison of

calculated burning velocity versus the number of images used (Figure 4.1) shows that an asymptotic burning velocity estimation is reached as the number of images become greater than 10-15 images.

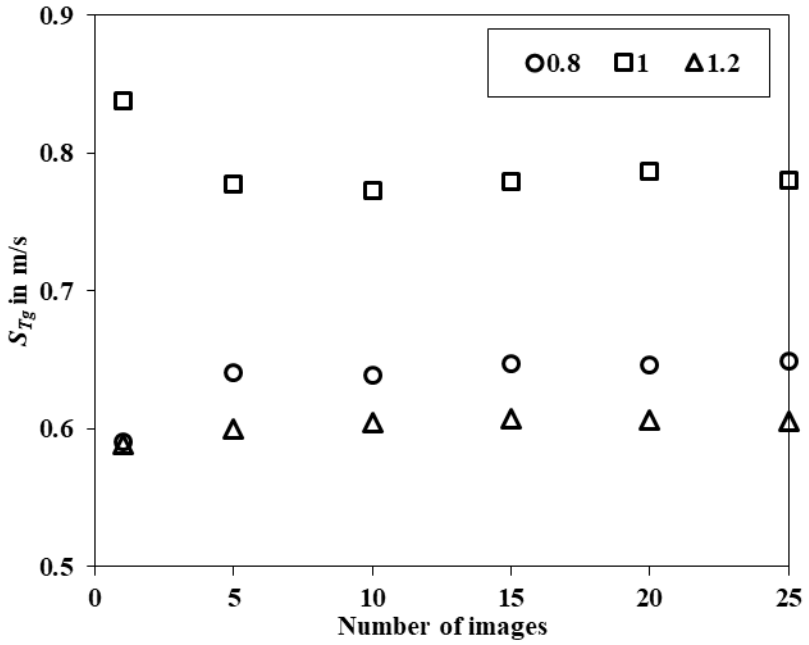

Figure 4.1: Effect of number of images versus estimated turbulent burning velocity for gaseous premixed flame at 30 lpm, u'_{rms} = 0.65 m/s.

For all the 25 images processed, the flame edges are carefully handpicked manually using a MATLAB program. Since the uncertainty associated with the edge selection by hand is not quantified, the quantified error bars are calculated as the standard deviation of the burning velocity from 25 images. The 25 flame images used for this case of coal at 25 g/m^3 at u'_{rms} = 0.65 m/s along with the edges tracked are shown below (Figure 4.2):

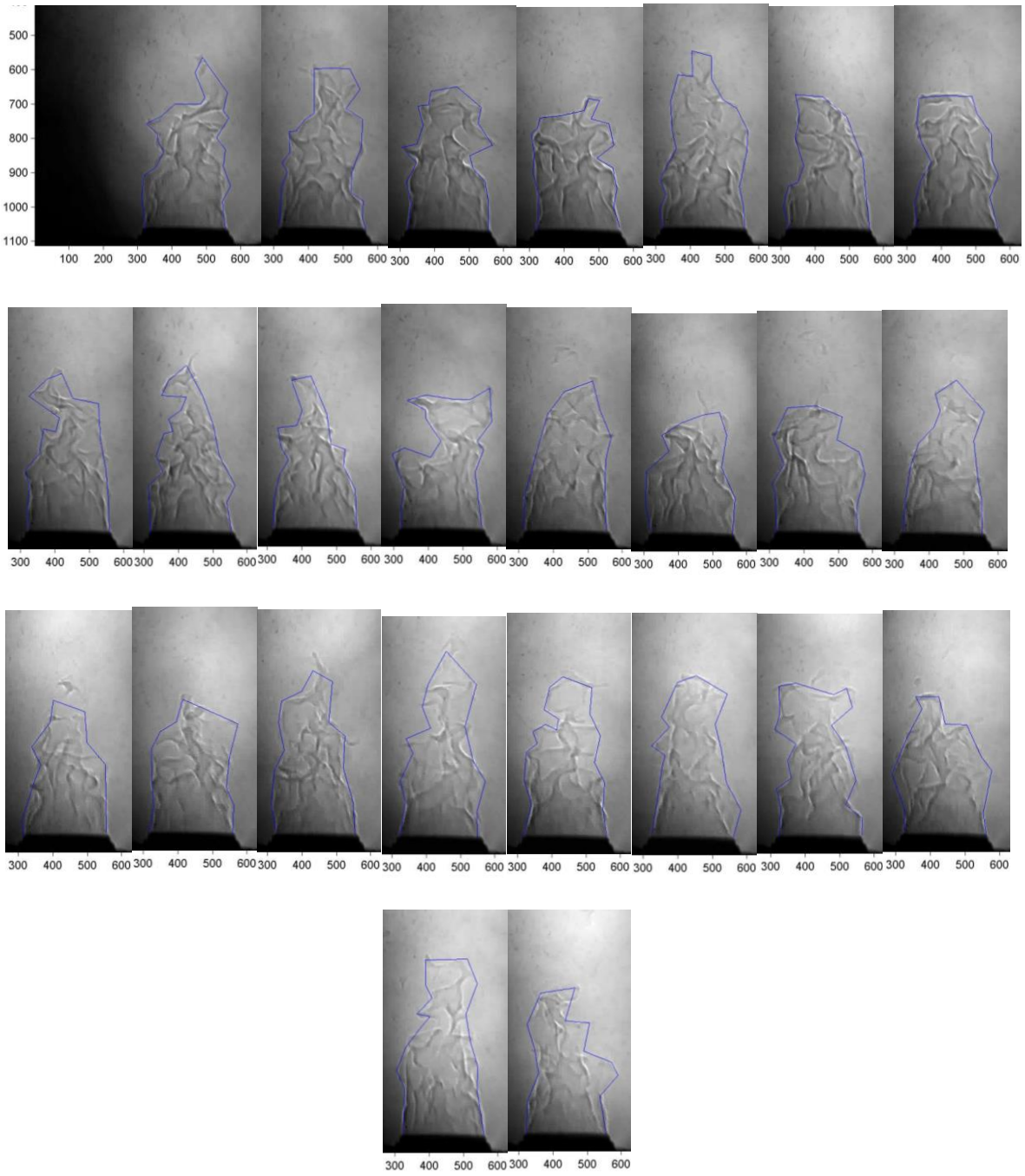

Figure 4.2: Sample manually selected flame edges of 25 flame images for 30 lpm, coal at 25 g/m^3.

The mean flame height is used to estimate the half cone angle, α.

$$S_T = \bar{u} \sin \alpha \qquad (4.1)$$

where, $\bar{u}$ is the mean flow velocity and α is the half cone angle. Figure 4.3 shows the sample shadowgraph image and the averaged flame image used for estimating the half cone angle.

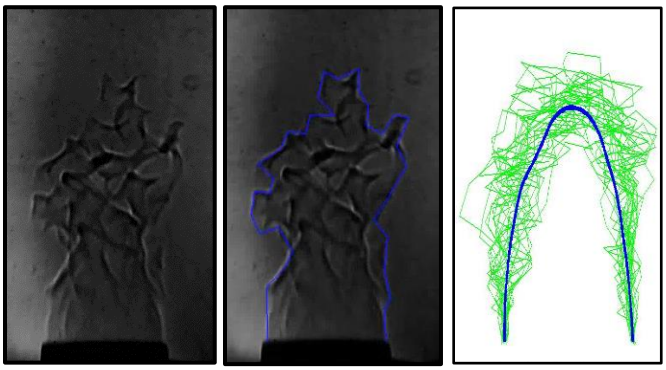

Figure 4.3: Shadowgraph flame image and Averaged flame image.

This approach to estimate the turbulent burning velocity by averaging the measured flame height was validated against the data from the research of Kobayashi et al. [40] in the previous study by Rockwell and Rangwala [19]. This is reproduced in the Figure 4.4 below. A good agreement is observed between the two sets of data. Kobayashi et al. [40] also used a perforated plate generated turbulence in their study. Also, it should be noted that Kobayashi et al. [40] used the angle method to extract the turbulent burning velocity from Schlieren images of turbulent flames. Similar approach has been adopted in the current study after confirming the validity of this methodology.

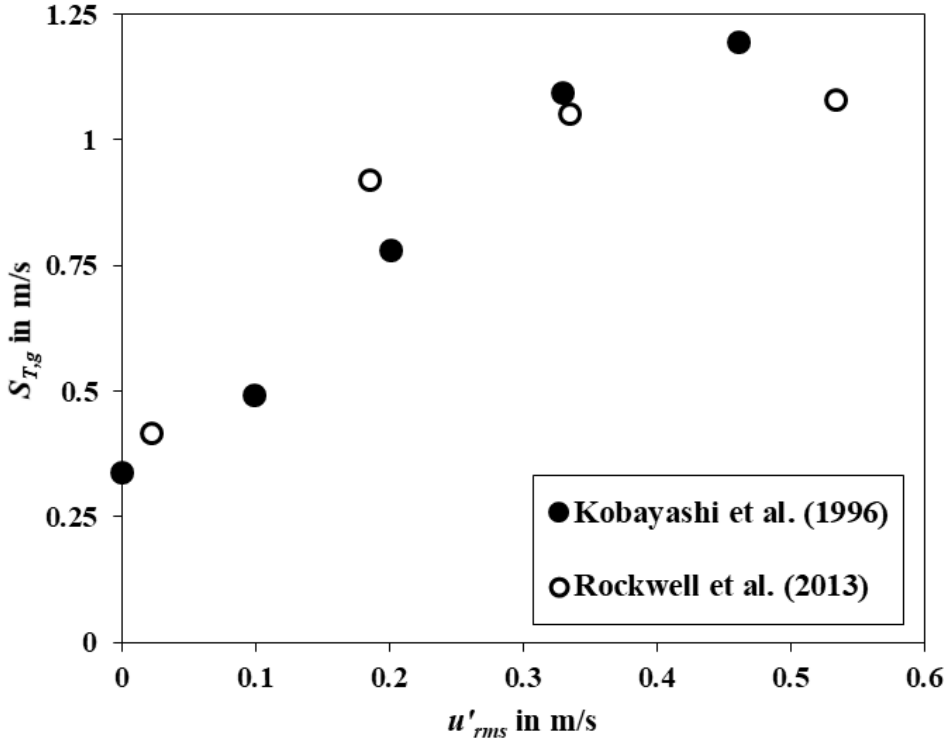

Figure 4.4: Validation of Turbulent Burning Velocity measurements. Reproduced from Rockwell and Rangwala [19]**.**

4.4 Experimental results and discussion

4.4.1 Turbulent combustion regime

Turbulent flow, characterized as $u = \bar{u} + u'$, where u is the flow velocity, $\bar{u}$ is the average flow velocity, u' is the fluctuating component of the flow velocity. The turbulent intensity, estimated as the root mean square (rms) of fluctuating component of flow velocity.

$$u'_{rms} = \sqrt{\frac{u\prime_1^2 + u\prime_2^2 + u\prime_3^2 \ldots\ldots + u\prime_n^2}{n}} \qquad (4.2)$$

The integral length scale (l_0) of turbulence is calculated as presented in Brunn [45].

$$l_0 = \bar{u} \int_0^{\infty} \rho_u(\tau)\, d\tau \qquad (4.3)$$

Where, $\bar{u}$ is the average flow velocity and $\rho_u(\tau)$ is the autocorrelation of the velocity fluctuation. The calculated value of l_0 (2.7 mm - 2.9 mm) is comparable to the perforated plate hole diameter of 3 mm. The total methane-air flow rates of 30, 35, and 40 liters per minute create a range of turbulent intensities of 0.65 to 0.88 m/s (Table 4.1).

Table 4.1: Turbulent intensity and integral length scale

Flow regime	Flow rate (lpm)	Avg. flow velocity $\bar{u}$ (m/s)	u'_{rms} (m/s)	% u'_{rms}	l_0 (mm)
Laminar	10	1.01	-	-	-
Turbulent	30	3.03	0.646	21.3	2.9
	35	3.53	0.718	20.3	2.8
	40	4.04	0.882*	21.8	2.7

* *For sodium bicarbonate experiments, the turbulent intensity measured at 40 lpm was u'_{rms} = 0.82 m/s. This is due to the use of a different perforated plate for these test conditions.*

The turbulent combustion regime, in which the current experiments exist, is investigated with a plot of u'_{rms}/S_L vs. l_0/δ_L, commonly referred to as the Borghi diagram [83]–[85], [46]. This is presented in Figure 4.5. The line $Re_T = 1$ separates the turbulent flame regimes ($Re_T > 1$) from laminar flames ($Re_T < 1$, lower-left region in the diagram). In this present study, while investigating the turbulent combustion regime, the turbulent Reynolds number ($Re_T = \frac{u'_{rms} l_0}{\nu}$) is approximately, 10 in the hot region and 100 in the cold region. This is because of an increase in viscosity by an order of magnitude in hot region.

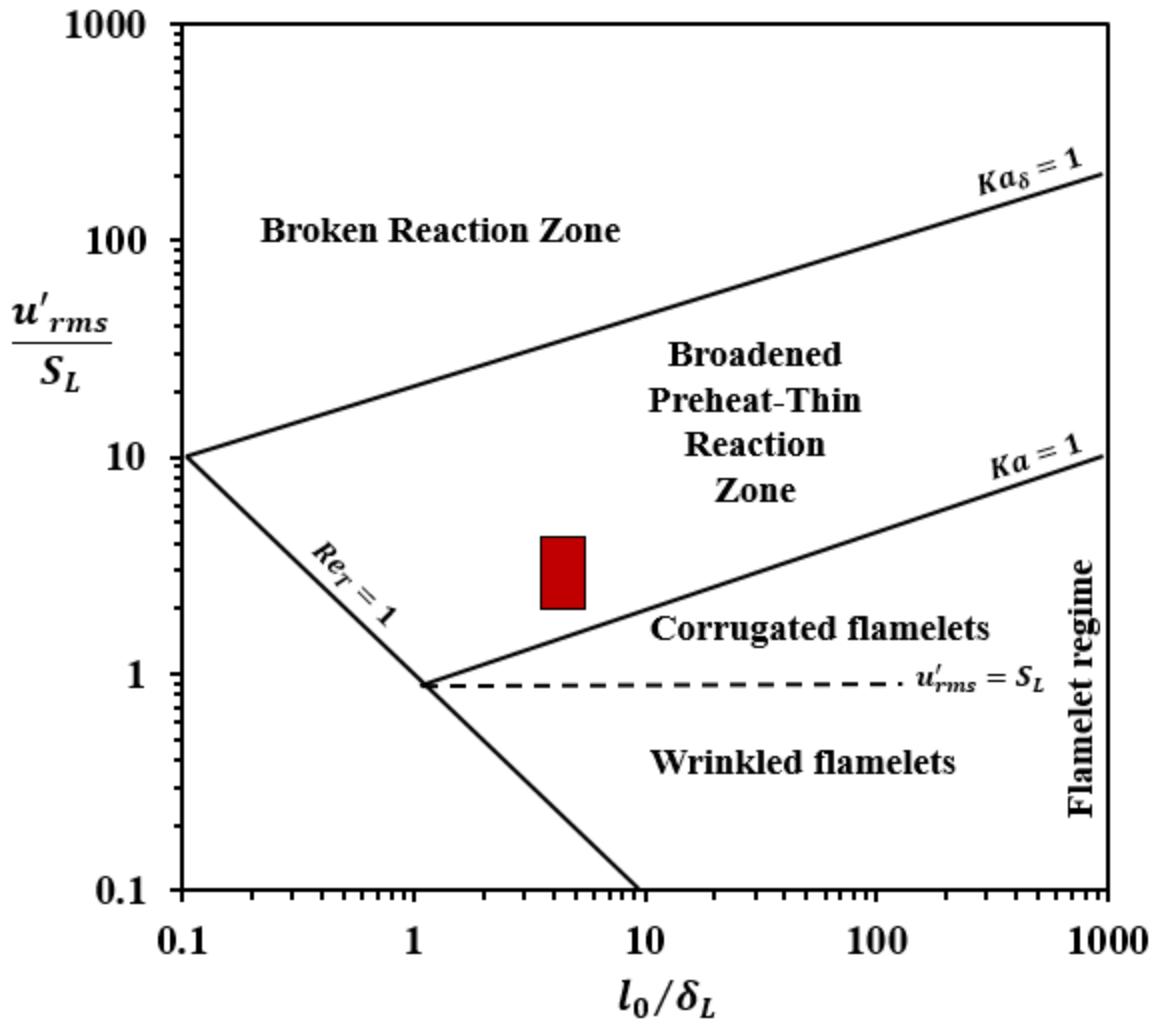

Figure 4.5: Borghi diagram [83]–[85] [46]**, shaded area represents turbulent combustion regime for the current experiments.**

When the turbulent intensity u'_{rms} is less than the laminar burning velocity (S_L), the laminar flame front propagation dominates over the turnover velocity of even the large eddies, hence turbulence does not affect flame front to corrugate, but will rather try to push and wrinkle the flame front. This region ($u'_{rms} < S_L$, lower-right region in the diagram) is called the wrinkled flamelet regime. As the turbulent intensity starts dominating the laminar burning velocity ($u'_{rms} > S_L$), there is a kinematic interaction between turbulent eddies and laminar flame front resulting in the

corrugation of flame front. This region (u'_{rms}> S_L) is called corrugated flamelet regime. In this region *Ka* < 1, flame thickness is less than the Kolmogorov length scale, the flame structure is embedded in smallest of eddies (Kolmogorov scale) and no perturbations in flame structure is observed. The boundary where *Ka* = 1 is called Klimov-Williams (K-W) limit, is equivalent to the condition where the flame thickness is equal to the Kolmogorov length scale. When this boundary is crossed, the smallest eddies can interact with the flame structure but only in the preheat zone of the flame zone. As a result the preheat layer is predicted to broaden but the reaction layer is predicted to remain at laminar flame thickness. In the broken reaction zone the Kolmogorov scale eddies can enter the reaction layer resulting in enhanced heat loss to the preheat zone resulting in local heat loss leading to local flame extinguishments. This occurs at high Karlovitz and Reynolds numbers. These flame regimes are presented in the Figure 4.6.

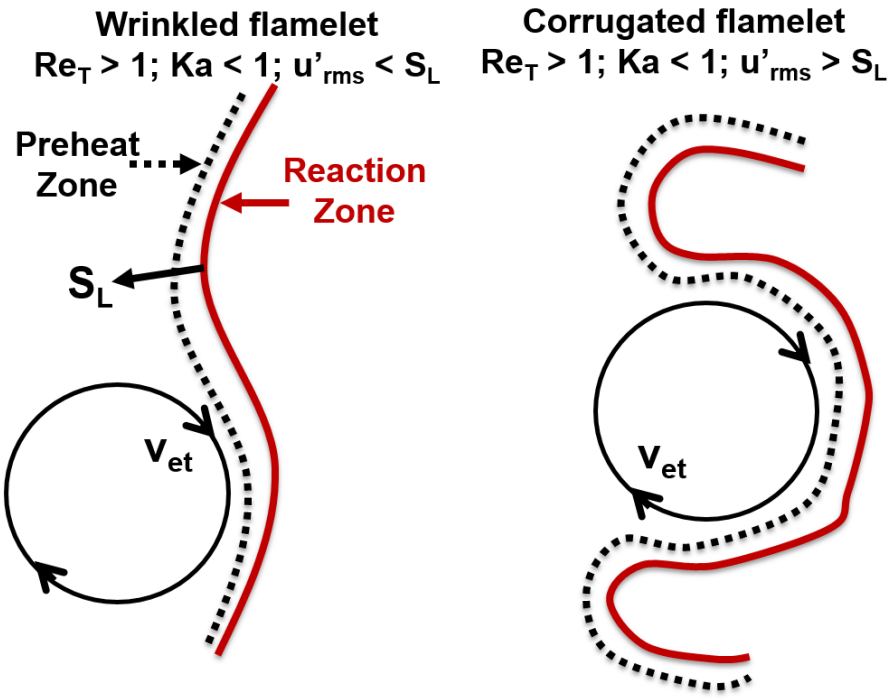

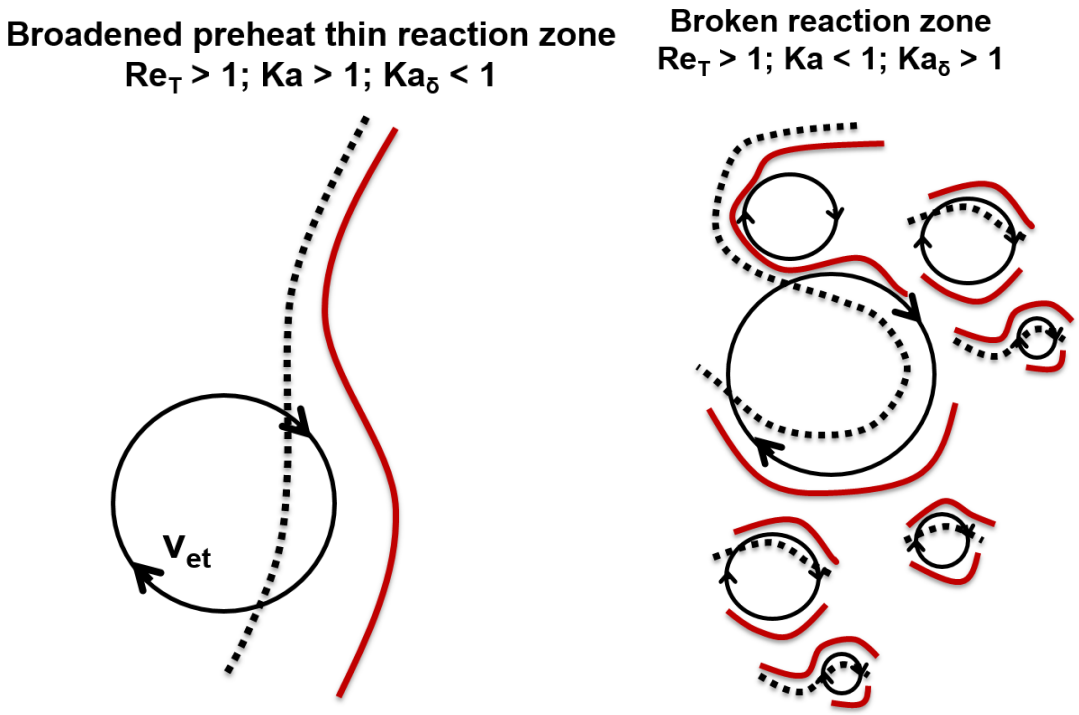

Figure 4.6: Flame regimes in Borghi diagram.

Figure 4.6 has been developed based on lecture series by Chakravarthy [86].

While estimating the regime in Borghi diagram in this study, the flame thickness is defined similar to Peters [46] as $\delta_L = \frac{D^*}{S_L}$, where D^* is thermal diffusivity estimated at an elevated reaction zone temperature. The reaction zone temperature differs with the gas phase equivalence ratio (ϕ_g = 0.8, 1.0 & 1.2) and the corresponding thermal diffusivity, D^* varies between 0.000186 m^2/s to 0.000216 m^2/s. Damköhler number (*Da*) defined as $\frac{S_L\, l_0}{u'_{rms}\, \delta_L}$ represents the ratio of flow time scale to the chemical time scale. A large Damköhler number indicates that the reaction rate is fast, and thus, a shorter chemical time scale.

Table 4.2: Damköhler number, Karlovitz number and Turbulent Reynolds number for the cases studied.

	u'_{rms}	ϕ_g = 0.8	ϕ_g = 1.0	ϕ_g = 1.2
Da	0.65	1.2	2.3	2.1
	0.72	1.0	2.1	1.8
	0.88	0.8	1.6	1.5
Ka	0.65	2.7	1.3	1.5
	0.72	3.2	1.5	1.7
	0.88	4.5	2.0	2.4
Re_T	0.65	10.0	8.6	9.2
	0.72	11.0	9.5	10.1
	0.88	13.0	11.2	11.9

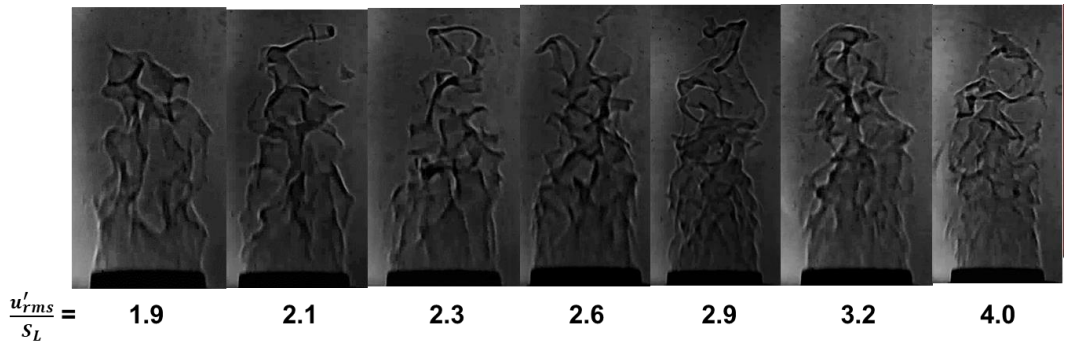

Figure 4.7: Flame structure in the broadened preheat-thin reaction zone regime.

Damköhler numbers (*Da*) and Karlovitz numbers (*Ka*) estimated for the test cases are greater than one (~ 1-5) (Table 4.2), thus indicating that the regime of the current experiments is within the rectangular gray shaded region (Figure 4.5) identified as Broadened Preheat-Thin Reaction zone [43], [44], [46]. Thus, the combustion regime studied in this experimental cases, the preheat layer is broadened and the reaction layer remains thin at the laminar thickness. The flame structure

in this regime as observed from the current experiments are shown in Figure 4.7. However, the above analysis has been conducted without considering the effect of particles. The effect of particles on the turbulence is very important and it is discussed in the next section.

4.4.2 Turbulence modulation

The studies investigating the interaction between particle-gas in cold flow and its effect on the gas-phase turbulent intensity shows that particle size, particle density, and particle loading influence turbulence modulation. Prior studies without considering combustion, using non-dimensional numbers indicate both attenuation and augmentation of the turbulent intensity with the addition of particles and this is still an active area of research.

4.4.2.1 Length scale analysis

Gore and Crowe [74] analyzed a wide range of experimental data and found a relationship between the characteristic length scales of two phases, particle diameter to the turbulent integral length scale (d_p/l_0) to explain turbulent modulation (Figure 4.8). When d_p/l_0 is greater than 0.1, the presence of particles increase the turbulent intensity, whereas if $d_p/l_0 < 0.1$ particles attenuate the turbulent intensity. In general, when the particle size is very small as compared to the turbulent length scale, they tend to follow the turbulent fluid motions. A more recent literature by Saber et al. [76] indicates that the cut-off value for this ratio to enhance turbulence is $d_p/l_0 > 0.25$. In the current experiments, for the d_p range of 75–90 µm, d_p/l_0 varies from 0.026 to 0.033 as indicated in Figure 4.8. This would imply that the particles do not enhance the turbulent intensity in the current range of experiments (Figure 4.8). But this analysis with the ratio of length scale does not provide an insight into the effect of particle loading (concentration). Further analysis using the volumetric loading (ϕ_v) of the particles at different concentrations were performed similar to Elgobashi [77].

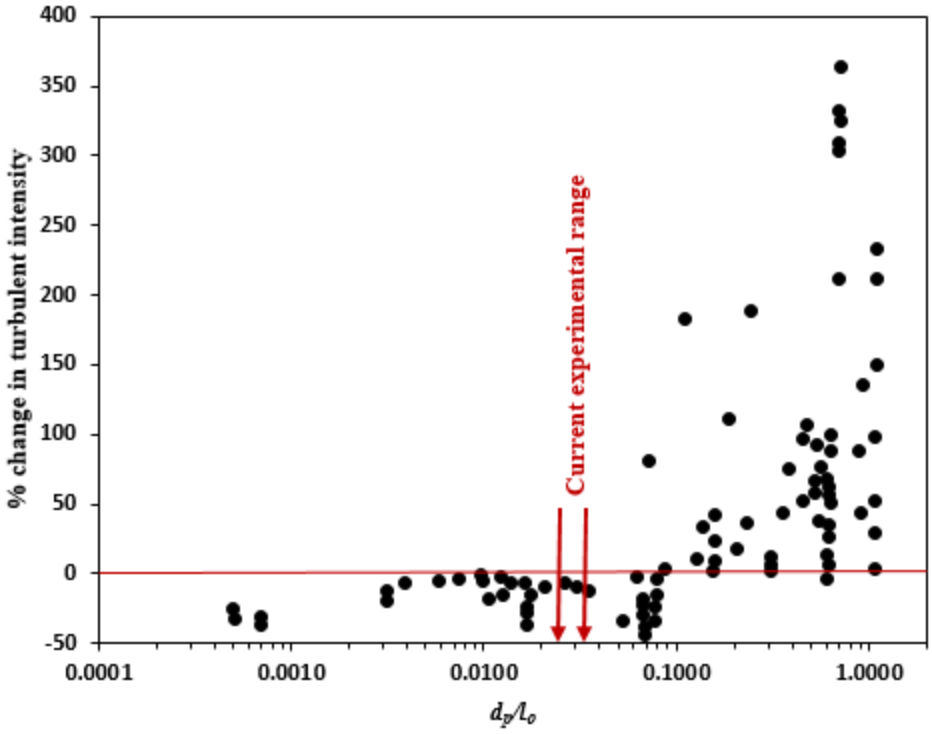

Figure 4.8: Length scale analysis to check the change in turbulent intensity.

Note: Figure 4.8 uses the data points as presented by Crowe and Gore [74]. They present experimental data from the following studies: Levy and Lockwood [87], Hetsroni and Sokolov [88], Tsuji et al. [73], Modarress et al. [89], Modarress et al. [90], Lee and Durst [72], Tsuji and Morikawa [73], Shuen et al. [91], Parthasarathy and Faeth [92], Zissalmar and Molerus [93], Sun and Faeth [94], Maeda et al. [71], Theofanous and Sullivan [95], Wang et al. [96].

4.4.2.2 Effect of particle concentration

The volumetric loading of particles, defined as volume fraction of particles in the total flow rate, is estimated as $\phi_v = \frac{V_{p,total}}{V_{p,total} + V_f}$; where, $V_{p,total}$ is the total volume occupied by particles and V_f is the volume of fluid. It should be specified that even though the same mass based concentration (mass loading) has been used in this study to compare the concentration effects of different dust

types, the heavier dusts (larger density) will have less number of particles for the same mass concentration (e.g., sand will have less number of particles as compared to coal at the same concentration of 25 g/m^3). This in turn will result in lesser volumetric loading which is dependent on the number of particles. This is evident from the ϕ_v presented in Table 4.3. The classification map (Figure 4.9) by Elgobashi [77], [78] suggests that the cold flow interaction between particle-gas for current experiments is in the regime of 2-way coupling, where the momentum exchange between the particles and carrier phase turbulence is large enough to alter the turbulence structure. Further based on the ratio of particle response time and Kolmogorov time scale, it is seen that the presence of particle in the concentration range studied enhance turbulence in the order as sand > sodium bicarbonate > coal.

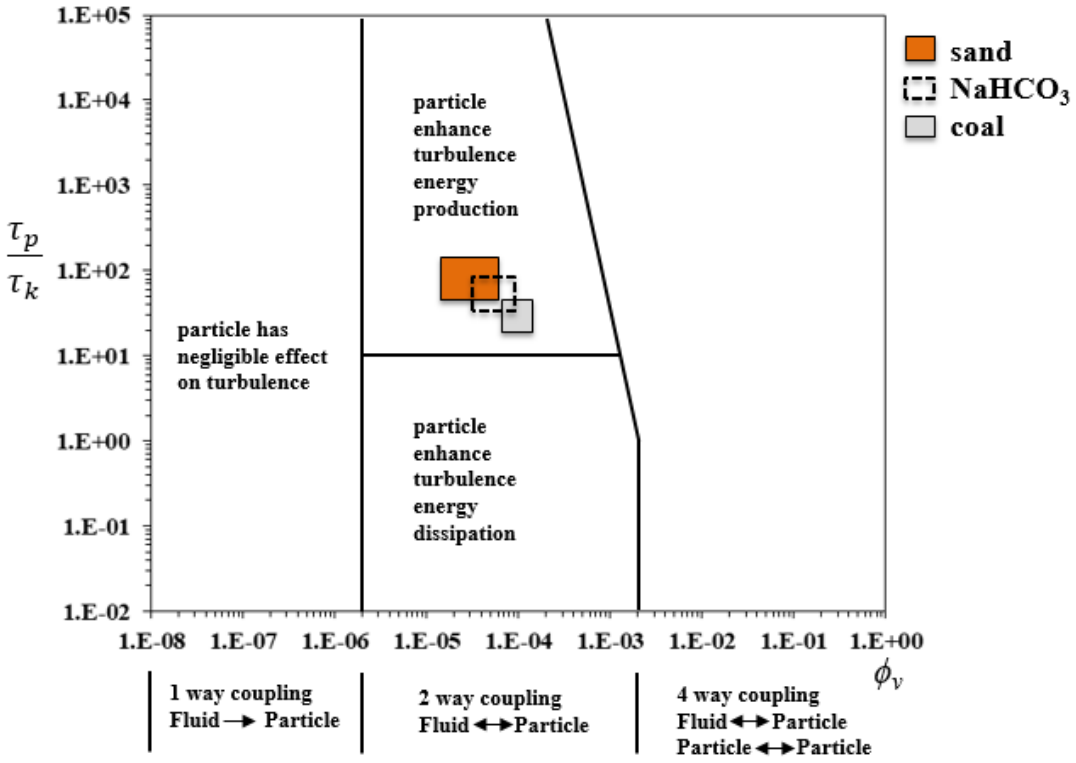

Figure 4.9: Classification map for particle-laden turbulent flows, adopted from [77] **indicating the current particle regime.**

4.4.2.3 Time scale analysis

At a constant volumetric loading, the turbulence attenuation is a strong function of Stokes number (*St*) and it can be used to describe the alteration of carrier phase turbulence [79]. Stokes number characterizes the responsiveness of the particles to the fluid-phase turbulent fluctuations. It is defined as the ratio of particle response time to fluid response time [80]. The fluid response time is an appropriate timescale of flow, in this case expressed as the eddy turnover time [81].

$$St = \frac{\tau_p}{\tau_e} \qquad (4.4)$$

where, τ_p is the particle response time and τ_e is the fluid response time expressed as eddy turnover time. $\tau_p = \frac{\rho_p \, d_p^2}{18 \, \mu_f}$ and $\tau_e = \frac{l_0}{u'_{rms}}$ where, ρ_p is the particle density, d_p is the particle diameter, μ_f is the dynamic viscosity of fluid, l_0 is the integral turbulent length scale, $u'_{rms}$is the turbulent intensity. Prior studies suggest a critical value of $St = \frac{\tau_p}{\tau_e} \sim 1$ to differentiate the enhancement (> 1) and attenuation (< 1) of turbulence.

The *St* for all the dusts considered in the current study, over the range of three different flow velocities used, are greater than one and of the order of *O* (~ 1) to *O* (~ 10) indicating a slight enhancement in turbulent intensity. The resulting relative motion between particles and fluid produces vortex shedding that tend to enhance the turbulent intensity. Table 4.3 presents all the above analyses for the current study.

Table 4.3: Ratio of characteristic length scales, volumetric loading, and Stokes number.

Particle type	ρ_p (kg/m^3)	d_p (µm)	u_f (m/s)	$\frac{d_p}{l_0}$	ϕ_v	*St*
Coal	492	75-90	3.03	0.026 – 0.031	5 x 10^{-5} – 1.5 x 10^{-4}	1.9 - 2.8
			3.53	0.027 - 0.032		2.2 - 3.2
			4.04	0.028 – 0.033		2.8 – 4.0

Sand	1490	75-90	3.03	0.026 – 0.031	1.7 x 10^{-5} – 5 x 10^{-5}	5.8 – 8.3
			3.53	0.027 - 0.032		6.7 - 9.6
			4.04	0.028 – 0.033		8.4 – 12.1
$NaHCO_3$	801	75-90	3.03	0.026 – 0.031	3.1 x 10^{-5} – 9.4 x 10^{-5}	3.1 – 4.5
			3.53	0.027 - 0.032		3.6 – 5.1
			4.04	0.028 – 0.033		4.5 – 6.5

All the above analysis is based on the particle-gas flow without considering any phase changes and chemical reaction. A prior study, which analyzed the effect of a flame zone at the exit of the burner on the turbulence modulation of upstream flow of reactants, is rare in the literature. With the analogy of spray combustion in droplet cloud, an attempt to study the vaporization of particle cloud and the effect of turbulence on the vaporization rate of particles is explained in the next section.

4.4.2.4 Turbulence and particle vaporization

In analogy to the spray combustion [97]–[103] Group combustion number (G), and vaporization Damköhler number (Da_v) analysis were carried out. For this purpose, vaporization time scale of a single particle, $\tau_v = \left(\frac{\rho_p}{\rho_g}\right)\left(\frac{r_p^2}{\alpha_g}\right)$; diffusion time scale, $\tau_c = \frac{r_c^2}{\alpha_g}$; characteristic time scale for the variation of mass and thermal energy after vaporization of particle defined as $\tau_g = \frac{3}{4\pi\alpha_g r_p n}$ and turbulent time scale $\tau_e = \frac{l_o}{u'_{rms}}$ as summarized previously by Urzay [98] were used, where thermal diffusivity (α_g) and density (ρ_g) were estimated for the gaseous reactants at elevated reaction zone temperature, T_g = 1200 K. The inner diameter of the Bunsen burner was used as the particle cloud diameter, r_p represent particle radius and n is the number of particles per unit volume. Only coal and sodium bicarbonate particles are considered for this analysis because

of their vaporizing nature. The Group combustion number defined as, $G = \frac{\tau_c}{\tau_g}$ is estimated to be in the O (~ 1) in the cases studied, ranging between 1.6 - 5.1 for coal and 0.9 - 3.2 for sodium bicarbonate. This indicates that the time needed for the diffusion of heat from the flame into the cloud is long enough to vaporize the particles, which further suggest that the combustion can take place either as internal group combustion or as external sheath combustion depending on the particle concentration [98]. For the dust concentration considered in this study it can be concluded that at lower dust concentration, an internal group combustion takes place with a combination of single particle combustion surrounded by a diffusion flame. Whereas, as the dust concentration increases the combustion regime shifts towards an external sheath combustion regime due to the lack of complete vaporization of interior particles. Figure 4.10 is recreated for particle combustion in analogy to the spray combustion regimes as per Urzay [98].

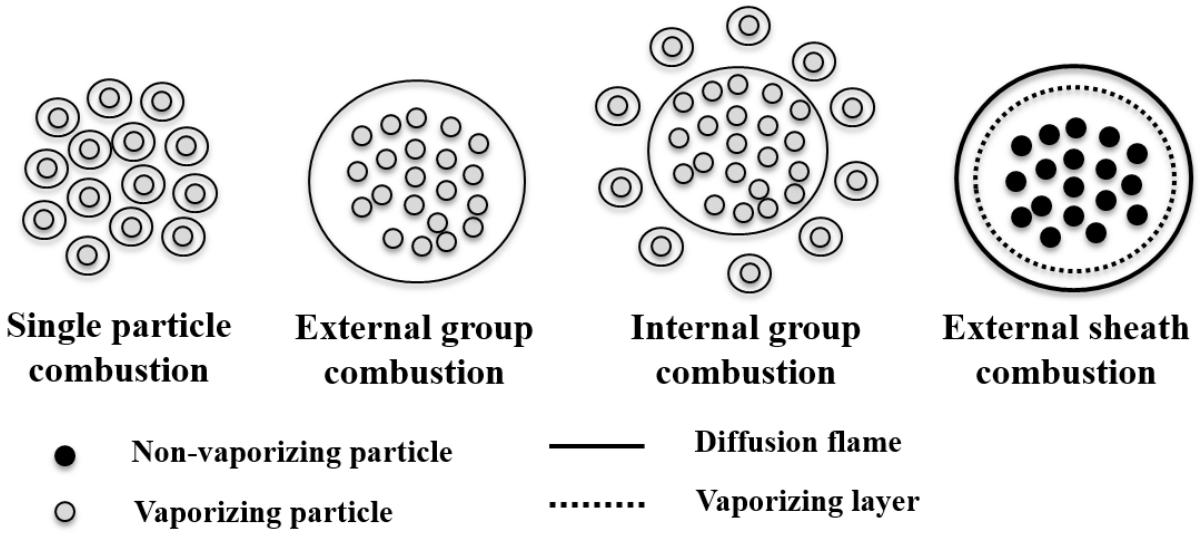

Figure 4.10: Vaporizing particle combustion regimes in analogy to spray combustion regimes.

The effect of turbulence on the vaporization rate of particles has been studied using vaporization Damköhler number defined by Gökalp [100], $Da_v = \frac{\tau_e}{\tau_v}$. Prior studies [101], [102] with droplets indicate that for $Da_v > 0.1$, the effect of ambient turbulence is negligible on the evaporation rate whereas for $0.0001 < Da_v < 0.1$, it was seen that the turbulence have a significant effect on increasing the evaporation rate. In general, the vaporization rate from the particle decreases with an increase in the Da_v and becomes independent of turbulence as Da_v approaches unity [103]. In the current test cases, turbulent time scale defined by the eddy turnover time is smaller by an order than the vaporization time scale, and the resultant Da_v is in the range of 0.17 – 0.36 for coal and in the range of 0.11 – 0.22 for Sodium bicarbonate particles. Hence, overall the turbulence has negligible or minor effects on the vaporization rate of the particle. Based on the Da_v values estimated, it can be concluded that the vaporization rate will be accelerated more for sodium bicarbonate than coal at the same level of turbulence. Further it can be seen that, as the turbulent intensity increase the vaporization rate will also increase, due to the lower values of Da_v. Table 4.4 presents the above analysis for the current study.

Table 4.4: Group combustion number and vaporization Damköhler number for test cases with coal and sodium bicarbonate.

Particle type	ρ_p (kg/m^3)	d_p (µm)	u'_{rms} (m/s)	G	Da_v
Coal	492	75-90	0.65	1.4 – 5.1	0.25 – 0.36
			0.72		0.22 – 0.31
			0.88		0.17 – 0.25
$NaHCO_3$	801	75-90	0.65	0.9 – 3.2	0.15 – 0.22
			0.72		0.13 – 0.19
			0.82		0.11 – 0.16

4.4.2.5 Change in the particle size

The particles may grow or shrink in size while passing through the flame zone. Some particles may shrink in size due to the release of volatiles and off gassing. Other particles may grow in size due to deposition of the volatiles from neighboring particles or from the resulting char deposition on the surface resulting in decreased vaporization [97]. Thus we cannot expect particle diameter to continuously decrease as they vaporize, compared to a droplet scenario. The uncertainties due to these effects are not rigorously considered in the current analysis. However an observation from the pre-burn and post-burn microscopic images (Figure 4.11) of coal, sand and sodium bicarbonate reflect that the above said changes in the particle size occurs while it passes through the flame zone. For coal and sodium bicarbonate, a reduction in the particle size has been observed and it is more significant for sodium bicarbonate. For these particles the certain off gassing of volatiles has resulted in this effect. Interestingly, the sand particles have fused together and has resulted in an increase in the post burn size of sand. The typical melting temperature of sand is around 1700 ^{o}C. However the shorter residence time in the flame zone and sudden cooling to the product side temperature and further to atmospheric temperature of sand may have resulted in fusing. Further, it can be inferred from the correlations presented in the earlier sections for length scale and time scale analysis that an increase in the diameter will result in increase in the Stokes number and the turbulent intensity in the flame zone.

Particle type	Pre-burn	Post-burn
Coal	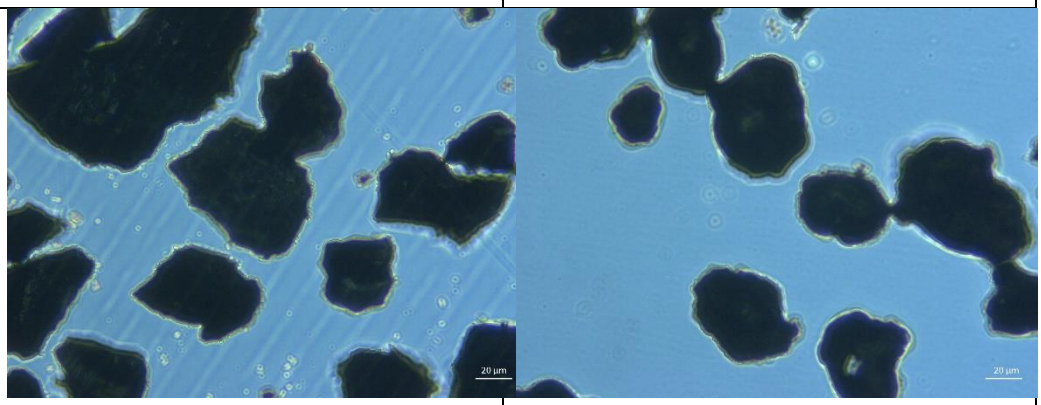	
Sand	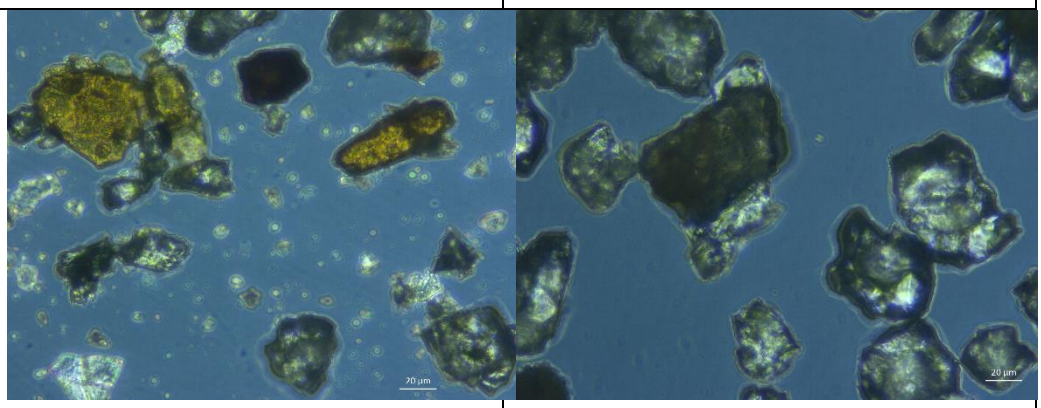	
Sodium Bicarbonate	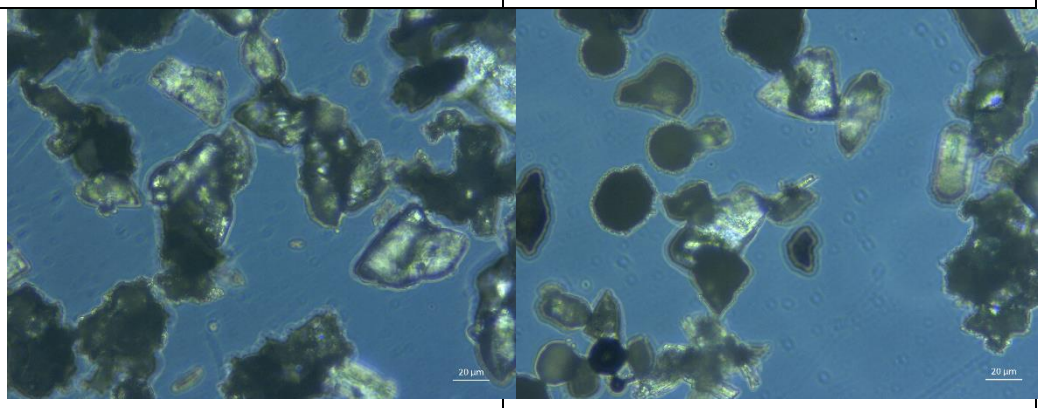	

Figure 4.11: Dust pre-burn and post burn microscopic images.

Furthermore, the broadened preheat zone regime in the test cases studied will preheat the gases and particles at the downstream of the flame front. The study by Wabel et al. [43] indicates that the broadened preheat zone thickness is a critical variable that attenuates the incoming turbulence

to the flame front. The off-gassing from the vaporizing particles begin from the preheat zone and eventually lead to the variation in particle density and particle diameter, hence again affecting the turbulence intensity very near the flame zone. Future research is required to better understand the relevant turbulence variation in the presence of flame zone and its effect on the turbulent burning velocity.

4.4.3 Variation of turbulent burning velocity

Figure 4.12 shows the set of shadowgraph flame images taken at dust concentration of 50 g/m^3 and at ϕ_g = 1.0 for different dust types studied. One observation, which can be clearly made is that, with the increase in the turbulent intensity, the flame becomes more wrinkled and corrugated for all the dusts considered. The tip of the flame front starts to break up, especially at the higher turbulent intensities. In addition, it is seen that different dust types have also affected the flame shape. It is evident from the flame images that, sand particles, which do not release any volatiles, resulted in forming clearer flame edges. The effect of volatile release is more predominant with the addition of coal as compared to $NaHCO_3$. This is due to the difference in decomposition mechanism of the coal and sodium bicarbonate, which are discussed in the next section along with the variation of turbulent burning velocity at the conditions tested.

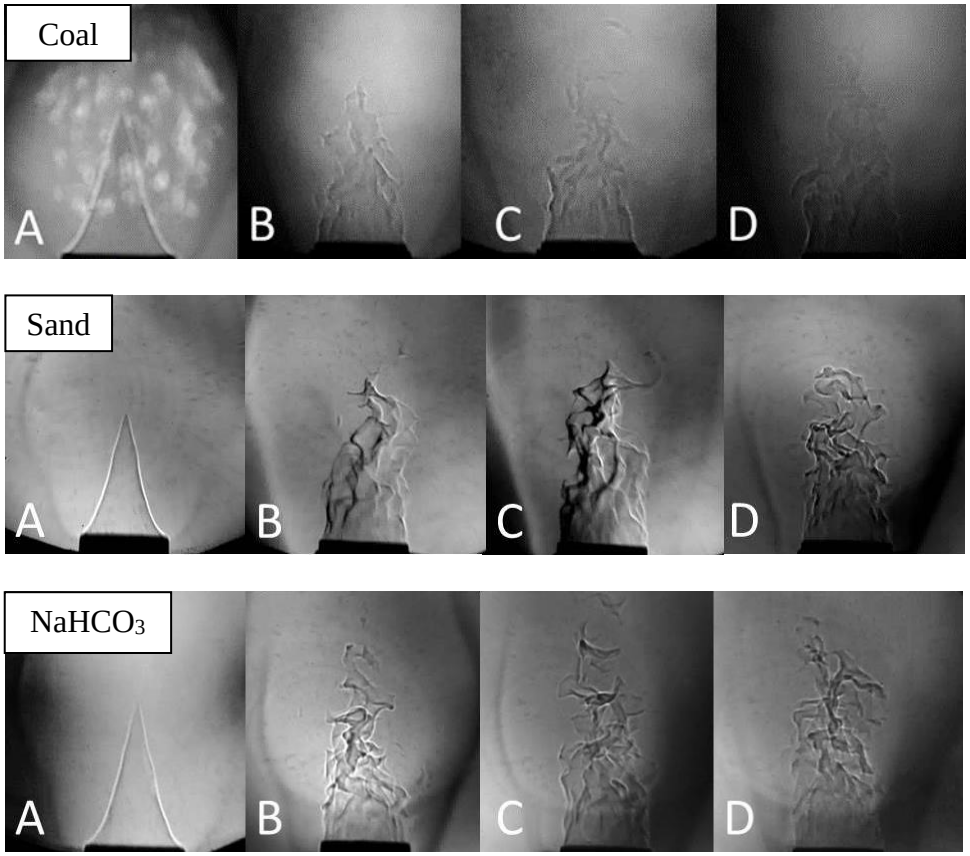

Figure 4.12: Turbulent flame images

Coal 75-90 µm at 50 g/m^3 and ϕ_g = 1.0, A) Laminar; B) u'_{rms} = 0.65 m/s; C) u'_{rms} = 0.72 m/s; D) u'_{rms} = 0.88 m/s.

Sand 75-90 µm at 50 g/m^3 and ϕ_g = 1.0 – A) Laminar; B) u'_{rms} = 0.65 m/s; C) u'_{rms} = 0.72 m/s; D) u'_{rms} = 0.88 m/s.

Sodium Bicarbonate 75-90 µm at 50 g/m^3 and ϕ_g = 1.0 – A) Laminar; B) u'_{rms} = 0.65 m/s; C) u'_{rms} = 0.72 m/s; D) u'_{rms} = 0.82 m/s.

Figure 4.13, Figure 4.14, Figure 4.15, shows the variation of measured turbulent burning velocity of different dust types at different dust concentrations, turbulent intensities and equivalence ratios. These variations are depicted for u'_{rms} = 0.65 m/s, 0.72 m/s and 0.88 m/s in

Figure 4.13, Figure 4.14, and Figure 4.15, respectively. As explained earlier, the experimentally estimated turbulent burning velocity (S_T) by averaged flame height approach [19], [82] has been adopted here. The maximum value of standard deviation of turbulent burning velocity estimated by averaging 25 images for all the cases of gas, coal, sand and sodium bicarbonate are 10 %, 16 %, 13 % and 12 % respectively from the mean S_T value. The error bars represent the standard deviation of mean turbulent burning velocity estimated for all the data points.

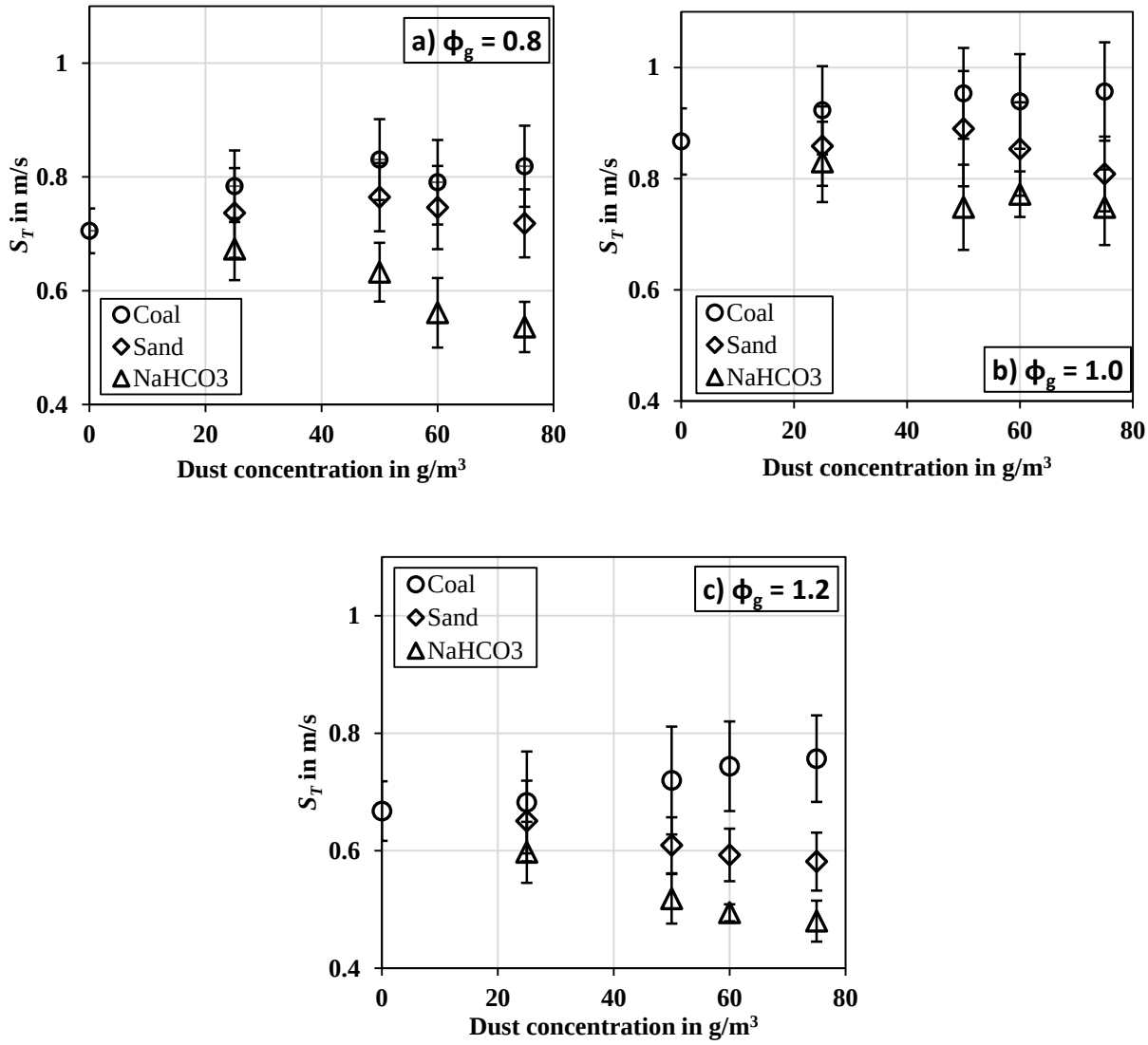

Figure 4.13: Variation of S_T at u'_{rms} = 0.65 m/s.

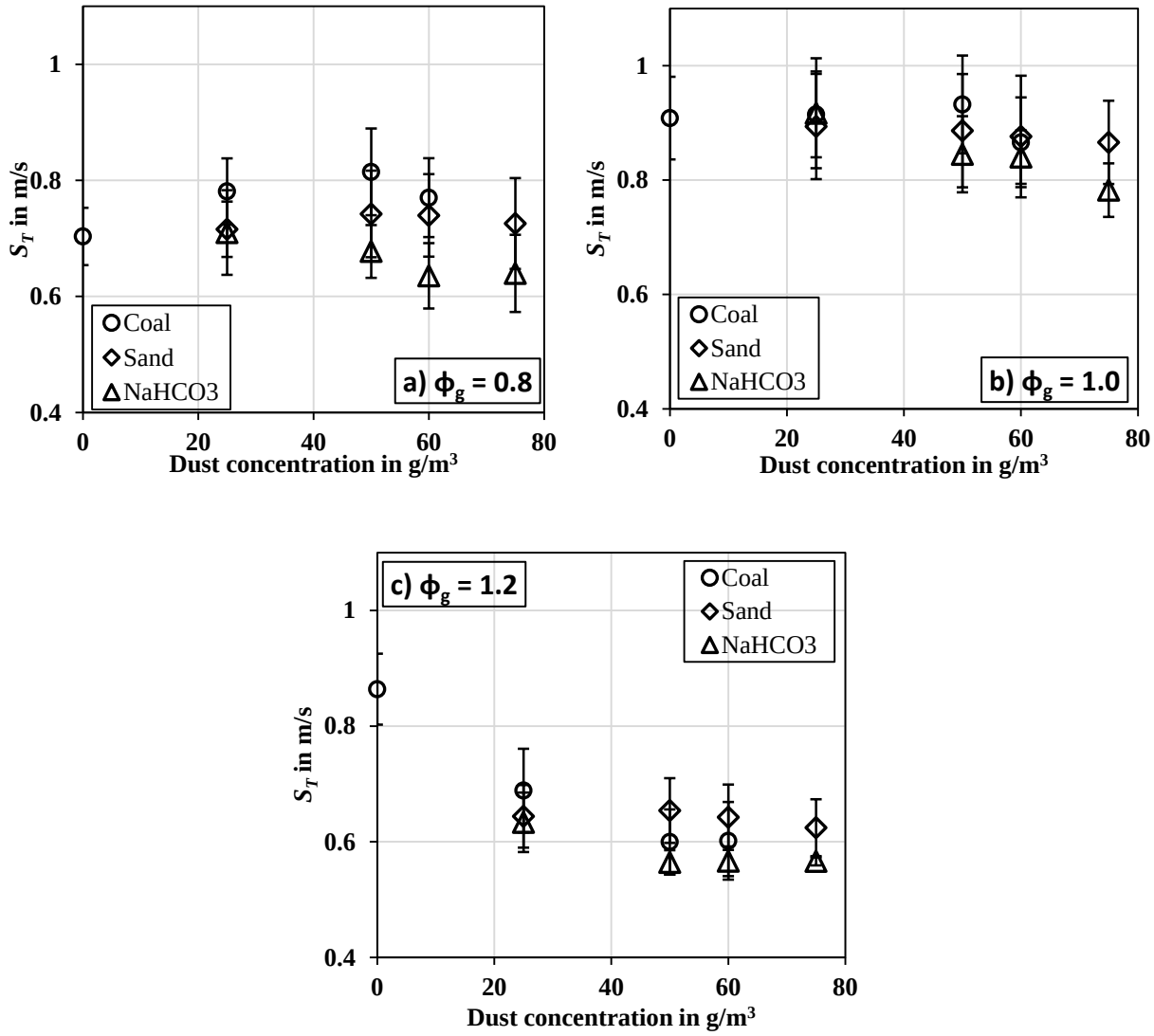

Figure 4.14: Variation of S_T at u'_{rms} = 0.72 m/s.

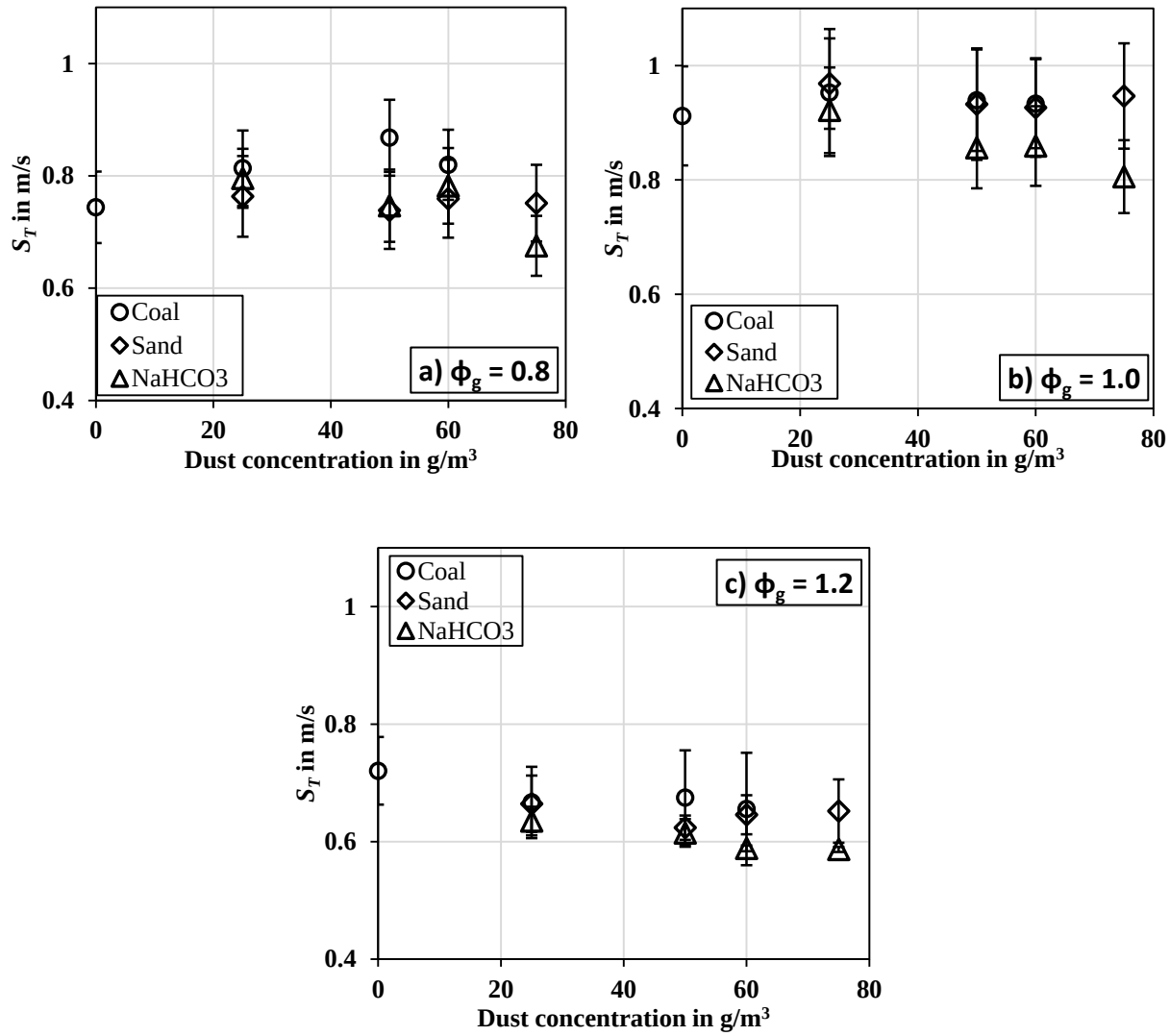

Figure 4.15: Variation of S_T at u'_{rms} = 0.88 m/s for coal & sand; S_T at u'_{rms} = 0.82 m/s for $NaHCO_3$.

In general, it is observed that an increase in the turbulent intensity, increases the S_T for both gaseous and dust entrained premixed flames. This is consistent with the observations of earlier studies [19], [40]. Increase in S_T is irrespective of the type of the dust added. However, it is noted that the rate of increase of S_T differs with different dust types. Coal and sodium bicarbonate have heterogeneous effect of absorbing the heat from flame zone and then releasing volatiles, whereas

sand acts only by absorbing heat from the flame zone. As the dust particles are introduced to a gaseous flame, at smaller concentrations (0-50 g/m^3), greater effect in the rate of increase or decrease of the burning velocity is observed. At larger concentrations of ~ 60-75 g/m^3 of dust particles, a decrease in the burning velocity is observed due to the dampening effect on the turbulent intensity at higher volumetric loading of particles along with the effect of broadened preheat zone. At higher concentration of particles, the interspace distance between the particles decreases which lowers the temperature diffused in the interspaces of the particle cloud and heating of the individual particles, thus further reducing the release of volatiles. But at higher turbulent intensities this effect is diminished due to the increased vaporization rate as evident from the decrease of Da_v (Table 4.4). This explains the overall decrease in the S_T at higher concentrations of coal and sodium bicarbonate particles at higher turbulent intensities (Figure 4.14 - Figure 4.15). At fuel rich equivalence ratios, the addition of all the dusts except coal at low turbulent intensity (0.65 m/s), results in decreasing the S_T. At high turbulent intensities of u'_{rms} = 0.72 and 0.88 m/s, the addition of coal also results in a decrease in S_T for a fuel rich mixture, ϕ_g = 1.2. The addition of coal particles in fuel lean and stoichiometric mixtures resulted in an increase in the S_T till a specific concentration (~ 50 g/m^3) and beyond which at higher concentrations, resulted in decreasing the burning velocity. The volatile released by coal is predominantly methane (CH_4) and hence there is a local increase in the equivalence ratio [19], [59]. At higher turbulent intensities with larger vaporization rate, this effect becomes predominant and the burning velocity decreases even lesser than sand cases (Figures 4.14.b, 4.14.c, 4.15.b, 4.15.c).

Sand particles used in this study (silica), act only as heat sinks and thus affect the burning velocity without releasing any volatiles. It is noted that the S_T values with sand interaction at higher turbulent intensities and stoichiometric and fuel rich conditions are comparable to or higher than

that of coal cases. This could be due to the heating of the sand particles resulting in re-radiation from the particle to the flame zone along with the fact that sand particle maintains its shape and hence have the same surface area of contact as it passes through the flame zone. The Stokes number for sand particles are higher than that of coal and $NaHCO_3$ (Table 4.3), hence results in higher turbulent intensity for the same volumetric loading. The mass transfer on the surface of coal and sodium bicarbonate due to volatilization also play a role in controlling turbulence modulation, which is not possible in the case of sand. It is also observed earlier from the post-burn pictures of sand that fusing of sand particles has resulted in an increase in the diameter. Further, sand particles also have the most pronounced edges, which at higher concentrations may lead to enhancement in turbulent intensity. The detailed effects of different particle types and shape effects on turbulent modulation in reacting flows need to be studied further. An attempt to relate this effect using empirical model coefficients is explained in the next section.

Addition of sodium bicarbonate always decreases the S_T. This can be related to the effect of release of volatiles in the form of CO_2 and H_2O. As presented in prior study [62], sodium bicarbonate decomposition reaction at high temperature is an endothermic reaction and complete decomposition of $NaHCO_3$ happens in two steps. $NaHCO_3$ reacts at a temperature of 270^{o}C.

$$2\ NaHCO_3 \rightarrow Na_2CO_3 + CO_2 + H_2O. \qquad (4.5)$$

The sodium carbonate formed as a result of this decomposition, is a relatively stable salt. But at a higher temperature of around 851^{o}C, Na_2CO_3 also reacts to release more CO_2.

$$Na_2CO_3 \rightarrow Na_2O + CO_2 \qquad (4.6)$$

The endothermic reaction, resulting in flame enthalpy reduction also indicates the heterogeneous effect of $NaHCO_3$, as it acts as a heat sink to release volatiles while diluting the local equivalence ratio of the mixture. As noted before through Da_v analysis, sodium bicarbonate has higher

vaporization rate and this is increased at higher turbulent intensities resulting in the decrease of turbulent burning velocity due to larger release of CO_2 and H_2O.

A complete chemical inhibition and resulting flame extinction with the addition of $NaHCO_3$ has not been observed in the turbulent premixed flames for the range of concentrations studied. Our earlier study [104] in chapter 3 with laminar premixed flame inhibition by $NaHCO_3$ particles of 75-90µm indicated that 75 g/m^3 and 125 g/m^3 $NaHCO_3$ were required to extinguish the methane-air laminar flame of equivalence ratio 0.8 and 1.2, respectively. The maximum $NaHCO_3$ concentration that was tested in turbulent flame conditions is 100 g/m^3 and no flame extinction was observed. Based on the laminar flame extinction results, we can conclude that concentration of $NaHCO_3$ more than 100 g/m^3 will be required for flame extinction of turbulent premixed flames.

4.4.4 Correlation coefficients for turbulent burning velocity

Earliest models for predicting turbulent burning velocity for gaseous mixtures was derived by Damkohler [105] and Schelkin [106], takes the form as:

$$\frac{S_{Tg}}{S_{Lg}} = 1 + \frac{u'_{rms}}{S_{Lg}} \quad , \qquad (4.7)$$

Following which, many studies [85], [107]–[109] followed this correlation which attempted to reproduce experimental data on turbulent burning velocities, mostly for gaseous pre-mixtures. There were many modifications done based on the scale and intensity of turbulence to arrive at a generalized equation of the form:

$$\frac{S_{Tg}}{S_{Lg}} = 1 + C\left(\frac{u'_{rms}}{S_{Lg}}\right)^n \quad , \qquad (4.8)$$

where, n is known as bending (nonlinear) component and C is the parameter indicating the influence of turbulence. Note that this classical form of equation was mainly used for gaseous

mixtures until Dahoe [85] implemented them with 20-L explosion vessel experiments with dust-air mixtures. In general for gaseous mixtures, the turbulent burning velocity increases linearly at smaller turbulent intensity and with the increase in the intensity it increases more slowly. At very high levels of turbulence ($u'_{rms} \gg S_{Lg}$), the turbulent burning velocity becomes independent of laminar burning velocity.

An attempt to incorporate the above correlation using the present experimental data has been done by the following equation:

$$\frac{S_T}{S_L} = 1 + C\left(\frac{u'_{rms}}{S_{Lg}}\right)^n \quad , \qquad (4.9)$$

Here on the LHS, the turbulent burning velocity of gas-dust mixtures, S_T values are non-dimensionalized using corresponding S_L values at same concentration of dust, obtained from prior chapters [60], [107]. The u'_{rms} values are non-dimensionalized by S_{Lg}, which is the laminar burning velocity of gaseous methane-air mixtures [44]. Table 4.5 presents model coefficients, which represent the best fit of the experimental values from each of the pre-mixture condition tested in this study. The proposed correlation for particle-gas pre-mixture also does not account for the effect of particle concentration, which has a great influence in the burning velocity of hybrid flames.

Table 4.5: Predicted model coefficients from experimental results.

Pre-mixture Condition	*C*	*n*
Gas (CH_4 + air)	0.90	0.70
Hybrid (CH_4 + air + coal)	0.85	0.60
Hybrid (CH_4 + air + sand)	1.70	0.35
Hybrid (CH_4 + air + $NaHCO_3$)	0.90	1.0

Figure 4.16 presents the experimentally obtained S_T/S_L values along with the predicted trend of variation of the same using the above empirical correlation. As compared to the gaseous mixture, addition of coal results in smaller S_T/S_L ratio. This is due to the fact that addition of coal presents a similar trend in the burning velocity variation for both laminar and turbulent flames. Whereas sand and sodium bicarbonate addition results in a decreasing trend in the laminar burning velocity [104], which ultimately results in a larger S_T/S_L values than coal and gaseous cases. The influence of turbulence presented by *C* value, in increasing the burning velocity is found to be greater with the addition of sand as compared to other particles and gaseous case studied. The *C* value for gaseous, coal added and $NaHCO_3$ added pre-mixtures are around the same value of 0.90, 0.85 and 0.90 respectively. Whereas with the addition of sand, *C* value is almost doubled to 1.70. This also supports the earlier argument that sand particles owing to an increase in size, having higher particle density and potential particle-particle collisions results in enhancing turbulence as compared to coal and $NaHCO_3$. This resulting in higher S_T values for sand at higher turbulent intensities. Further, the bending component for the case of sand indicates the rate of increase of S_T/S_L is much smaller as compared to other cases. This could be due to the lack of any volatiles released either to improve the equivalence ratio or to dilute the pre-mixture like other particles considered. Sodium Bicarbonate produces a near linear variation ($R^2 = 0.75$) of S_T/S_L, with a slope of 0.9, indicating that the turbulent burning velocity (S_T) is almost the sum of laminar burning velocity (S_L) and turbulent intensity (u'_{rms}).

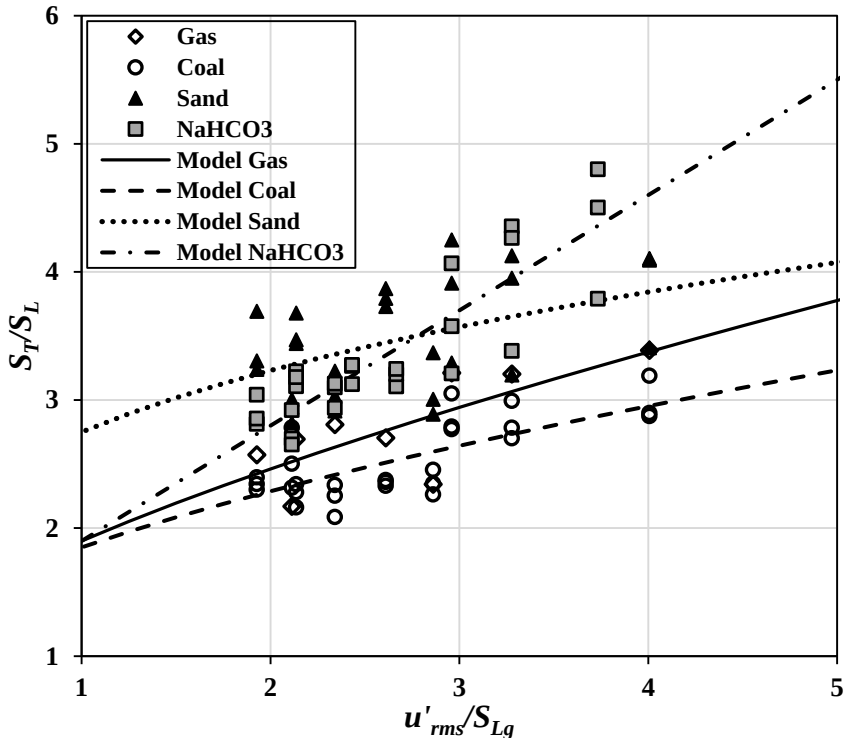

Figure 4.16: Correlation model coefficients for premixed methane-air-dust flames analyzed.

Above equation can be applied to gaseous mixtures with single *C* and *n* values, as has been done by earlier work. However, dust-air mixtures need multiple *C* and *n* values [19], [85] because of additional factors like dust type, size and concentration, which would influence the burning velocity as well as modulate turbulent intensity. Only the LHS of the equation 4.7 considers the effect of dust and dust concentration, where the effect of dust concentration is in built in the burning velocity values. In order to consider the effect of dust concentration, the RHS of equation 4.7 is modified by replacing S_{Lg} with S_L (laminar burning velocity of gas-dust mixture) resulting in the modified equation as:

$$\frac{S_T}{S_L} = 1 + C\left(\frac{u'_{rms}}{S_L}\right)^n \quad , \qquad (4.8)$$

Figure 4.17 presents the modified plot between the non-dimensional turbulent burning velocities versus turbulent intensity.

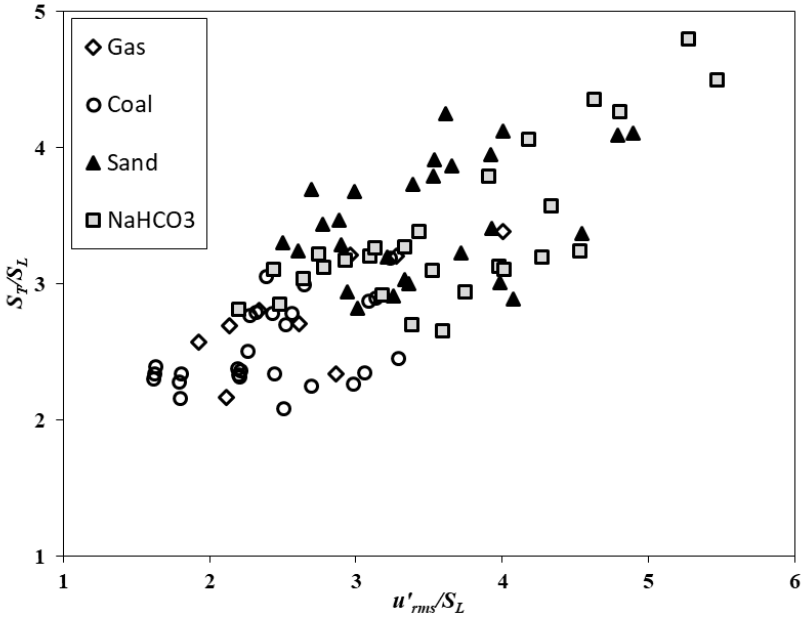

Figure 4.17: Modified non-dimensional turbulent burning velocity versus turbulent intensity.

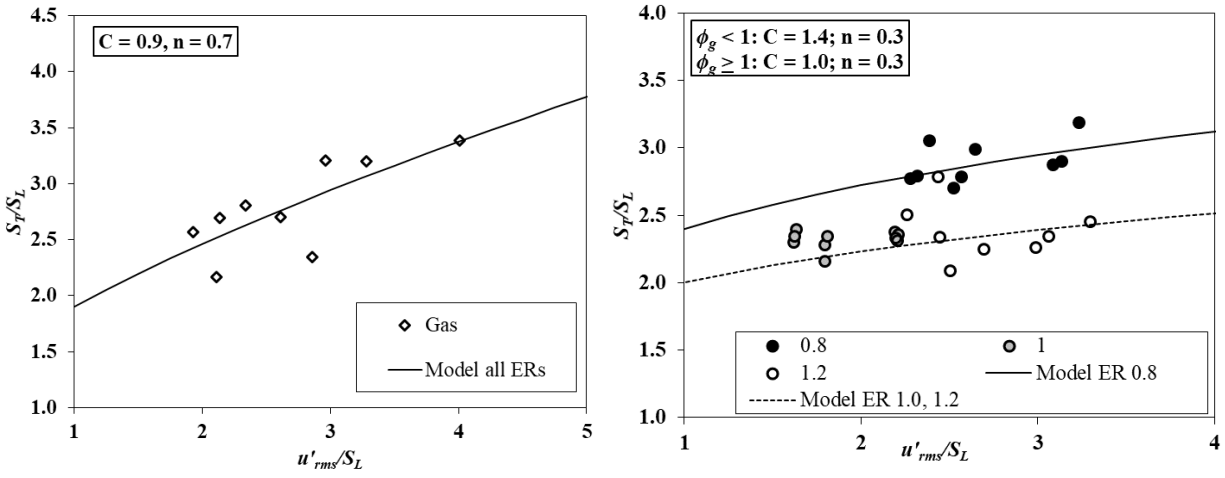

(a) Gas (b) Coal

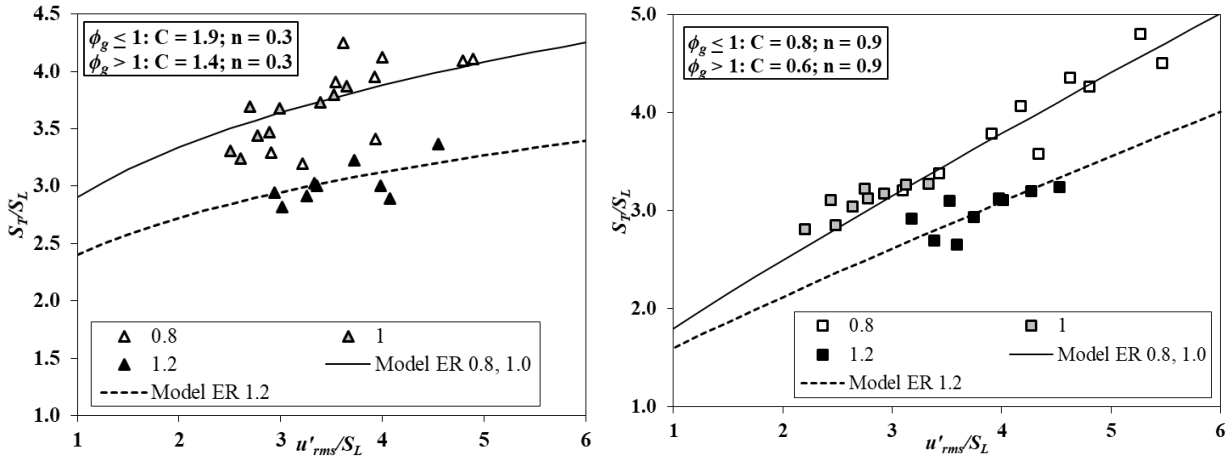

(c) Sand (d) Sodium bicarbonate

Figure 4.18: Modified correlation plots for a) gas; b) coal; c) sand; d) sodium bicarbonate.

Analyzing different types of dusts independently (Figure 4.18) indicates that two sets of model constants are necessary. This transition of model constants are dictated by the gas phase equivalence ratio as the main stream mixture ratio is still predominant over the change in equivalence ratio due to dust addition (for coal and sodium bicarbonate). The equivalence ratio at which the transition occurs differs with the dust type. The observation for coal is consistent with that of Rockwell [19] where $\phi_g < 1$ and $\phi_g \geq 1$can be grouped with two separate model constants. Whereas for sand and sodium bicarbonate the distinct constants are used for $\phi_g \leq 1$ and $\phi_g > 1$. The model constants are presented in Table 4.6. As observed before, close to straight line fit is observed for sodium bicarbonate model results.

Table 4.6: Modified model coefficients.

Pre-mixture Condition	***Equivalence ratio***	***C***	***n***
Gas (CH_4 + air)	All ϕ_g	0.9	0.7
Hybrid (CH_4 + air + coal)	$\phi_g < 1$	1.4	0.3

	$\phi_g \geq 1$	1.0	0.3
Hybrid (CH_4 + air + sand)	$\phi_g \leq 1$	1.9	0.3
	$\phi_g > 1$	1.4	0.3
Hybrid (CH_4 + air + $NaHCO_3$)	$\phi_g \leq 1$	0.8	0.9
	$\phi_g > 1$	0.6	0.9

No effect of particle size has been considered in the correlation and hence the model coefficients used above is limited to the 75-90 μm particles, concentration range and the turbulent intensity range studied in the current work. Overall, the correlation coefficients predicted in this study is indicative of how the current study with the interaction of particles on gaseous pre-mixture differ from the gaseous cases, which is typically done using this correlation. The results clearly indicate the distinction of these model coefficients (*C* and *n*) as a result of the addition of particles, and different types of particles. A larger database across a wider range of turbulent intensities (u'_{rms}/S_L) is required to provide a more predictive correlation for wider range of all parameters involved. This can ultimately be used in modeling purposes.

4.5 Conclusions

This chapter presents the variation of turbulent burning velocity of premixed methane-air-dust flames as a function of dust concentration, dust type, turbulent intensity and equivalence ratio of gaseous pre-mixture using a turbulent Bunsen burner type experimental platform. Dust type and concentration play a major role in deciding the trend of variation of turbulent burning velocity, S_T. Coal particles tend to increase S_T with the release of volatiles (methane), except for fuel rich conditions and higher concentrations of coal at larger turbulent intensities. Sodium bicarbonate addition decrease the burning velocity at all the concentrations, turbulent intensities, and

equivalence ratios tested. This is attributed to the absorption of energy and the release of CO_2 and H_2O. The time scale analysis for the vaporization of particle shows $NaHCO_3$ has higher evaporation rate than coal at same level of turbulence. An increase in the turbulent intensity increases the vaporization rate of particles. Sand particles exhibit a tendency to increase the S_T at smaller concentrations, and lower turbulent intensities. At a higher turbulent intensity and ϕ_g = 1.0 to 1.2, S_T values due to the addition of sand becomes comparable to or higher than that of coal. The turbulence modulation exhibited by different particles and concentration is evident in these observations.

Several observations are made from three independent characteristic time scale analysis performed using the experimental data. First, the chemical and convective times in gas phase confirm the broadened preheat thin reaction zone regime in the current test cases, which has the effect of attenuating turbulence and the resulting turbulent burning velocity. Second, the particle time scale analysis (Stokes number) show that the effect of particles and particle concentration is to slightly enhance the turbulence and increase the turbulent burning velocity at lower concentrations. Third, the time scale analysis of particle vaporization (vaporization Damköhler number) indicate an increase in the vaporization rate for particles (coal and sodium bicarbonate) resulting in a decrease in their turbulent burning velocities at higher concentrations and turbulent intensities. The absence of this effect for inert (sand) results in higher turbulent burning velocities at higher concentrations. A unified approach to couple this complex phenomenon of turbulence, particle interaction, particle vaporization and combustion in particle laden premixed gaseous flames is the direction for future research.

5 Radiative fraction of turbulent premixed methane-air-dust flames

5.1 Chapter abstract

This chapter presents the results from measurements of the radiative fraction of heat released by methane-air-dust turbulent premixed flames and discusses the effect of dust particles (75-90 μm) on the radiative heat released. Radiative heat flux measurements are captured from burner stabilized methane-air-dust premixed flames at different equivalence ratios (ϕ_g = 0.8, 1.0, 1.2), and turbulent intensities (u'_{rms} = 0.65, 0.72, 0.88 m/s) using different dust types (coal, sand and sodium bicarbonate) and dust concentrations (λ_p = 25, 50, 75 g/m^3). The effect of these parameters on the resulting radiative fraction of heat released (X_r) is investigated. It is identified that the addition of dust particles increase the radiative fraction irrespective of the dust type due to the radial and axial extension of flame. An increase in the turbulent intensity decreases the radiative fraction. Addition of coal dust results in the maximum radiative fraction of heat released, whereas sand and sodium bicarbonate results in approximately similar average radiative fraction values. With the addition of coal dust, the radiative fraction of premixed methane-air flames become comparable to that of methane-air diffusion flames. The range of radiative fractions of methane-air gaseous turbulent premixed flame is found to be 2.7% - 6%, whereas the addition of coal, sand and sodium bicarbonate results in an increased range of X_r values of 10.5% - 17.5%, 7.6% - 11.5%, and 8.5% - 12.7% respectively.

5.2 Introduction and related literature

Thermal radiation is an important factor in flame spread, both during premixed flame propagation and in spread to other nearby combustible materials. It also plays an important role to evaluate the scale of fire as it accounts for bulk of the heat transferred to the surroundings and is the cause of numerous injuries to industrial workers and first responders. From the perspective of fire, thermal radiation properties of non-premixed flames have been studied widely because of their sooty nature and the resulting large radiative heat losses [110]. It is verified [111] that radiative heat transfer from the flame is dependent mainly on the fuel type and fuel size. Radiative fraction of diffusion flame typically varies from 10% to 60%. Owing to its relatively low radiative loss, premixed flames are historically less investigated for their thermal radiation properties.

One of the first of relatively few studies on radiation characteristics of axisymmetric turbulent premixed jet flames was conducted by Ji et al. [112] and reported the spectral radiation properties of turbulent jet premixed methane-air flames. The effect of radiation heat loss on the flame propagation speed, especially at the lean or near lean flammability limit have been investigated in various research studies [113], [114]. Shoshin et al. [114] proposed that radiative heat losses from the flame in a low velocity region that appears below very lean flames resulted in flame extinction. This also shows the effect of thermal radiation heat loss on premixed flame stability. Studies on laminar flame propagation through organic dust cloud indicate that thermal radiation from flame zone to the preheat zone and vaporization zone significantly increases the burning velocity [115]. There are studies reporting the radiation heat loss from non-premixed turbulent jet flames [116]. Fujimori el al. [117] presented the effect of preheated air on increasing the radiative fraction of methane flames and reported that the radiative fraction of methane jet flames reached a maximum value of 0.5 at 1230 K preheated air. With regard to the measurement of radiative heat flux from

flames, Sivathanu and Gore [118], estimated total radiant output of turbulent jet flames from the measurement of radiative heat flux at a single point location. Studies (Hamins, [119]) with pool fires indicate that single point measurement of heat flux can be used to get a good estimate of radiative fraction, if measured at appropriate radial and axial distance from the flame. The near-field and far-field behavior of modeling approaches and its impact on the radiative fraction of heat estimation in jet fires was reviewed by Hankinson and Lowesmith [120].

The explosion incidents occurring in coal mines are one type of scenario in which a premixed flame propagation is accompanied by coal dust entrainment. The risk of dust explosions have amplified with an increased material processing in many process industries [121]). The combustible dust interaction with flames are generally studied from the perspective of flame propagation or combustibility of the dust itself. Relatively less attention has been given to study the thermal radiation properties of these hybrid mixture flame conditions. The specific objective of this chapter of thesis is to estimate the radiative fraction of heat released from dust entrained turbulent premixed methane-air flame conditions at different dust concentrations and turbulent intensities.

Coal, sand and sodium bicarbonate particles with size range of 75-90 μm have been used to compare the effect of different dust types in this work. Coal is used purely from a hazard (flash fire) perspective. Most underground coal deposits release methane gas which along with coal dust result in an explosion hazard (Amyotte and Pegg, [122]; Brune et al. [123]). The study (Im and Ahluwalia, [124]) on coal combustion product radiation properties suggest that radiative heat transfer from particulate is dominant as compared to gaseous emissions and the radiation characteristics are dependent on the particle size and type. The practice of rock dust inerting has been used extensively in order to prevent the formation of explosive dust-gas mixtures in

underground mines (Harris et al. [125]). The rock dust added as inert in coal mines should pass at least 70% through a 200-mesh (75 μm) sieve (Sapko et al. [126]). For this study, sand (silica) is used as inert. Christophe et al. [127] observed that the addition of SiC particles to methane-air flames promotes the thermal radiation greatly due to their higher emissivity even though there was a drop in the flame temperature. Sodium Bicarbonate ($NaHCO_3$) is a dry chemical fire extinguishing agent thus act as a chemical inhibitor apart from being a heat sink. Because of the heat sink and suppressive nature of sand and sodium bicarbonate respectively and their application as flame inhibitors, it is expected that they reduce the radiative fraction of flame. However, the results indicate this is not always the case. A qualitative trend in the variation of radiative fraction is presented in this chapter by processing the experimentally obtained radiative heat flux measurements and flame images from burner stabilized turbulent premixed flames.

5.3 Experimental set-up and procedure

The Bunsen burner experimental set-up used in this study is explained in Chapter 2. The important components of the experimental set-up as shown in Figure 5.1 include a combustion chamber with a burner nozzle, dust feeder, and an exhaust hood. Mass flow controlled methane-air mixtures at equivalence ratios of ϕ_g = 0.8, 1.0, and 1.2 are used to produce fuel lean, stoichiometric, and fuel rich premixed gaseous flames. A particle screw feeder is used to inject dust (75-90 μm) at different concentrations into the methane-air flow creating the hybrid flame. Turbulent intensity (u'_{rms}) is altered by adjusting the flow velocity. The methane-air flow rates of 30, 35, and 40 liters per minute create turbulent intensities of 0.65, 0.72, and 0.88* m/s (*at 40 lpm for the experiments conducted with $NaHCO_3$, u'_{rms} measured was 0.82 m/s) respectively. A water cooled heat flux gauge has been fixed at 25 mm vertical distance and 33 mm radial distance from

the burner exit and center of the burner respectively, in order to capture the heat flux measurements. Multiple flame images extracted from videos captured at 30 fps are used to estimate the average flame height. The maximum value of standard deviation of individual flame height values from the mean flame height is found to be 12%, 11% and 11% for coal, sand and sodium bicarbonate respectively.

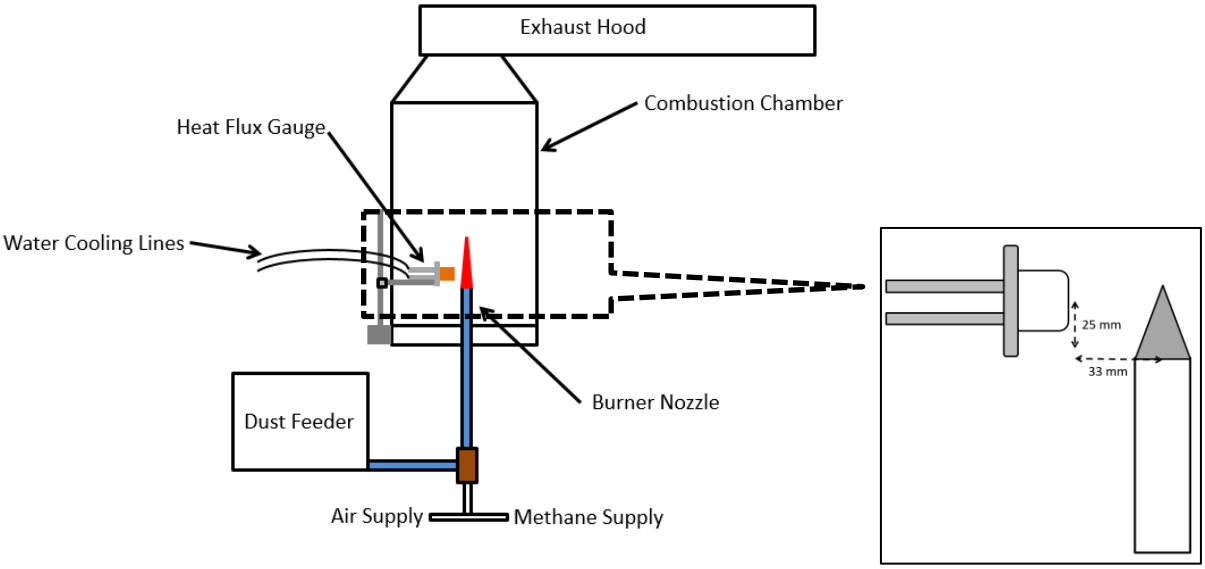

Figure 5.1: Experimental set-up and heat flux gauge location.

5.4 Estimation of radiative fraction

Radiative heat flux ($\dot{q}_r''$) measurements are captured using a water cooled heat flux gauge at a single point location at the exit plane of the burner and parallel to the axis of the flame, located at 25 mm vertical distance and 33 mm radial distance from the burner exit and centerline of the burner respectively. Prior study (Sivathanu and Gore, [118]) with jet diffusion flames have shown that a single point measurement of heat flux from appropriate location from the flame can provide a good

estimate of radiative fraction. The resulting radiative heat release rate ($\dot{q}_r$) is estimated by solid flame model using:

$$\dot{q}_r = \frac{A_f \, \dot{q}_r''}{\tau \, F} \qquad (5.1)$$

where F is the flame geometric view factor and A_f is the surface area of flame. Atmospheric transmissivity, τ is assumed to be unity. In order to estimate F and A_f, classical cylindrical flame model (Shokri and Beyler, [128]) is adopted with diameter of the flame, D_f equal to the average flame diameter. In order to account for the radial expansion effects of the flame, an average flame diameter is estimated by measuring different diameters (d_1, d_2, d_3,…d_n) through the flame length and averaging them for each cases (Figure 5.2.a). The average flame diameter is calculated as:

$$D_f = \frac{\sum_{i=1}^{n} d_i}{n} \qquad (5.2)$$

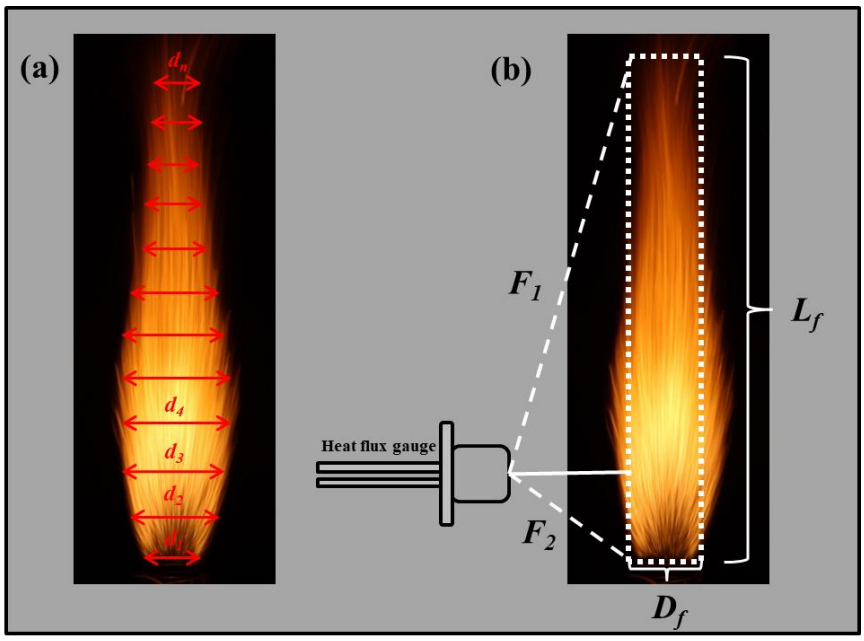

Figure 5.2: (a) Average flame diameter estimation, (b) View factor estimation.

The geometric view factor of the flame is calculated by:

$$F = F_1 + F_2 \qquad (5.3)$$

where F_1 and F_2 represents view factors from the top and bottom section of the flame respectively (Figure 5.2.b). They are estimated using the expression:

$$F_{ij} = \frac{1}{\pi D}\tan^{-1}\left(\frac{L}{\sqrt{D^2-1}}\right) + \frac{L}{\pi}\left[\frac{A-2D}{D\sqrt{AB}}\tan^{-1}\sqrt{\frac{A(D-1)}{B(D+1)}} - \frac{1}{D}\tan^{-1}\sqrt{\frac{D-1}{D+1}}\right] \qquad (5.4)$$

where $D = \frac{x}{R}; x = 33\ mm; R = \frac{D_f}{2};$

$$L = \frac{l}{R}; l = (L_f - 25)\ mm\ for\ F_1; l = 25\ mm\ for\ F_2$$

$$A = (D+1)^2 + L^2; B = (D-1)^2 + L^2$$

Flame surface area is then calculated using,

$$A_f = \pi D_f L_f \qquad (5.5)$$

where L_f is the flame height calculated by averaging the flame height values of 25 images for each condition tested. The total heat release rate, $\dot{q}_{T,g}$ from the gaseous pre-mixture is obtained from:

$$\dot{q}_{T,g} = H_{c,methane} \cdot x_{methane} \cdot \left(\frac{moles}{cc}\right)_{reactants} \cdot \dot{V}_{reactants} \qquad (5.6)$$

where $H_{c,methane}$ is the heat of combustion of methane, 800 kJ/mol; $x_{methane}$ is the number of moles of methane; $\left(\frac{moles}{cc}\right)_{reactants} \cdot \dot{V}_{reactants}$represents the molar burning rate of the reactants where $\dot{V}_{reactants}$ is the volumetric flow rate of the gaseous reactants. Similarly the total heat release rate, $\dot{q}_{T,p}$ from the particles is obtained from:

$$\dot{q}_{T,p} = H_{c,p} \cdot \lambda_p \cdot \dot{V}_{reactants} \qquad (5.7)$$

where $H_{c,p}$ is the heat of combustion of particle, 31.3 kJ/g for coal and -1.61 kJ/g for $NaHCO_3$; and λ_p is the particle concentration. The total heat release rate is estimated as:

$$\dot{q}_T = \dot{q}_{T,g} + \dot{q}_{T,p} \qquad (5.8)$$

The particle heat release rate increase the total heat release rate with coal and decrease the total heat release rate with sodium bicarbonate. In the current experiments coal resulted in an increase of premixed methane-air gas heat release rate by 21.5% to 93.2% whereas the addition of sodium bicarbonate resulted in a decrease of premixed methane-air gas heat release rate by 1.1% to 4.8% owing to the endothermic nature of the reactions. From the above, the radiative fraction is estimated from the ratio of radiative heat release rate to the total heat release rate as follow:

$$X_r = \frac{\dot{q}_r}{\dot{q}_T} \qquad (5.9)$$

where $\dot{q}_T$ is the the total heat release rate of the reactants. The heating, decomposition, and possible combustion of the particles will depend on various factors such as particle size, residence time, particle temperature and turbulent intensity (Chapter 4). The current analysis assume heat of combustion from all the particles considered for each concentrations. This thesis chapter intends to present a qualitative variation of the radiative fraction of turbulent premixed flames with the influence of dust addition and the results are presented in the following section.

5.5 Results and discussion

5.5.1 Variation of radiative heat flux

The variation of radiative heat flux for turbulent premixed methane-air flame with turbulent intensity is presented in Figure 5.3. Radiative heat flux measured from the tests considered with coal, sand and sodium bicarbonate respectively are presented in Figs. 5.4-5.6 by normalizing the respective heat flux values with that of gaseous flame radiative heat flux measurements obtained at corresponding turbulent intensities. For all the radiative flux measurements, uncertainty analysis was conducted. The standard deviation of heat flux measurements for experiments with coal dust

varied between 5.6% - 13.1%; for experiments with sand varied between 11.7% - 22.9%; for experiments with $NaHCO_3$ dust varied between 11.1% - 26.7%. A larger scatter in the data is observed for the flame inhibitors, i.e. sand and $NaHCO_3$.

For gaseous premixed flames, an increase in the turbulent intensity results in a decrease in the radiative heat flux measured irrespective of the equivalence ratio of the mixture. Whereas for a given turbulent intensity, the radiative heat flux increases in the order $\phi_g = 1 > 1.2 > 0.8$.

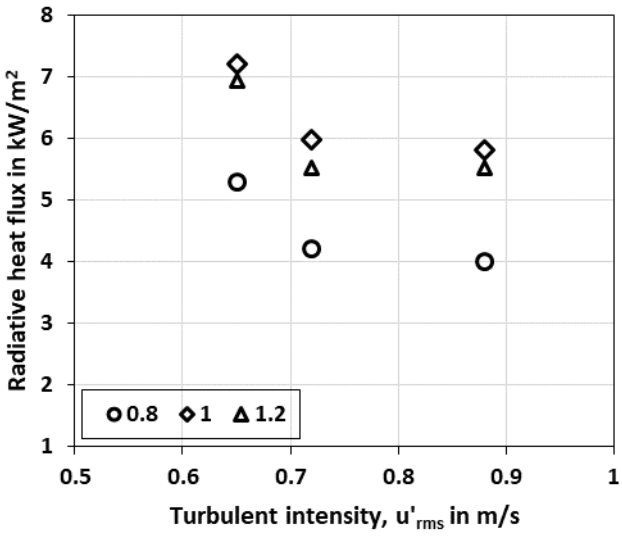

Figure 5.3: Variation of radiative heat flux for turbulent premixed methane-air flames.

In general, it is observed (Figure 5.4) that with the addition of coal dust, there is almost a linear increase in the radiative heat flux values against the concentration of coal dust. The normalized heat flux values of premixed methane-air-coal flames varied in the range of 1.11 to 2.07. It is also noted that the radiative heat flux values increases with an increase in the turbulent intensity. Further, as the gas phase equivalence ratio increases ϕ_g = 0.8 to 1.2, the normalized radiative heat flux value decreases with the addition of coal dust.

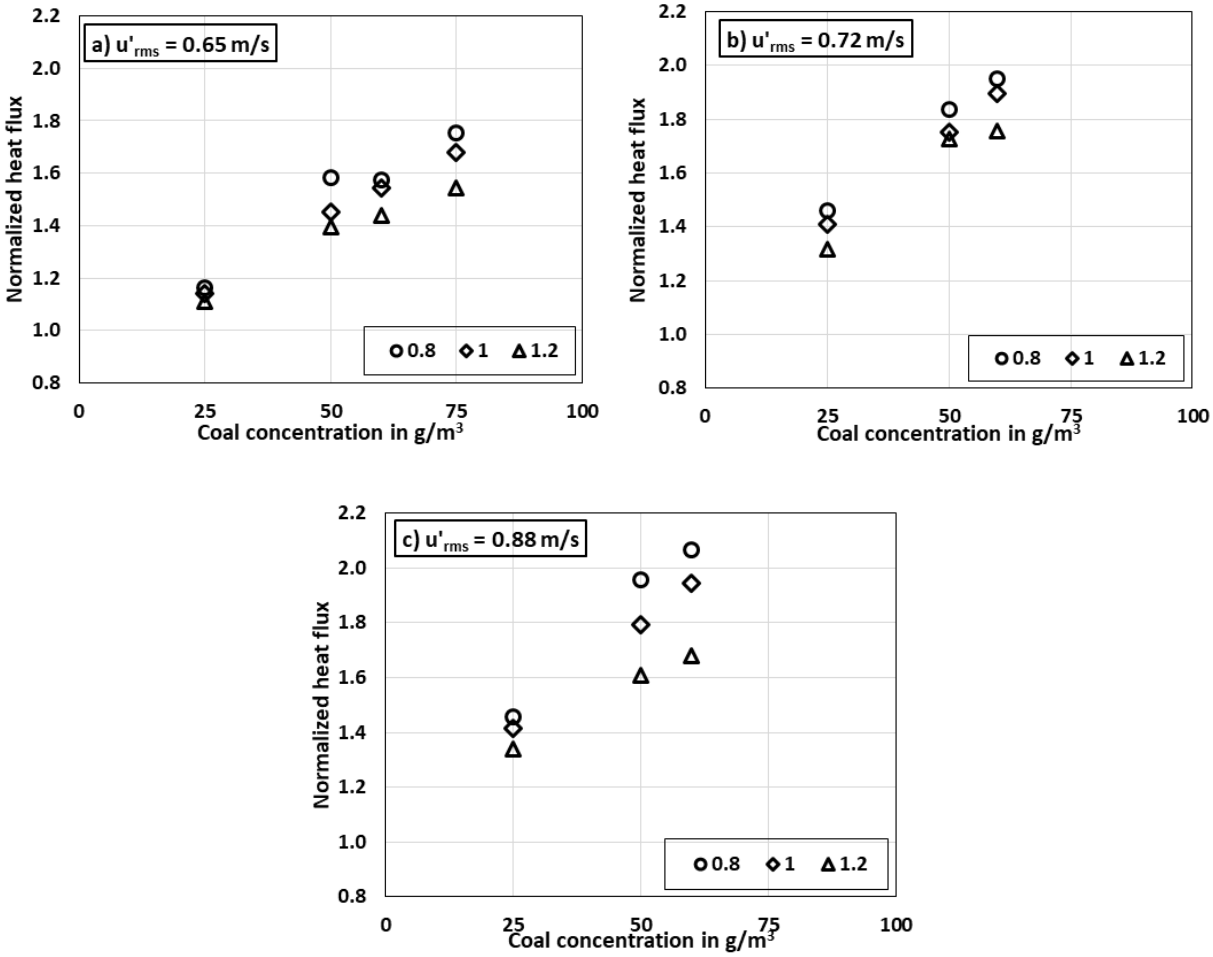

Figure 5.4: Variation of normalized heat flux for turbulent premixed methane-air-coal flames.

The addition of inert particles sand has a decreasing effect in the radiative heat flux values (Figure 5.5). The normalized heat flux values from methane-air-sand flames are always less than 1 and varied between the ranges of 0.76 to 0.98. This is again reflective of the heat sink nature of sand resulting in reduced flame temperature. An increase in the concentration of sand has negligible effect on the radiative heat flux values and the effect of gas phase equivalence ratio is similar to the trend of radiative heat flux variation for gas only premixed flames.

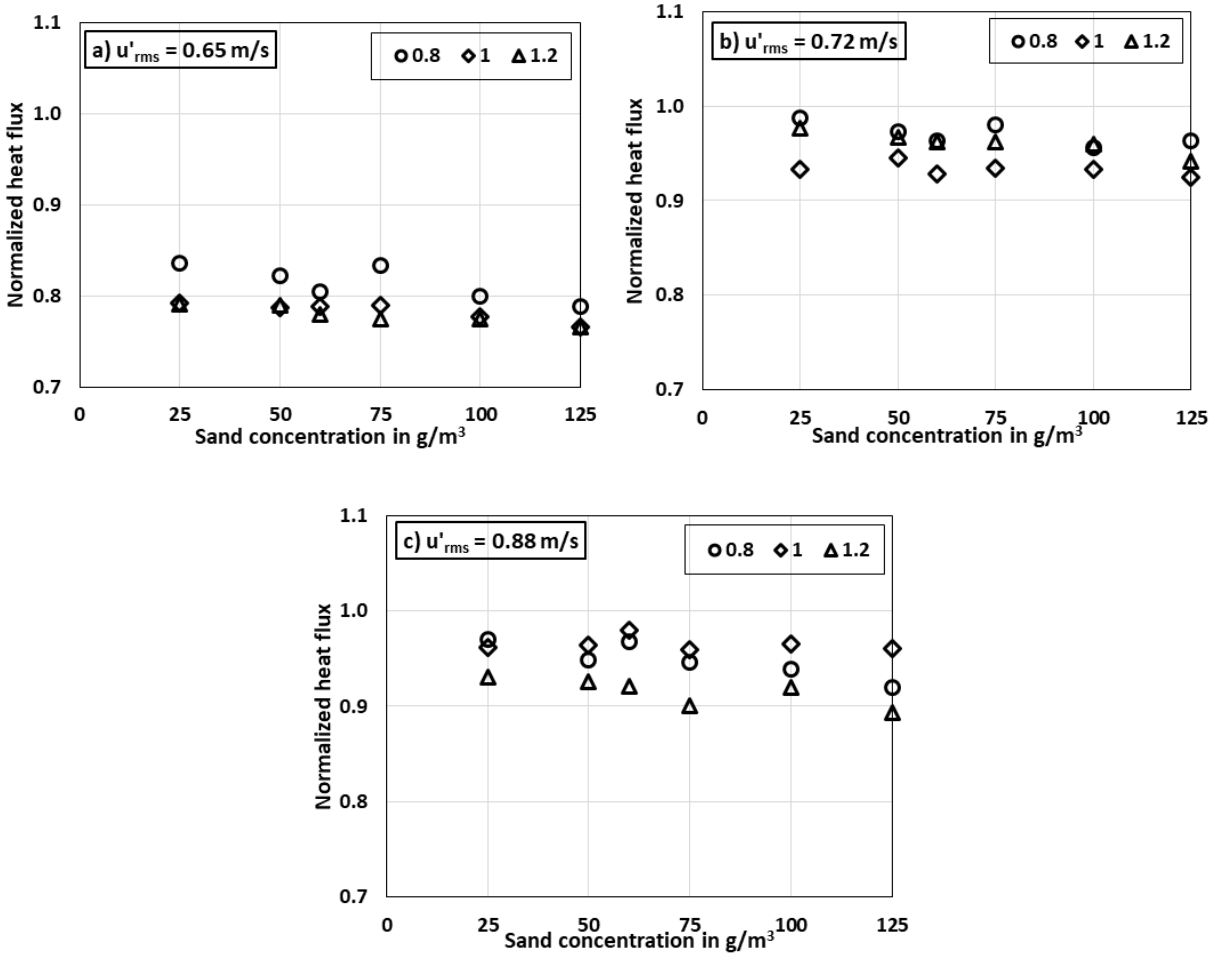

Figure 5.5: Variation of normalized heat flux for turbulent premixed methane-air-sand flames.

The radiative heat flux emitted by the premixed flames with the addition of sodium bicarbonate dust is different from that of coal and sand. With an increase in the concentration of sodium bicarbonate the normalized radiative heat flux decreases, indicating a chemical suppressive effect of $NaHCO_3$ due to reduced flame temperature. It is noted that as the turbulent intensity increases the normalized radiative heat flux values increases. This could be due to the increased vaporization of $NaHCO_3$ resulting in an increased release of CO_2 and H_2O. The normalized heat flux values varied from 0.47 to 1.14.

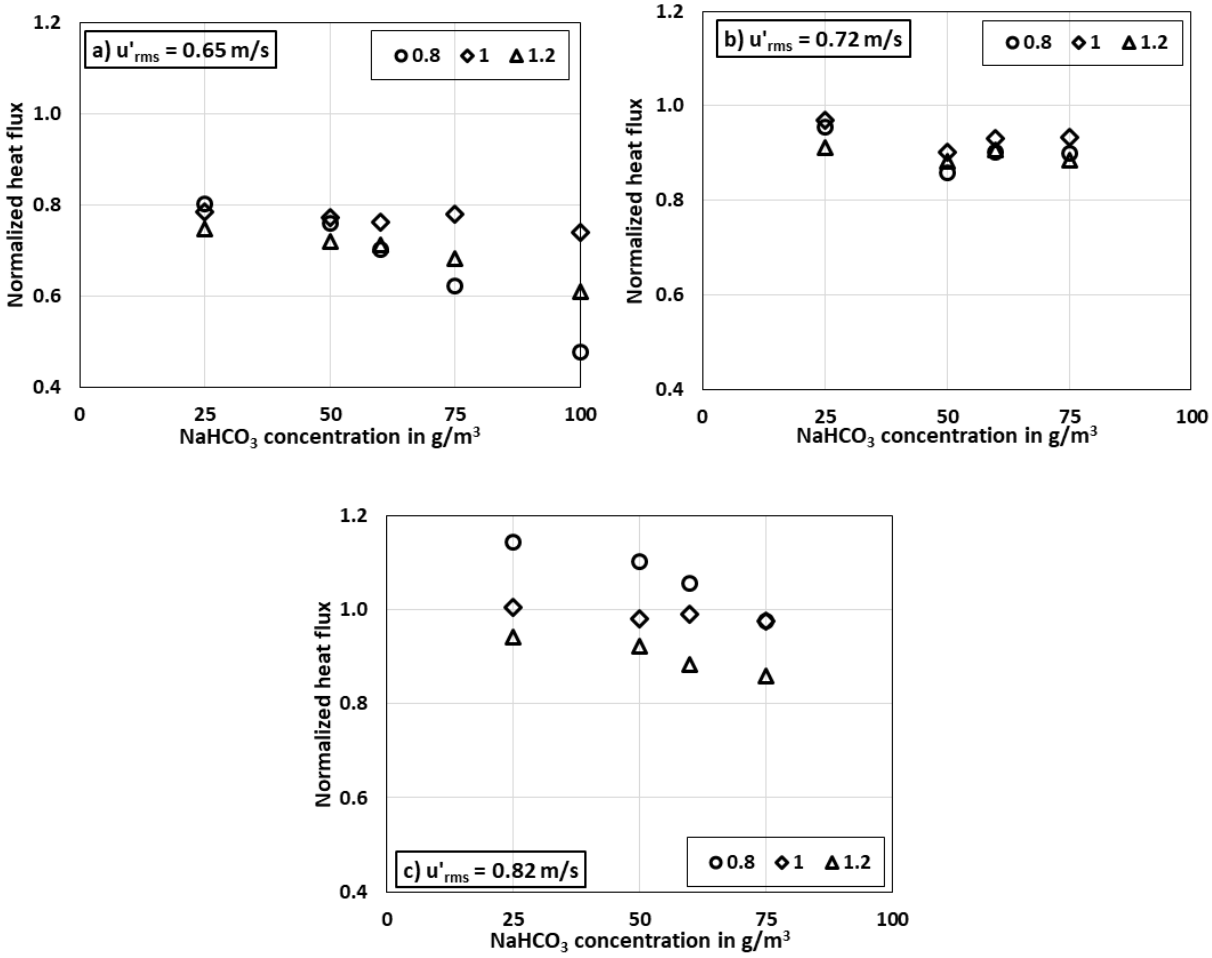

Figure 5.6: Variation of normalized heat flux for turbulent premixed methane-air-$NaHCO_3$ flames.

5.5.2 Variation of radiative fraction of heat released

The variation of radiative fraction from the tests considered with coal, sand and sodium bicarbonate, respectively, are presented in Figs. 5.9-5.11. In general, addition of dusts, irrespective of the dust type results in an increase in radiative fraction of the heat released as compared to the gas only flame. This is owing to the significant effect of dusts on the flame shape, size and luminosity. The radiative fraction of heat released from a particular fuel will vary with change in

flame or fire size (Markstein, [129]). It can be verified from Figs. 5.2 and 5.3 that the particle addition results in considerable radial and axial extension of the flame. A radial expansion factor, defined as $\delta_r = \frac{D_f}{d_i}$, ratio of average flame diameter to the inner diameter of the burner indicate that the type of the dust influences the average diameter of the flame. The radial expansion factor δ_r increased in the order of coal (δ_r = 1.52) > sodium bicarbonate (δ_r = 1.48) > sand (δ_r = 1.36) > gas (δ_r = 1). Clearly, the particles that generate volatiles have greater radial expansion as compared to sand which does not release any volatiles.

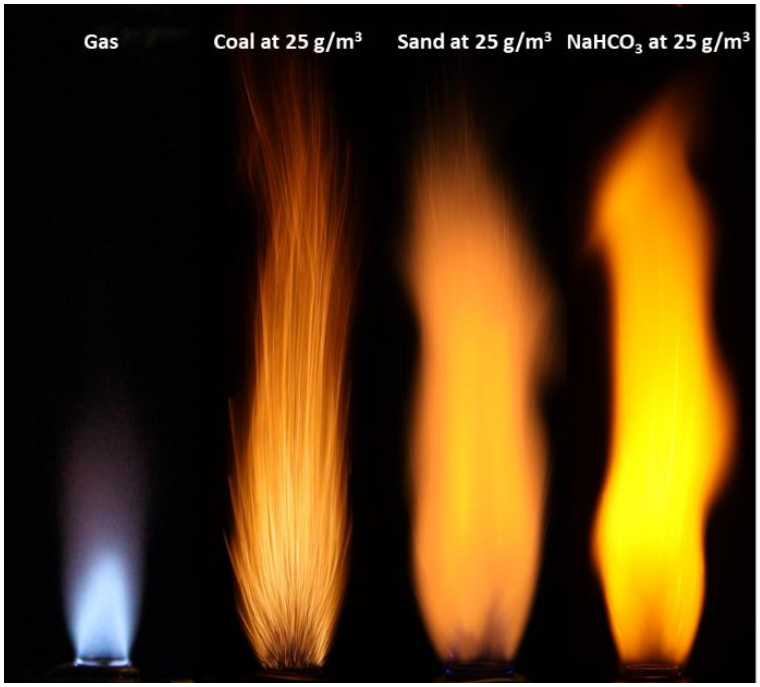

Figure 5.7: Instantaneous flame images showing the effect of particle addition at 25 g/m^3 on methane-air stoichiometric flame at u'_{rms}= 0.65 m/s.

It is obvious from Figure 5.7 that the addition of particles significantly increases the premixed gas burner flame height. This effect is quantified in Figure 5.8.a and Figure 5.8.c and it

significantly affects the radiative properties of premixed gas-dust premixed flames. Figure 5.8 explains this effect clearly as the sample plots indicate the effects of dust concentration, turbulent intensity and equivalence ratio on the average flame height. In this study, an increase in the turbulent intensity has been achieved by increasing the total flow rate of the gaseous mixture resulting in a high-momentum flame with longer flame height (Figure 5.8.b). The effect of equivalence ratio also becomes more prominent with the addition of dusts (Figure 5.8.c). The average flame height is less for stoichiometric methane-air case in gas only condition, whereas with the addition of particles, the flame height increases consistently with equivalence ratio. The higher flame temperature in the stoichiometric condition results in particles to transfer heat to further axially length as compared to the fuel lean condition. For fuel rich condition with particles, the presence of a larger outer zone of high temperature diffusion results in further increase in the average flame length.

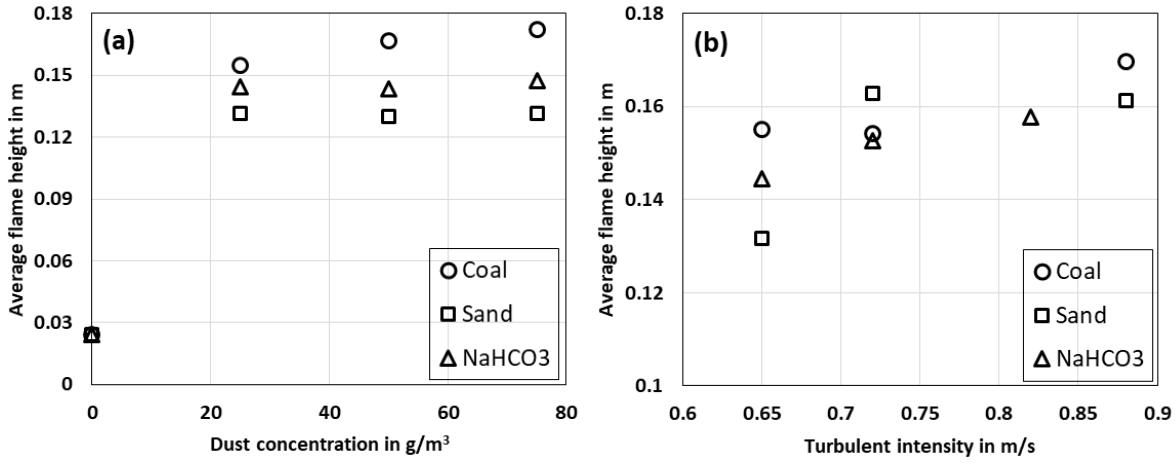

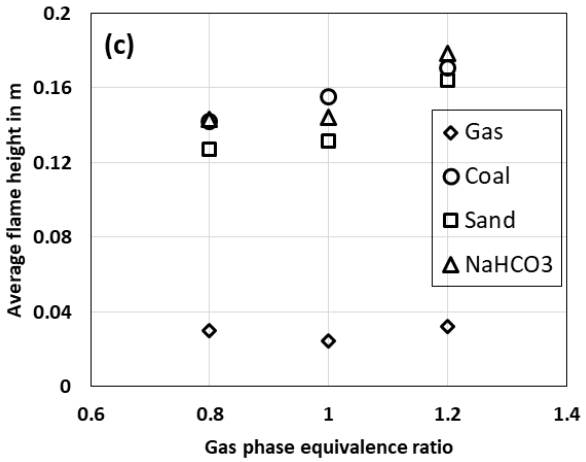

Figure 5.8: Variation of average flame height with (a) dust concentration at u'_{rms} = 0.65 m/s for stoichiometric methane-air flame; (b) turbulent intensity at λ_p = 25 g/m^3 for stoichiometric methane-air flame; (c) gas phase equivalence ratio at u'_{rms} = 0.65 m/s and at λ_p = 25 g/m^3.

It is observed that the type of the dust influence the radiative fraction of heat released. The flame radiation properties typically depend on the flame temperature and combustion species. Most often the premixed methane-air flame radiation is attributed to CO_2, H_2O, CO and CH_4 as the soot volume fraction is much small as compared to the non-premixed flames. It has been observed from the current study that the luminous emissions become significant with the addition of dusts. Dusts will absorb and emit radiation depending on the size and type of the particle. From the three dusts considered in this study, coal results in the maximum radiative fraction of heat. This is not only due to the additional effects of volatiles released in the form of methane adding to the gaseous emission but also from the continuous emission of hot soot particles with in the flame. This extends to visible spectrum resulting in luminous flames.

Even though sand and sodium bicarbonate are considered to be flame suppressants and thus expected to have resulted in smaller radiative heat flux values than gaseous premixed flames, their

addition result in an enhancement of radiative fraction of total heat released. As we have seen before sodium bicarbonate decomposition starts at 270 ^{o}C and this reaction is endothermic with an enthalpy change of 135 kJ/mol. The presence of sodium ions result in a luminous flame (Figure 5.7) and along with the presence of intermediate salts enhances the overall radiative fraction of heat released.

An increase in the concentration of coal (Figure 5.9) leads to an increase in the X_r until a certain concentration (~ 50 g/m^3) and then X_r levels off with further increase in the concentration. The value of 50 g/m^3 for plateau concentration is just below reported Minimum Explosible Concentrations (MEC) for Pittsburgh Seam Coal, which is in the range 60 g/m^3 to 80 g/m^3, depending on vessel size and igniter energy (Cashdollar and Hertzberg, [130], Cashdollar and Chatrathi, [131]). There is not much variation of X_r observed with an increase in the concentration of sand (Figure 5.10). Addition of $NaHCO_3$ shows a decrease in the value of X_r at dust concentrations of 75 g/m^3 for fuel lean and fuel rich conditions (Figure 5.11). Even though the decomposition of $NaHCO_3$ results in release of radiation absorption species such as CO_2 and H_2O, the decomposition reaction of $NaHCO_3$ is endothermic. This becomes predominant for fuel lean and fuel rich conditions resulting in a reduction in average flame temperature and hence reducing the radiative fraction at higher concentrations. Further, at higher particle concentration, the volumetric loading of the particle increases; this results in decreased inter particle spaces, restricting the diffusion of heat to individual particles and reduced particle decomposition. This explains the levelling off behavior of X_r at higher particle concentrations.

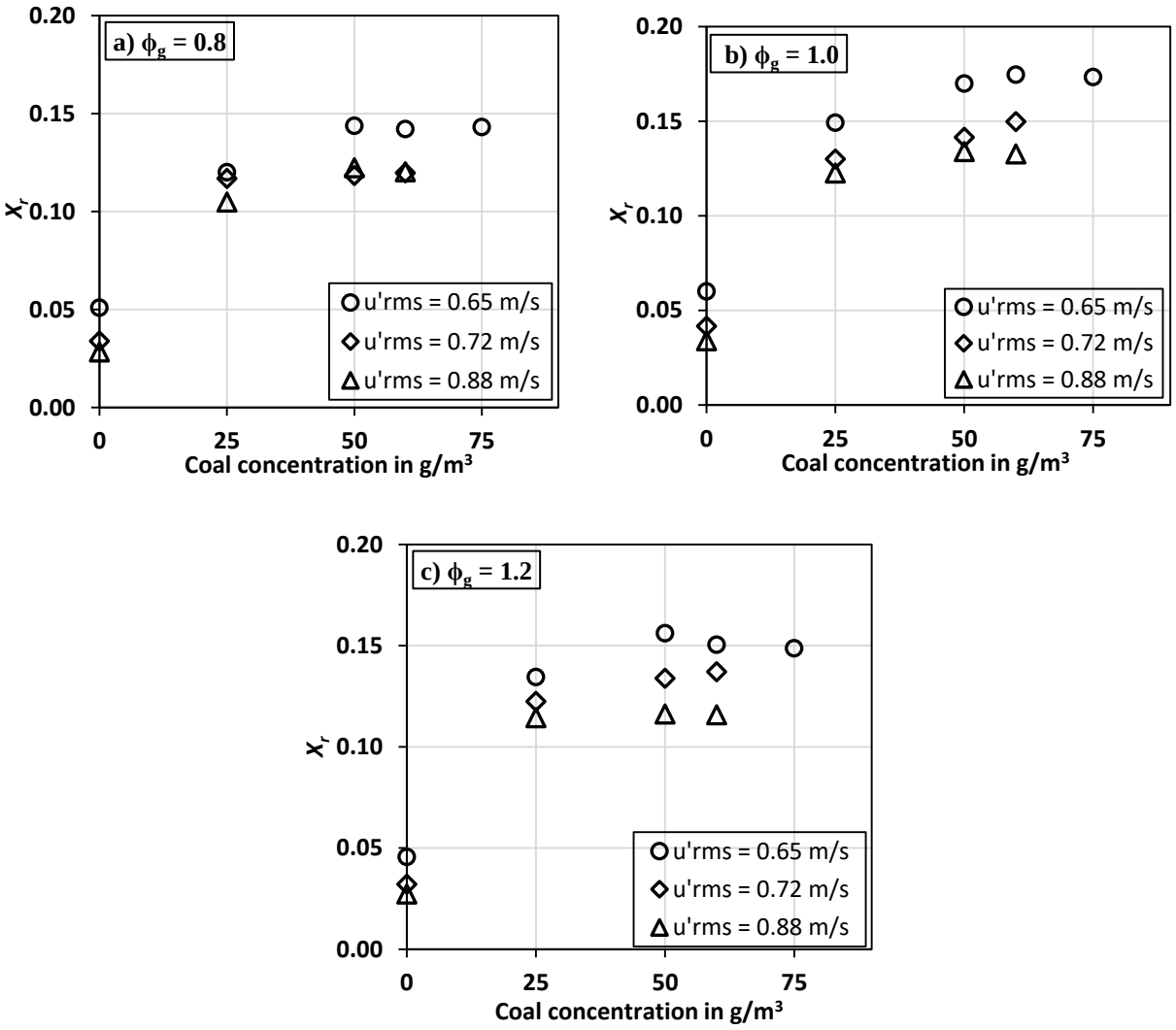

Figure 5.9: Variation of radiative fraction with the addition of coal.

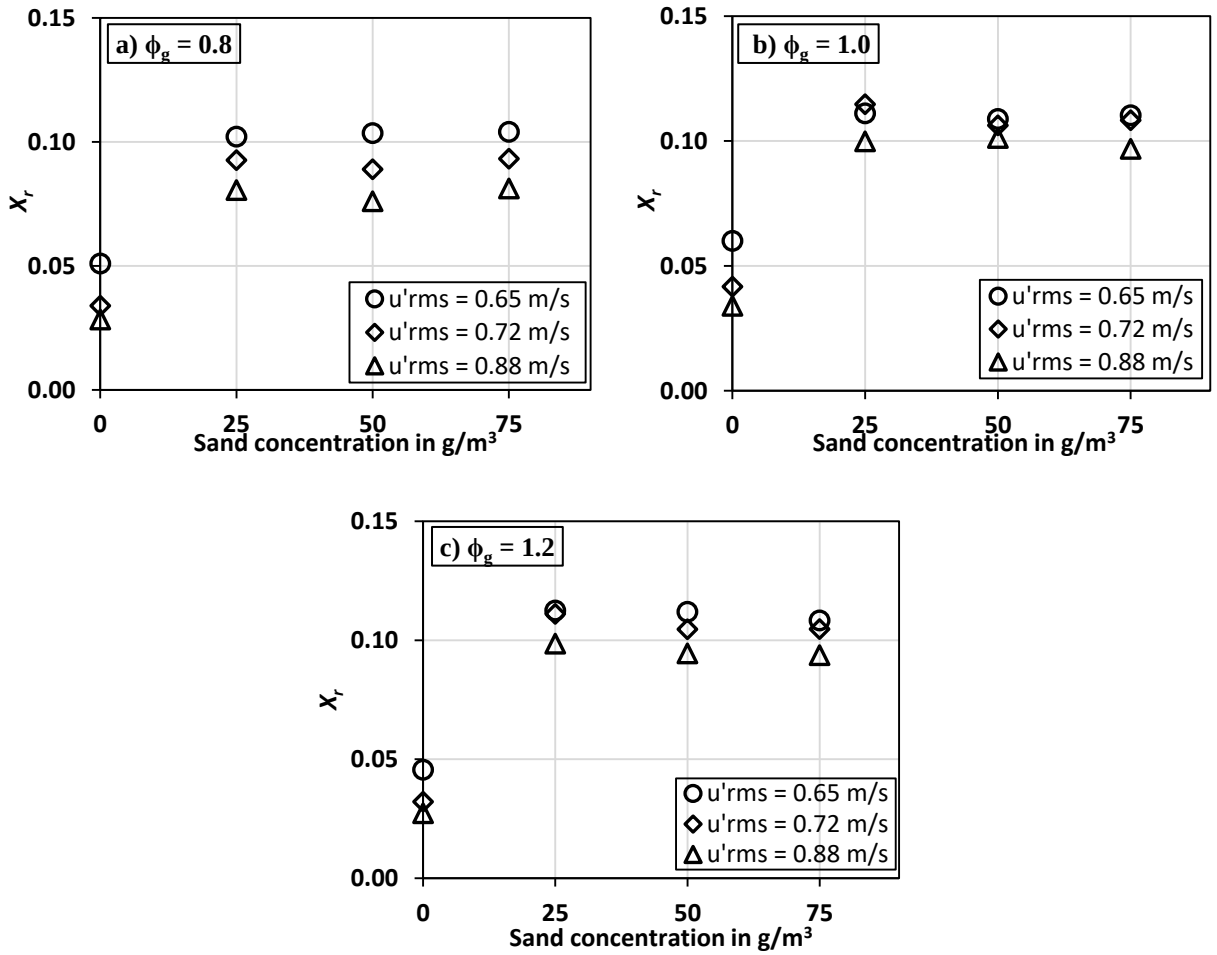

Figure 5.10: Variation of radiative fraction with the addition of sand.

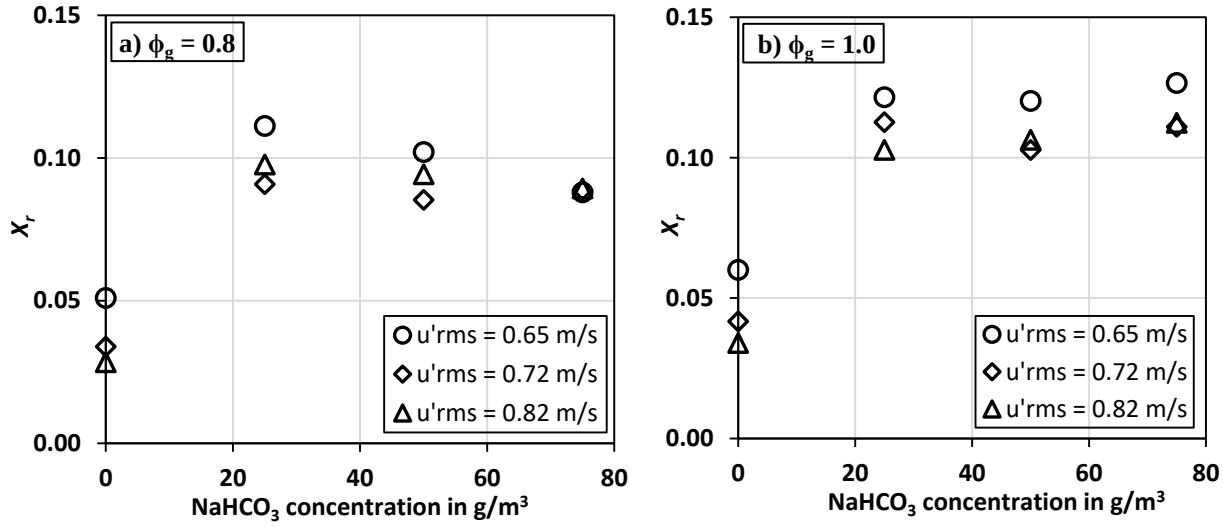

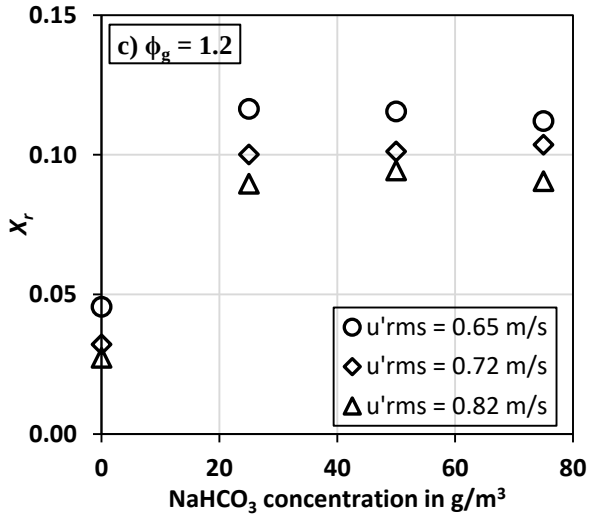

Figure 5.11: Variation of radiative fraction with the addition of sodium bicarbonate.

The rate of increase of radiative fraction with particle addition decreases with an increase in the turbulent intensity. This can be attributed to an increase in the average flow velocity resulting in a shorter residence time of the particle. This observation is consistent with that observed in turbulent jet flames (Wu et al. [132]), where with an increase in the velocity, a decrease in the radiative fraction has been reported.

Table 5.1: Radiative fraction from different pre-mixture conditions.

Pre-mixture condition	**No. of cases studied**	**Max. % X_r**	**Min. % X_r**	**Max. $\dot{q}_r''$ (kW/m^2)**	**Min. $\dot{q}_r''$ (kW/m^2)**
Methane-Air	9	6.00	2.73	7.20	4.0
Methane-Air-Coal	27	17.46	10.48	12.09	5.83
Methane-Air-Sand	27	11.47	7.60	5.70	3.79
Methane-Air-NaHCO3	27	12.66	8.53	5.84	3.29

Table 5.1 presents the minimum and maximum values of radiative fraction of heat release rate and radiative heat flux measured from all the cases studied with specific dust particles. The range of radiation fraction of heat released by gaseous methane-air premixed flame was between 2.7% - 6%. Table 5.1 indicates that the effect of dust addition in a gas premixed flame is to always increase the radiative heat fraction of heat released even though the measured radiative heat flux increases or decreases depending on the property of the dust added. The addition of coal results in a significant increase in the radiative fraction as well as the radiative heat flux. The average radiative fraction from premixed flame conditions with coal addition is around in the range of 10.5% – 17.5% this is comparable to that of methane-air jet diffusion flames (~ 20%) analyzed in prior studies (Alpert, [133]). This is because of the release of volatiles from coal particles, which are predominantly methane, resulting in a highly fuel rich flame conditions. Sand and sodium bicarbonate, being thermal and chemical flame suppressants, results in reducing the flame temperature and hence reduce the radiative heat flux of gas premixed flames. However, their influence in flame size has resulted in increasing the radiative fraction of heat released from the gas premixed flames. The radiative fractions with the addition of sand ranges from 7.6% - 11.5% and that of sodium bicarbonate ranges from 8.5% - 12.7%. The addition of $NaHCO_3$ results in slightly higher value of X_r as compared to sand, this could be due to the release of CO_2 and H_2O with the decomposition of $NaHCO_3$ at high temperature. The maximum value of radiative fraction is observed for stoichiometric methane-air gas mixture (ϕ_g = 1.0) and at low turbulent intensity considered (u'_{rms} = 0.65 m/s). With the addition of particles the maximum radiative fraction is observed at the higher dust concentration cases, 60-75 g/m^3. The minimum value of radiative fraction of heat released is observed at fuel lean methane-air gas mixture (ϕ_g = 0.8) and at high turbulent intensity (u'_{rms} = 0.82-0.88 m/s) considered. The results from this are clear indicative of

the influence of dusts on the flame temperature and flame size which ultimately affects the radiative fraction of heat released.

5.6 Conclusions

This chapter presents the radiative fraction of heat released by methane-air turbulent premixed flames with the addition of dust particles. Radiative heat flux measurements captured from burner stabilized methane-air-dust premixed flames at different equivalence ratios, and turbulent intensities were studied to understand the influence of different dust types (coal, sand and sodium bicarbonate) and dust concentrations. Results indicate that the addition of dust particles increase the radiative fraction of heat released irrespective of the dust type because of the radial and axial extension of the flame. An increase in the turbulent intensity decreases the X_r owing to shorter residence time of particles and an increased flame height. Addition of coal dust results in the maximum radiative fraction value of X_r = 17.46%, and behaves similar to methane jet diffusion flames at higher concentrations. However, sand and sodium bicarbonate results in maximum radiative fraction values of 11.5% and 12.6% respectively. The effect of dust concentration on X_r is to increase with the addition of coal, whereas with sand, dust concentration does not have much influence on X_r and an increase in sodium bicarbonate concentration has decreasing effect on both radiative fraction and radiative heat flux.

6 Summary and future directions

6.1 Summary

Interaction of dust particles with the gaseous premixed methane-air flames has been studied in this dissertation. The results obtained are quite useful to improve the understanding of burning velocity and radiative fraction of heat released from gas-dust premixed flames at atmospheric pressure conditions. This study focuses on the interaction of 75-90 μm sized combustible (coal), inert (sand), and dry chemical (sodium bicarbonate) particles on premixed methane-air flames. Both laminar and turbulent gaseous methane-air flames are used at fuel lean (ϕ_g = 0.8), stoichiometric (ϕ_g = 1.0) and fuel rich (ϕ_g = 1.2) equivalence ratios, for all the dusts studied. The influence of turbulence is studied through varying the turbulent intensities, u'_{rms} = 0.65, 0.72, 0.82, 0.88 m/s. The integral length scale of turbulence is maintained in the range of 2.7-2.9 mm, which is approximately equal to the perforated plate hole size (3 mm) used to generate turbulence. Along with the type of the dust, the concentration of dust is also very significant when they interact with flames. The dust concentrations are varied as λ_p = 0, 25, 50, 60, 75, 100 g/m^3 throughout the study. In addition, the flame extinction characteristics of sand and sodium bicarbonate particles are investigated on laminar flames whereas the radiative fraction of heat released from the gas-dust premixed flames are investigated for all the turbulent premixed flames.

Addition of sand and sodium bicarbonate always decreases the laminar burning velocity. At ϕ_g = 0.8, flame extinction occurs at 350 g/m^3 and 75 g/m^3 with sand and sodium bicarbonate

respectively; whereas at ϕ_g = 1.2 flame extinction occurs at 585 g/m^3 and 125 g/m^3 with sand and sodium bicarbonate, respectively. Flame extinction occurs at a lower particle concentration with sodium bicarbonate as compared to sand due to its heterogeneous nature. The concentration of sand resulting in flame extinction of lean and rich mixture is approximately 4.67 times higher as compared to that of sodium bicarbonate. The mathematical model developed based on heat sink nature of inert particles to predict the laminar burning velocity has been extended to generalize its applicability of flame extinction results and validated against the current experiments. The critical concentration of sand required for flame extinction predicted by mathematical model is in good agreement with experimental observations.

The results from turbulent premixed flames indicate that dust type and dust concentration play a major role in deciding the trend of variation of turbulent burning velocity, S_T. Coal particles tend to increase S_T with the release of volatiles (methane), except for fuel rich conditions and higher concentrations of coal at larger turbulent intensities. Sodium bicarbonate addition tends to decrease the burning velocity at all the concentrations, turbulent intensities, and equivalence ratios. The detailed time scale analysis conducted shows that the presence of particles in the concentration range considered tend to slightly enhance the cold flow turbulence whereas with the presence of flame zone, an increase in the turbulent intensity results in increasing the vaporization rate of the particles. This results in decreasing the turbulent burning velocity of methane-air mixtures with coal and sodium bicarbonate particles at higher concentrations and turbulent intensities. The time scale analysis for the vaporization of particle shows sodium bicarbonate has higher evaporation rate than coal at same level of turbulence. An increase in the turbulent intensity increases the vaporization rate of particles. Out of dust types examined, at smaller concentrations the turbulent burning velocity increases in the order coal > sand > sodium bicarbonate. But as the dust

concentration and turbulent intensity increases, the S_T values with sand becomes comparable to or greater than that of coal. Particle vaporization time scale analysis of particle vaporization (vaporization Damköhler number) indicates an increase in the vaporization rate for particles (coal and sodium bicarbonate) at higher turbulent intensities resulting in a decrease in their turbulent burning velocities at higher concentrations. The absence of this effect for sand along with an increase in the particle size results in higher turbulent burning velocities at higher concentrations.

The turbulence modulation exhibited by different particles and concentrations is evident in these observations. The chemical and convective times in gas phase confirm the broadened preheat thin reaction zone regime in the current test cases, which has the effect of attenuating turbulence the resulting turbulent burning velocity. The particle time scale analysis (Stokes number) show that the effects of particles and particle concentration are to slightly enhance the turbulence and increase the turbulent burning velocity at lower concentrations. Future research is necessary to couple these complex phenomenon of turbulence, particle interaction, particle vaporization and combustion in particle laden premixed gaseous flames. Model coefficients generated from the experimental data to estimate the turbulent burning velocity in these conditions show a clear distinction in the model coefficients between gaseous premixed flames versus gas-dust premixed flames.

The addition of dust particles always increases the radiative fraction of heat released, irrespective of the dust type, owing to the radial and axial extension of flame. An increase in the turbulent intensity decreases the radiative fraction due to shorter residence time of particles and an increased flame height. Addition of coal dust results in the maximum value of radiative fraction of heat released of X_r = 17.5%, and becomes comparable to that of methane jet diffusion flames at higher concentrations. However, adding sand and sodium bicarbonate gives approximately similar

average radiative fraction values. The range of radiative fractions of methane-air gaseous turbulent premixed flame is found to be 2.7% - 6%, whereas the addition of coal, sand, sodium bicarbonate and iron results in an increased range of X_r values of 10.5% - 17.5%, 7.6% - 11.5%, 8.5% - 12.7% and 9.4% - 15.1% respectively. In summary, a low radiating premixed flame becomes more radiative with the addition of dusts and with the addition of a combustible dust this becomes more significant.

6.2 Future directions

Future work includes:

- Conduct experiments to investigate the burning velocity of premixed flames interacting with a mixture of dust types, specifically to study the effects of inert and dry chemicals mixed with combustible dusts.
- Compare the hybrid mixture burning velocity results from constant pressure test conditions versus the constant volume test conditions.
- Study the extinction characteristics of turbulent premixed flames with inert and dry chemicals. This was attempted in the current study but the presence of the pilot flame in the burner prevented the turbulent flame from complete extinguishment and the limitations of the dust screw feeder prevented from going to higher particle concentrations.
- Extending the mathematical model to predict the burning velocity and extinction effects of dry chemicals (e.g., $NaHCO_3$) and validate with the experimental results. This will have a similar approach as that of mathematical model for coal particles [18], but need to be adjusted for the release of CO_2 and H_2O.

- Develop a theoretical model to predict the turbulent burning velocity of gas-dust premixed flames.
- Further clarify the turbulent combustion regime diagram to accommodate the turbulent modulation due to reacting or decomposing dusts.

7 Bibliography

[1] "Combustible Dust: An Explosion Hazard," *U. S. Chemical Safety Board*. [Online]. Available: https://www.osha.gov/dsg/combustibledust/.

[2] M. Griffon, "CSB Combustible Dust Incident Investigations Overview," in *Dust Explosion Hazards Symposium, Fire Protection Research Foundation*, 2011.

[3] S. Goroshin, F. D. Tang, A. J. Higgins, and J. H. S. Lee, "Laminar dust flames in a reduced-gravity environment," *Acta Astronaut.*, vol. 68, no. 7–8, pp. 656–666, 2011.

[4] *NFPA 68: Standard on Explosion Protection by Deflagration Venting*, 2013th ed. 2013.

[5] *NFPA 654: Standard for the Prevention of Fire and Dust Explosions from the Manufacturing, Processing, and Handling of Combustible Particulate Solids*, 2017th ed. 2017.

[6] M. Parekh, "Grain Dust Peril," *Ind. fire world*, vol. 13, no. 4, 1998.

[7] G. E. Andrews and D. Bradley, "Determination of burning velocities: A critical review," *Combust. Flame*, vol. 18, no. 1, pp. 133–153, 1972.

[8] *NFPA 69: Standard on Explosion Prevention Systems*, 1997th ed. 1997.

[9] *ASTM E1226-12a, Standard Test Method for Explosibility of Dust Clouds*. West Conshohocken, PA: ASTM International, 2012.

[10] *ISO 6184-1 Explosion protection systems - Part 1: Determination of explosion indices of combustible dusts in air*. 2005.

[11] R. K. Eckhoff, *Dust Explosions in the Process Industries*. Boston: Gulf Professional Publishing, 2003.

[12] A. D. Benedetto, A. Garcia-Agreda, O. Dufaud, I. Khalili, R. Sanchirico, N. Cuervo, L. Perrin, and P. Russo, "Flame Propagation of Dust and Gas-Air Mixtures in a Tube," in

Proceedings of 7th Mediterranean Combustion Symposium, Sardinia, Italy, 2011.

[13] S. R. Rockwell, *Influence of Coal Dust on Premixed Turbulent Methane–air Flames*. PhD thesis, Fire Protection Engineering, Worcester Polytechnic Institute., 2012.

[14] H. M. Cassel, A. K. D. Gupta, and S. Guruswamy, "Factors Affecting Flame Propagation through Dust Clouds," *Third Symp. Combust. Flame Explos. Phenom.*, pp. 185–190, 1949.

[15] J. Lee, S. Goroshin, and M. Kolbe, "Burning Velocity Measurements in Aluminum-Air Suspensions using Bunsen Type Dust Flames," in *Sixth International Microgravity Combustion Workshop*, 2001, pp. 221–224.

[16] Y. Liu, J. Sun, and D. Chen, "Flame propagation in hybrid mixture of coal dust and methane," *J. Loss Prev. Process Ind.*, vol. 20, no. 4, pp. 691–697, 2007.

[17] Y. Xie, V. Raghavan, and A. S. Rangwala, "Study of interaction of entrained coal dust particles in lean methane–air premixed flames," *Combust. Flame*, vol. 159, no. 7, pp. 2449–2456, 2012.

[18] M. Lee, S. Ranganathan, and A. S. Rangwala, "Influence of the reactant temperature on particle entrained laminar methane-air premixed flames," *Proc. Combust. Inst.*, vol. 35, no. 1, pp. 729–736, 2015.

[19] S. R. Rockwell and A. S. Rangwala, "Influence of coal dust on premixed turbulent methane–air flames," *Combust. Flame*, vol. 160, no. 3, pp. 635–640, 2013.

[20] R. A. Ogle, "Chapter 1 - Introduction to combustible dust hazards," in *Dust Explosion Dynamics*, R. A. Ogle, Ed. Butterworth-Heinemann, 2017, pp. 1–34.

[21] J.-H. Sun, R. Dobashi, and T. Hirano, "Combustion behavior of iron particles suspended in air," *Combust. Sci. Technol.*, vol. 150, no. November, pp. 99–114, 2000.

[22] P. Julien, *On the study of flames in aluminum and iron suspensions*. PhD Thesis, Mechanical

Engineering, McGill University, Montreal., 2016.

[23] N. I. Poletaev, A. N. Zolotko, and Y. A. Doroshenko, “Degree of dispersion of metal combustion products in a laminar dust flame,” *Combust. Explos. Shock Waves*, vol. 47, no. 2, pp. 153–165, 2011.

[24] G. Joulin and B. Deshaies, “On Radiation-Affected Flame Propagation in Gaseous Mixtures Seeded with ln´ert Particles,” *Combust. Sci. Technol.*, vol. 47, no. 5–6, pp. 299–315, 1986.

[25] M. Dewitte, J. Vrebosch, and A. van Tiggelen, “Inhibition and extinction of premixed flames by dust particles,” *Combust. Flame*, vol. 8, no. 4, pp. 257–266, 1964.

[26] M. L. Harris, E. S. Weiss, C. K. Man, S. P. Harteis, and G. V. Goodman, “Rock dusting considerations in underground coal mines,” in *Proc. of the 13th US/North American Mine Ventilation Symp.*, 2010, pp. 267–271.

[27] M. Faraday and C. Lyell, “Report on the subject of the explosion at the Haswell Collieries, and on the means of preventing similar accidents.,” *London, Edinburgh, Dublin Philos. Mag. J. Sci.*, vol. 26, pp. 16–35, 1845.

[28] H. K. Chelliah, “Flame inhibition/suppression by water mist: Droplet size/surface area, flame structure, and flow residence time effects,” *Proc. Combust. Inst.*, vol. 31, no. 2, pp. 2711–2719, 2007.

[29] J. W. Fleming, “Chemical Fire Suppressants: How can we replace Halon?,” in *Proc. Fall Technical Meeting of the Eastern States Combustion Institute, Raleigh, NC*, 1999.

[30] M. D. Rumminger and G. T. Linteris, “The role of particles in the inhibition of premixed flames by iron pentacarbonyl,” *Combust. Flame*, vol. 123, no. 1, pp. 82–94, 2000.

[31] J. D. Birchall, “On the mechanism of flame inhibition by alkali metal salts,” *Combust. Flame*, vol. 14, no. 1, pp. 85–95, 1970.

[32] G. T. Linteris, M. D. Rumminger, and V. I. Babushok, “Catalytic inhibition of laminar flames by transition metal compounds,” *Prog. Energy Combust. Sci.*, vol. 34, no. 3, pp. 288–329, 2008.

[33] T. Mitani and T. Niioka, “Extinction phenomenon of premixed flames with alkali metal compounds,” *Combust. Flame*, vol. 55, no. 1, pp. 13–21, 1984.

[34] D. Trees and K. Seshadri, “Experimental Studies of Flame Extinction by Sodium Bicarbonate (NaHCO3) Powder,” *Combust. Sci. Technol.*, vol. 122, no. 1–6, pp. 215–230, 1997.

[35] P. R. Amyotte, “Solid inertants and their use in dust explosion prevention and mitigation,” *J. Loss Prev. Process Ind.*, vol. 19, no. 2, pp. 161–173, 2006.

[36] M. G. Andac, F. N. Egolfopoulos, C. S. Campbell, and R. Lauvergne, “Effects of inert dust clouds on the extinction of strained, laminar flames at normal-and micro-gravity,” *Proc. Combust. Inst.*, vol. 28, no. 2, pp. 2921–2929, 2000.

[37] T. Mitani, “A flame inhibition theory by inert dust and spray,” *Combust. Flame*, vol. 43, no. Supplement C, pp. 243–253, 1981.

[38] G. Dong, B. Fan, B. Xie, and J. Ye, “Experimental investigation and numerical validation of explosion suppression by inert particles in large-scale duct,” *Proc. Combust. Inst.*, vol. 30, no. 2, pp. 2361–2368, 2005.

[39] C. A. Schneider, W. S. Rasband, and K. W. Eliceiri, “NIH Image to ImageJ: 25 years of image analysis.,” *Nat. Methods*, vol. 9, no. 7, pp. 671–675, Jul. 2012.

[40] H. Kobayashi, T. Tamura, K. Maruta, T. Niioka, and F. A. Williams, “Burning velocity of turbulent premixed flames in a high-pressure environment,” *Symp. Combust.*, vol. 26, no. 1, pp. 389–396, 1996.

[41] Y. Liu and B. Lenze, “The influence of the turbulence on the burning velocities of CH4-H2 mixtures,” *22nd Symp. Combust.*, vol. 22, no. 1, pp. 747–754, 1988.

[42] S. B. Pope, “Turbulent Premixed Flames,” *Annu. Rev. Fluid Mech.*, vol. 19, no. 1, pp. 237–270, 1987.

[43] T. M. Wabel, A. W. Skiba, and J. F. Driscoll, “Turbulent burning velocity measurements: Extended to extreme levels of turbulence,” *Proc. Combust. Inst.*, vol. 36, no. 2, pp. 1801–1808, 2017.

[44] T. M. Wabel, A. W. Skiba, J. E. Temme, and J. F. Driscoll, “Measurements to determine the regimes of premixed flames in extreme turbulence,” *Proc. Combust. Inst.*, vol. 36, no. 2, pp. 1809–1816, 2017.

[45] H. H. Bruun, *Hot wire anemometry : principles and signal analysis*. Oxford University Press, USA, 1995.

[46] N. Peters, *Turbulent Combustion*. Cambridge: Cambridge University Press, 2000.

[47] M. Lee, *Influence of the reactant temperature on particle entrained laminar methane-air premixed flames*. Worcester Polytechnic Institute, 2014.

[48] Yanxuan Xie, *Study of interaction of Entrained Coal Dust Particles in Lean Methane- Air Prtemixed Flames*. Worcester Polytechnic Institute, 2011.

[49] P. F. Thorne, “Inhibition of the combustion of liquid and gaseous fuels by finely divided inorganic salts: A literature review,” 1965.

[50] P. Kosinski, “Numerical investigation of explosion suppression by inert particles in straight ducts,” *J. Hazard. Mater.*, vol. 154, no. 1, pp. 981–991, 2008.

[51] L. Qiao, C. H. Kim, and G. M. Faeth, “Suppression effects of diluents on laminar premixed hydrogen/oxygen/nitrogen flames,” *Combust. Flame*, vol. 143, no. 1, pp. 79–96, 2005.

[52] J. D. Birchall, “On the mechanism of flame inhibition by alkali metal salts,” *Combust. Flame*, vol. 14, no. 1, pp. 85–95, 1970.

[53] W. A. Rosser, S. H. Inami, and H. Wise, “The effect of metal salts on premixed hydrocarbon—air flames,” *Combust. Flame*, vol. 7, pp. 107–119, 1963.

[54] P. Laffitte, R. Delbourgo, J. Comborieu, and J. C. Dumont, “The Influence of Particle Diameter on the Specificity of Fine Powders in the Extinction of Flames,” *Combust. Flame*, vol. 9, pp. 357–367, 1963.

[55] A. Hamins, “Flame extinction by sodium bicarbonate powder in a cup burner,” *Symp. Combust.*, vol. 27, no. 2, pp. 2857–2864, 1998.

[56] R. Friedman and J. B. Levy, “Survey of fundamental knowledge of mechanisms of action of flame extinguishing agents,” *WADC Tech. Rep.*, vol. 56, no. 568, 1957.

[57] P. Hoorelbeke, K. Van Wingerden, and V. U. Brussels, “Experimental study of inhibition of premixed flames,” in *International Colloquium on the Dynamics of Explosions and Reactive Systems*, 2009, pp. 20–23.

[58] H. K. Chelliah, A. K. Lazzarini, P. C. Wanigarathne, and G. T. Linteris, “Comparison of the fire suppression effectiveness of sodium bicarbonate particles and fine-water droplets in non-premixed and premixed flames,” in *Halon Options Technical Working Conference*, 2001, no. April, pp. 389–394.

[59] M. Lee, S. Ranganathan, and A. S. Rangwala, “Influence of the reactant temperature on particle entrained laminar methane-air premixed flames,” *Proc. Combust. Inst.*, vol. 35, no. 1, 2015.

[60] S. Ranganathan, M. Lee, V. Akkerman, and A. S. Rangwala, “Suppression of premixed flames with inert particles,” *J. Loss Prev. Process Ind.*, vol. 35, 2015.

[61] C. K. Law, *Combustion physics*, vol. 9780521870. Cambridge University Press, 2006.

[62] R. Skaggs, “Assessment of the fire suppression mechanics for HFC-227ea combined with NaHCO3,” in *Proceedings of 12th Halon Options Technical Working Conference*, 2002, pp. 1–11.

[63] S. R. Turns, *An introduction to combustion: concepts and applications*, 2nd ed., vol. 499. McGraw-Hill, 2000.

[64] B. Lewis and G. von Elbe, “Stability and Structure of Burner Flames,” *J. Chem. Phys.*, vol. 11, no. 2, pp. 75–97, 1943.

[65] B. Lewis and G. von Elbe, “CHAPTER V - Combustion Waves in Laminar Flow,” in *Combustion, Flames and Explosions of Gases (Third Edition)*, San Diego: Academic Press, 1987, pp. 215–417.

[66] G. von Elbe and M. Mentser, “Further Studies of the Structure and Stability of Burner Flames,” *J. Chem. Phys.*, vol. 13, no. 2, pp. 89–100, 1945.

[67] K. Seshadri, A. L. Berlad, and V. Tangirala, “The structure of premixed particle-cloud flames,” *Combust. Flame*, vol. 89, no. 3–4, pp. 333–342, 1992.

[68] S. G. Davis, P. C. Hinze, O. R. Hansen, and K. van Wingerden, “Does your facility have a dust problem: Methods for evaluating dust explosion hazards,” *J. Loss Prev. Process Ind.*, vol. 24, no. 6, pp. 837–846, 2011.

[69] *U S Chemical Safety and Hazard Investigation Board. Investigation Report: Combustible Dust Hazard Study*. 2006.

[70] A. E. Dahoe, R. S. Cant, and B. Scarlett, “On the Decay of Turbulence in the 20-Liter Explosion Sphere,” *Flow, Turbul. Combust.*, vol. 67, no. 3, pp. 159–184, Nov. 2001.

[71] M. Maeda, K. Hishida, and T. Furutani, “Optical measurements of local gas and particle

velocity in an upward flowing dilute gas–solids suspension.," *ASME Polyph. Flow Transp. Technol.*, 1980.

[72] S. L. Lee and F. Durst, "On the motion of particles in turbulent duct flows," *Int. J. Multiph. Flow*, vol. 8, no. 2, pp. 125–146, 1982.

[73] Y. Tsuji, Y. Morikawa, and H. Shiomi, "LDV measurements of an air-solid two-phase flow in a vertical pipe," *J. Fluid Mech.*, vol. 139, pp. 417–434, 1984.

[74] R. A. Gore and C. T. Crowe, "Effect of particle size on modulating turbulent intensity," *Int. J. Multiph. Flow*, vol. 15, no. 2, pp. 279–285, 1989.

[75] C. T. Crowe, "On models for turbulence modulation in fluid particle flows," *Int. J. Multiph. Flow*, vol. 26, pp. 719–727, 2000.

[76] A. Saber, T. S. Lundström, and J. G. I. Hellström, "Turbulent Modulation in Particulate Flow : A Review of Critical Variables," *Engineering*, no. October, pp. 597–609, 2015.

[77] S. Elghobashi, "On predicting particle-laden turbulent flows," *Appl. Sci. Res.*, vol. 52, no. 4, pp. 309–329, Jun. 1994.

[78] S. Elghobashi, "An Updated Classification Map of Particle-Laden Turbulent Flows," *IUTAM Symp. Comput. Approaches to Multiph. Flow*, vol. 81, pp. 3–10, 2006.

[79] C. Brennen, "Fundamentals of Multiphase Flows," *Cambridge Univ. Press*, vol. 128, p. 368, 2005.

[80] Y. Hardalupas, A. M. K. P. Taylor, and J. H. Whitelaw, "Velocity and particle-flux characteristics of turbulent particle-laden jets," *Proc. R. Soc. London A Math. Phys. Eng. Sci.*, vol. 426, no. 1870, pp. 31–78, 1989.

[81] M. Mandø, *Turbulence Modulation by Non-spherical Particles*. PhD Thesis, Aalborg: Aalborg Universitet, 2009.

[82] J. H. Grover, E. N. Fales, and A. C. Scurlock, “Turbulent flame studies in two-dimensional open burners,” *Symp. Combust.*, vol. 9, no. 1, pp. 21–35, 1963.

[83] R. Borghi, “On the Structure and Morphology of Turbulent Premixed Flames,” in *Recent Advances in the Aerospace Sciences: In Honor of Luigi Crocco on His Seventy-fifth Birthday*, Boston, MA: Springer US, 1985, pp. 117–138.

[84] N. Peters, “Laminar flamelet concepts in turbulent combustion,” *Symp. Combust.*, vol. 21, no. 1, pp. 1231–1250, 1988.

[85] A. E. Dahoe, *Dust Explosions: A Study of Flame Propagation*. PhD Thesis, Delft University of Technology, Delft, The Netherlands, 2000.

[86] S. R. Chakravarthy, “Mod-11 Lec-48 Turbulent Combustion 2,” 2016. [Online]. Available: https://www.youtube.com/watch?v=tMny1GeAjqM&list=PLbMVogVj5nJQDbg-ivB9ilWI9h3aJ78-y&index=48.

[87] Y. Levy and F. C. Lockwood, “Velocity measurements in a particle laden turbulent free jet,” *Combust. Flame*, vol. 40, pp. 333–339, 1981.

[88] G. Hetsroni and M. Sokolov, “Distribution of Mass, Velocity, and Intensity of Turbulence in a Two-Phase Turbulent Jet,” *J. Appl. Mech.*, vol. 38, no. 2, pp. 315–327, Jun. 1971.

[89] D. Modarress, S. Elghobashi, and H. Tan, “Two-component LDA measurement in a two-phase turbulent jet,” *AIAA J.*, vol. 22, no. 5, pp. 624–630, May 1984.

[90] D. Modarress, J. Wuerer, and S. Elghobashi, “An experimental study of a turbulent round two-phase jet,” *Chem. Eng. Commun.*, vol. 28, no. 4–6, pp. 341–354, Jul. 1984.

[91] J.-S. Shuen, A. S. P. Solomon, G. M. Faeth, and Q.-F. Zhang, “Structure of particle-laden jets - Measurements and predictions,” *AIAA J.*, vol. 23, no. 3, pp. 396–404, Mar. 1985.

[92] R. N. Parthasarathy and G. M. Faeth, “Structure of particle-laden turbulent water jets in still

water," *Int. J. Multiph. Flow*, vol. 13, no. 5, pp. 699–716, 1987.

[93] R. Zisselmar and O. Molerus, "Investigation of solid—liquid pipe flow with regard to turbulence modification," *Chem. Eng. J.*, vol. 18, no. 3, pp. 233–239, 1979.

[94] T.-Y. Sun and G. M. Faeth, "Structure of turbulent bubbly jets—I. Methods and centerline properties," *Int. J. Multiph. Flow*, vol. 12, no. 1, pp. 99–114, 1986.

[95] T. G. Theofanous and J. Sullivan, "Turbulence in two-phase dispersed flows," *J. Fluid Mech.*, vol. 116, pp. 343–362, 1982.

[96] S. K. Wang, S. J. Lee, O. C. Jones, and R. T. Lahey, "3-D turbulence structure and phase distribution measurements in bubbly two-phase flows," *Int. J. Multiph. Flow*, vol. 13, no. 3, pp. 327–343, 1987.

[97] K. Annamalai and W. Ryan, "Interactive processes in gasification and combustion-II. Isolated carbon, coal and porous char particles," *Prog. Energy Combust. Sci.*, vol. 19, no. 5, pp. 383–446, 1993.

[98] B. J. Urzay, "A revised spray-combustion diagram of diffusion-controlled burning regimes in fuel-spray clouds," *Annu. Res. Briefs, Cent. Turbul. Res. Stanford Univ.*, pp. 193–198, 2011.

[99] H. H. Chiu and T. M. Liu, "Group Combustion of Liquid Droplets," *Combust. Sci. Technol.*, vol. 17, no. 3–4, pp. 127–142, 1977.

[100] I. Gökalp, C. Chauveau, O. Simon, and X. Chesneau, "Mass transfer from liquid fuel droplets in turbulent flow," *Combust. Flame*, vol. 89, pp. 286–298, 1992.

[101] J. S. Wu, Y. J. Liu, and H. J. Sheen, "Effects of ambient turbulence and fuel properties on the evaporation rate of single droplets," *Int. J. Heat Mass Transf.*, vol. 44, no. 24, pp. 4593–4603, 2001.

[102] J. S. Wu, K. H. Hsu, P. M. Kuo, and H. J. Sheen, “Evaporation model of a single hydrocarbon fuel droplet due to ambient turbulence at intermediate Reynolds numbers,” *Int. J. Heat Mass Transf.*, vol. 46, no. 24, pp. 4741–4745, 2003.

[103] M. Birouk and I. Gökalp, “Current status of droplet evaporation in turbulent flows,” *Prog. Energy Combust. Sci.*, vol. 32, no. 4, pp. 408–423, 2006.

[104] S. Ranganathan, D. Petrow, S. R. Rockwell, and A. S. Rangwala, “Experimental Investigation of Laminar Premixed Methane-Air Flame Extinction with Sand and Sodium Bicarbonate Particles,” in *Proceedings of 10th U. S. National Combustion Meeting, MD*.

[105] G. Damköhler, *The effect of turbulence on the flame velocity in gas mixtures*. Washington: National Advisory Committee for Aeronautics: NACA-TM-1112, 1947.

[106] K. I. Schelkin, “On combustion in a turbulent flow,” Washington, 1947.

[107] N. Peters, “The turbulent burning velocity for large-scale and small-scale turbulence,” *J. Fluid Mech.*, vol. 384, pp. 107–132, 1999.

[108] K. N. C. Bray, “Turbulent flows with premixed reactants. In: Libby P.A., Williams F.A. (eds) Turbulent Reacting Flows.,” in *Topics in Applied Physics book series (TAP)*, Berlin, Heidelberg: Springer, 1980, pp. 115–183.

[109] F. A. Williams, *Combustion Theory*, 2nd ed. Addison-Wesley, 1985.

[110] S. J. Brookes and J. B. Moss, “Soot Production and Thermal Radiation from Turbulent Jet Diffusion Flames,” vol. 61, pp. 49–61, 1996.

[111] J. G. Quintiere and T. G. Cleary, “Heat flux from flames to vertical surfaces,” *Fire Technol.*, vol. 30, no. 2, pp. 209–231, 1994.

[112] J. P. Ji, J. Sivathanu, Y. R. Gore, “Thermal Radiation Properties of Turbulent Lean Premixed Methane Air,” vol. 28, pp. 391–398, 2000.

[113] F. J. Higuera and V. Muntean, “Effect of radiation losses on very lean methane/air flames propagating upward in a vertical tube,” *Combust. Flame*, vol. 161, no. 9, pp. 2340–2347, 2014.

[114] Y. Shoshin, G. Gorecki, J. Jarosinski, and T. Fodemski, “Experimental study of limit lean methane/air flame in a standard flammability tube using particle image velocimetry method,” *Combust. Flame*, vol. 157, no. 5, pp. 884–892, 2010.

[115] A. Haghiri and M. Bidabadi, “Modeling of laminar flame propagation through organic dust cloud with thermal radiation effect,” *Int. J. Therm. Sci.*, vol. 49, no. 8, pp. 1446–1456, 2010.

[116] S.-M. Jeng, M.-C. Lai, and G. M. Faeth, “Nonluminous Radiation in Turbulent Buoyant Axisymmetric Flames,” *Combust. Sci. Technol.*, vol. 40, no. 1–4, pp. 41–53, 1984.

[117] T. Fujimori, Y. Hamano, and J. Sato, “Radiative heat loss and NOx emission of turbulent jet flames in preheated air up to 1230 K,” *Proc. Combust. Inst.*, vol. 28, no. 1, pp. 455–461, 2000.

[118] Y. R. Sivathanu and J. P. Gore, “Total radiative heat loss in jet flames from single point radiative flux measurements,” *Combust. Flame*, vol. 94, no. 3, pp. 265–270, 1993.

[119] A. Hamins, M. Klassen, J. Gore, and T. Kashiwagi, “Estimate of flame radiance via a single location measurement in liquid pool fires,” *Combust. Flame*, vol. 86, no. 3, pp. 223–228, 1991.

[120] G. Hankinson and B. J. Lowesmith, “A consideration of methods of determining the radiative characteristics of jet fires,” *Combust. Flame*, vol. 159, no. 3, pp. 1165–1177, 2012.

[121] S. G. Davis, P. C. Hinze, O. R. Hansen, and K. Van Wingerden, “Does your facility have a dust problem: Methods for evaluating dust explosion hazards,” *J. Loss Prev. Process Ind.*, vol. 24, no. 6, pp. 837–846, 2011.

[122] P. R. Amyotte and M. J. Pegg, “Explosion hazards in underground coal mines,” *Toxicol. Environ. Chem.*, vol. 40, no. 1–4, pp. 189–199, 1993.

[123] J. F. Brune, K. L. Cashdollar, and R. K. Zipf, “Explosion Prevention in United States Coal Mines. NIOSHTIC2 Number: 20032689,” in *Proceedings of the 32nd International Conference of Safety in Mines Research Institutes, Beijing, China: National Center for International Exchange & Cooperation on Work Safety (SAWS)*, 2007, pp. 121–125.

[124] K. H. Im and R. K. Ahluwalia, “Radiation properties of coal combustion products,” *Int. J. Heat Mass Transf.*, vol. 36, no. 2, pp. 293–302, 1993.

[125] M. L. Harris, K. L. Cashdollar, C. Man, and E. D. Thimons, “Mitigating Coal Dust Explosions in Modern Underground Coal Mines. NIOSHTIC2 Number: 20036230,” in *Mine Ventilation: Proceedings of the Ninth International Mine Ventilation Congress, New Delhi, India, Panigrahi DC, ed., New Delhi, India: Oxford & IBH Publishing Co. Pvt. Ltd.*, 2009, p. 1:143-149.

[126] M. J. Sapko, K. L. Cashdollar, and G. M. Green, “Coal dust particle size survey of US mines,” *J. Loss Prev. Process Ind.*, vol. 20, no. 4, pp. 616–620, 2007.

[127] P. Christophe, B. M. Rim, G. Mohamed, S. Khashayar, and F. Jérôme, “Thermal radiation in dust flame propagation,” *J. Loss Prev. Process Ind.*, vol. 49, no. Part B, pp. 896–904, 2017.

[128] M. Shokri and C. L. Beyler, “Radiation from Large Pool Fires,” *J. Fire Prot. Eng.*, vol. 1, no. 4, pp. 141–149, 1989.

[129] G. H. Markstein, “Relationship between smoke point and radiant emission from buoyant turbulent and laminar diffusion flames,” *Symp. Combust.*, vol. 20, no. 1, pp. 1055–1061, 1985.

[130] K. L. Cashdollar and M. Hertzberg, “20-l explosibility test chamber for dusts and gases,” *Rev. Sci. Instrum.*, vol. 56, no. 4, pp. 596–602, 1985.

[131] K. L. Cashdollar and K. Chatrathi, “Minimum Explosible Dust Concentrations Measured in 20-L and 1-M3 Chambers,” *Combust. Sci. Technol.*, vol. 87, no. 1–6, pp. 157–171, 1993.

[132] L. Wu, N. Kobayashi, Z. Li, and H. Huang, “Numerical Study of the Effects of Oxygen Concentration and Fuel Jet Velocity on Thermal Radiation in Methane and Propane Turbulent Diffusion Flames,” *Can. J. Chem. Eng.*, vol. 93, no. 9, pp. 1567–1576, 2015.

[133] R. L. Alpert, “Radiation from Turbulent-Jet Flames and Wall Fires,” *11th Jt. Meet. UJNR Panel Fire Res. Saf.*, 1989.

8 Appendices

8.1 Dust feeder calibration curves

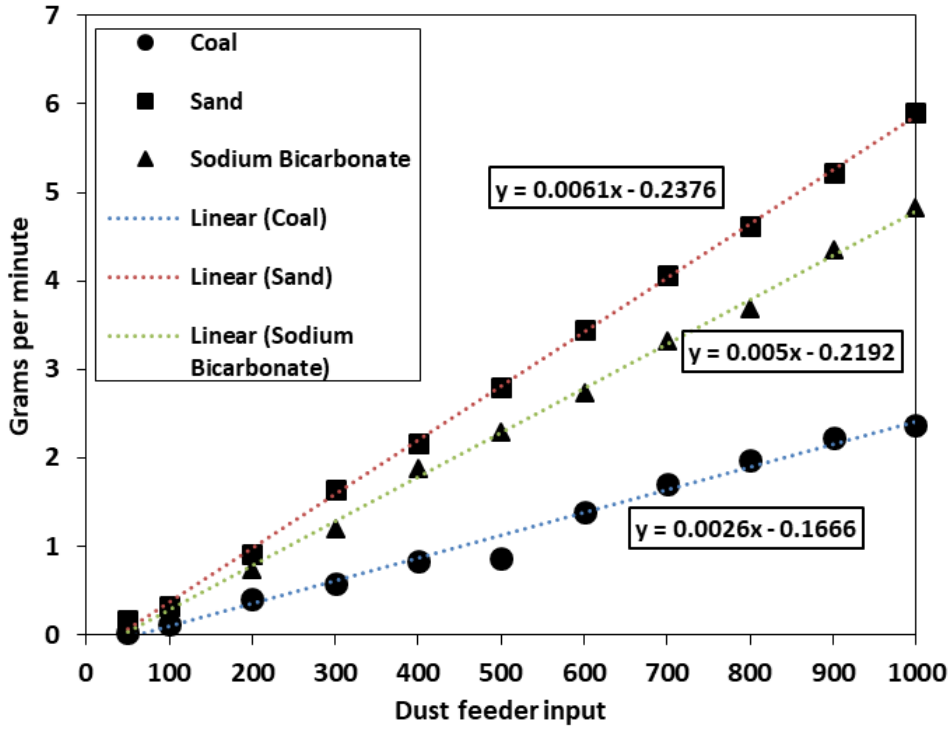

Figure 8.1: Dust feeder calibration curves for laminar test cases at 10 lpm.

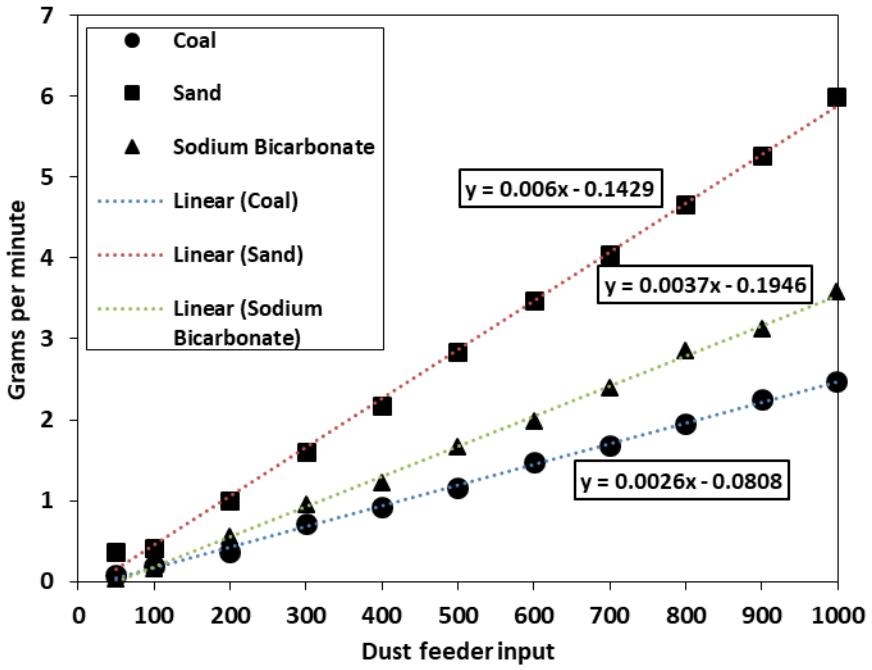

Figure 8.2: Dust feeder calibration curves for turbulent tests at 30 lpm.

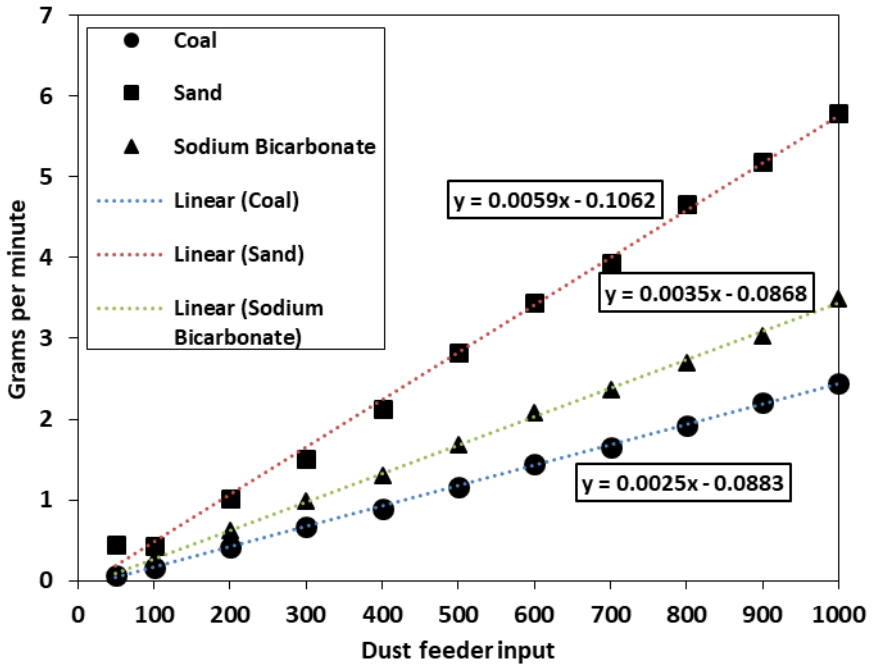

Figure 8.3: Dust feeder calibration curves for turbulent tests at 35 lpm.

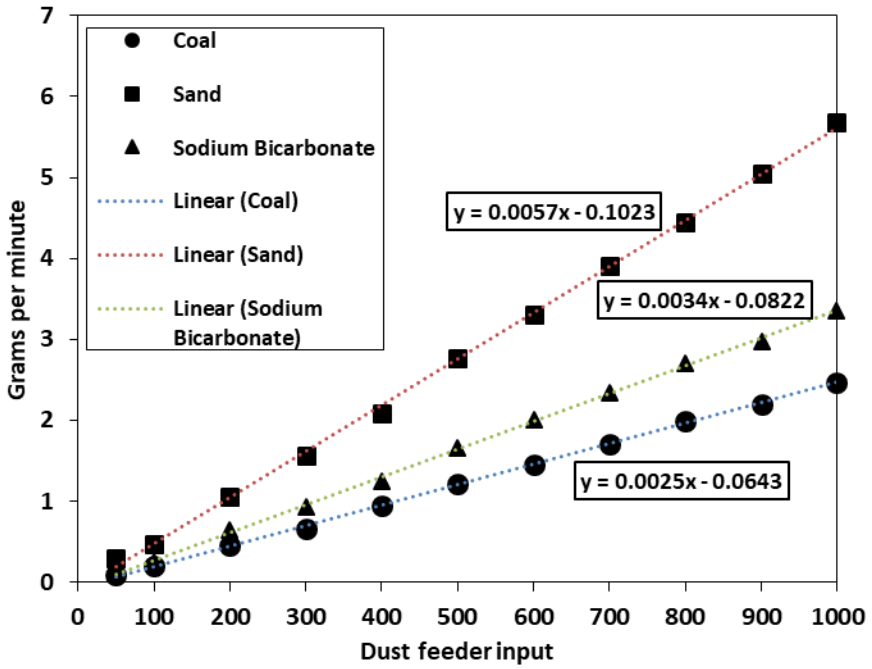

Figure 8.4: Dust feeder calibration curves for turbulent tests at 40 lpm.

8.2 Experimental matrices

Experimental Matrix: Shaded numbers indicate dust feeder input setting										
75-90 µm coal-methane-air premixed flame										
	Air	Methane	Dust Concentration (g/m^3)							
ϕ_g	**lpm**	**lpm**	**25**	**50**	**75**	**100**	**125**	**150**	**175**	**200**
0.8	9.23	0.775	160	256	352	449	545	641	737	833
1	9.05	0.950	160	256	352	449	545	641	737	833
1.2	8.88	1.119	160	256	352	449	545	641	737	833

Experimental Matrix: Shaded numbers indicate dust feeder input setting												
75-90 µm sand-methane-air premixed flame												
	Air	Methane	Dust Concentration (g/m^3)									
ϕ_g	**lpm**	**lpm**	**25**	**50**	**75**	**100**	**125**	**150**	**200**	**300**	**400**	**500**	**585**
0.8	9.23	0.775	80	121	162	203	244	285	367	531	695	859	998
1	9.05	0.950	80	121	162	203	244	285	367	531	695	859	998
1.2	8.88	1.119	80	121	162	203	244	285	367	531	695	859	998

Experimental Matrix: Shaded numbers indicate dust feeder input setting										
75-90 μm sodium bicarbonate-methane-air premixed flame										
	Air	Methane	Dust Concentration (g/m^3)							
ϕ_g	**lpm**	**lpm**	**25**	**50**	**75**	**100**	**125**	**150**	**175**	**200**
0.8	9.23	0.775	94	144	194	244	294	344	394	444
1	9.05	0.950	94	144	194	244	294	344	394	444
1.2	8.88	1.119	94	144	194	244	294	344	394	444

Experimental Matrix: Shaded numbers indicate dust feeder input setting						
30 lpm, u'_{rms} = 0.65 m/s, 75-90 μm coal-methane-air premixed flame						
	Air	Methane	Dust Concentration (g/m^3)			
ϕ_g	**lpm**	**lpm**	**25**	**50**	**60**	**75**
0.8	27.68	2.325	320	608	723	896
1	27.15	2.851	320	608	723	896
1.2	26.64	3.357	320	608	723	896
35 lpm, u'_{rms} = 0.72 m/s, 75-90 μm coal-methane-air premixed flame						
	Air	Methane	Dust Concentration (g/m^3)			
ϕ_g	**lpm**	**lpm**	**25**	**50**	**60**	**75**
0.8	32.29	2.712	385	735	875	x
1	31.67	3.326	385	735	875	x
1.2	31.08	3.917	385	735	875	x
40 lpm, u'_{rms} = 0.88 m/s, 75-90 μm coal-methane-air premixed flame						
	Air	Methane	Dust Concentration (g/m^3)			
ϕ_g	**lpm**	**lpm**	**25**	**50**	**60**	**75**
0.8	36.9	3.1	426	826	986	x
1	36.2	3.801	426	826	986	x
1.2	35.52	4.476	426	826	986	x

Experimental Matrix: Shaded numbers indicate dust feeder input setting								
u'_{rms} = 0.65 m/s, 75-90 μm sand-methane-air premixed flame								
	Air	Methane	Dust Concentration (g/m^3)					
ϕ_g	**lpm**	**lpm**	**25**	**50**	**60**	**75**	**100**	**125**
0.8	27.68	2.325	149	274	324	399	524	649
1	27.15	2.851	149	274	324	399	524	649
1.2	26.64	3.357	149	274	324	399	524	649
u'_{rms} = 0.72 m/s, 75-90 μm sand-methane-air premixed flame								
	Air	Methane	Dust Concentration (g/m^3)					

ϕ_g	lpm	lpm	25	50	60	75	100	125
0.8	32.29	2.712	166	315	374	463	611	760
1	31.67	3.326	166	315	374	463	611	760
1.2	31.08	3.917	166	315	374	463	611	760
u'_{rms} = 0.88 m/s, 75-90 µm sand-methane-air premixed flame								
	Air	Methane	Dust Concentration (g/m^3)					
ϕ_g	**lpm**	**lpm**	**25**	**50**	**60**	**75**	**100**	**125**
0.8	36.9	3.1	193	369	439	544	720	895
1	36.2	3.801	193	369	439	544	720	895
1.2	35.52	4.476	193	369	439	544	720	895

Experimental Matrix: Shaded numbers indicate dust feeder input setting							
u'_{rms} = 0.65 m/s, 75-90 µm $NaHCO_3$-methane-air premixed flame							
	Air	Methane	Dust Concentration (g/m^3)				
ϕ_g	**lpm**	**lpm**	**25**	**50**	**60**	**75**	**100**
0.8	27.68	2.325	255	458	539	661	863
1	27.15	2.851	255	458	539	661	863
1.2	26.64	3.357	255	458	539	661	863
u'_{rms} = 0.72 m/s, 75-90 µm $NaHCO_3$-methane-air premixed flame							
	Air	Methane	Dust Concentration (g/m^3)				
ϕ_g	**lpm**	**lpm**	**25**	**50**	**60**	**75**	**100**
0.8	32.29	2.712	275	525	625	775	x
1	31.67	3.326	275	525	625	775	x
1.2	31.08	3.917	275	525	625	775	x
u'_{rms} = 0.82 m/s, 75-90 µm $NaHCO_3$-methane-air premixed flame							
	Air	Methane	Dust Concentration (g/m^3)				
ϕ_g	**lpm**	**lpm**	**25**	**50**	**60**	**75**	**100**
0.8	36.9	3.1	318	612	730	907	x
1	36.2	3.801	318	612	730	907	x
1.2	35.52	4.476	318	612	730	907	x

8.3 Standard deviation of laminar burning velocities

Table 8.1: Standard deviation of laminar burning velocity measurements for methane-air-sand premixed flames.

Standard deviation in m/s						
	75-90 µm sand-methane-air premixed flame					
	Air	Methane	Dust Concentration (g/m^3)			
ϕ_g	**lpm**	**lpm**	**25**	**50**	**75**	**100**
0.8	9.23	0.775	0.0189	0.0114	0.0135	0.0134
1	9.05	0.950	0.0156	0.0116	0.0139	X
1.2	8.88	1.119	0.0121	0.0106	0.0098	0.0106

Table 8.2: Standard deviation of laminar burning velocity measurements for methane-air-$NaHCO_3$ premixed flames.

Standard deviation in m/s						
	75-90 µm sodium bicarbonate-methane-air premixed flame					
	Air	Methane	Dust Concentration (g/m^3)			No Dust
ϕ_g	**lpm**	**lpm**	**25**	**50**	**75**	**0**
0.8	9.23	0.775	0.0119	0.0157	x	0.0101
1	9.05	0.950	0.0202	0.0240	0.0170	0.0193
1.2	8.88	1.119	0.0125	0.0131	0.0126	0.0158

8.4 Turbulent burning velocities

Table 8.3: Turbulent burning velocity measurements for methane-air-coal premixed flames.

Turbulent Burning Velocity in m/s							
	u'_{rms} = 0.65 m/s, 75-90 µm coal-methane-air premixed flame						
	Air	Methane	Dust Concentration (g/m^3)				No Dust
ϕ_g	**lpm**	**lpm**	**25**	**50**	**60**	**75**	**0**
0.8	27.68	2.325	0.7837	0.8304	0.7907	0.8187	0.7052
1	27.15	2.851	0.9230	0.9534	0.9388	0.9567	0.8670
1.2	26.64	3.357	0.6822	0.7195	0.7437	0.7567	0.6675

	35 lpm, u'_{rms} = 0.72 m/s, 75-90 µm coal-methane-air premixed flame						
	Air	Methane	Dust Concentration (g/m^3)				No Dust
ϕ_g	**lpm**	**lpm**	**25**	**50**	**60**	**75**	**0**
0.8	32.29	2.712	0.7810	0.8146	0.7702	x	0.7034
1	31.67	3.326	0.9148	0.9323	0.8660	x	0.9083
1.2	31.08	3.917	0.6886	0.5997	0.6015	x	0.8638
	40 lpm, u'_{rms} = 0.88 m/s, 75-90 µm coal-methane-air premixed flame						
	Air	Methane	Dust Concentration (g/m^3)				No Dust
ϕ_g	**lpm**	**lpm**	**25**	**50**	**60**	**75**	**0**
0.8	36.9	3.1	0.8135	0.8679	0.8196	x	0.7439
1	36.2	3.801	0.9529	0.9394	0.9334	x	0.9119
1.2	35.52	4.476	0.6667	0.6749	0.6556	x	0.7205

Table 8.4: Turbulent burning velocity measurements for methane-air-sand premixed flames.

Turbulent Burning Velocity in m/s								
	u'_{rms} = 0.65 m/s, 75-90 µm sand-methane-air premixed flame							
	Air	Methane	Dust Concentration (g/m^3)					
ϕ_g	**lpm**	**lpm**	**25**	**50**	**60**	**75**	**100**	**125**
0.8	27.68	2.325	0.7366	0.7644	0.7461	0.7184	0.7113	0.6919
1	27.15	2.851	0.8585	0.8899	0.8533	0.8084	0.8167	0.7921
1.2	26.64	3.357	0.6506	0.6092	0.5928	0.5815	0.5615	0.5524
	u'_{rms} = 0.72 m/s, 75-90 µm sand-methane-air premixed flame							
	Air	Methane	Dust Concentration (g/m^3)					
ϕ_g	**lpm**	**lpm**	**25**	**50**	**60**	**75**	**100**	**125**
0.8	32.29	2.712	0.7158	0.7423	0.7397	0.7256	0.6910	0.6976
1	31.67	3.326	0.8937	0.8864	0.8762	0.8659	0.8301	0.7972
1.2	31.08	3.917	0.6440	0.6540	0.6425	0.6243	0.6004	0.6157
	u'_{rms} = 0.88 m/s, 75-90 µm sand-methane-air premixed flame							
	Air	Methane	Dust Concentration (g/m^3)					
ϕ_g	**lpm**	**lpm**	**25**	**50**	**60**	**75**	**100**	**125**
0.8	36.9	3.1	0.7634	0.7385	0.7594	0.7514	0.7247	0.7208
1	36.2	3.801	0.9686	0.9325	0.9267	0.9469	0.9286	0.9525
1.2	35.52	4.476	0.6644	0.6239	0.6458	0.6521	0.5973	0.6241

Table 8.5: Turbulent burning velocity measurements for methane-air-$NaHCO_3$ premixed flames.

Turbulent Burning Velocity in m/s							
	u'_{rms} = 0.65 m/s, 75-90 µm $NaHCO_3$-methane-air premixed flame						
	Air	Methane	Dust Concentration (g/m^3)				
ϕ_g	**lpm**	**lpm**	**25**	**50**	**60**	**75**	**100**
0.8	27.68	2.325	0.6732	0.6326	0.5613	0.5363	x
1	27.15	2.851	0.8301	0.7483	0.7719	0.7485	x
1.2	26.64	3.357	0.5972	0.5181	0.4943	0.4801	x
	u'_{rms} = 0.72 m/s, 75-90 µm $NaHCO_3$-methane-air premixed flame						
	Air	Methane	Dust Concentration (g/m^3)				
ϕ_g	**lpm**	**lpm**	**25**	**50**	**60**	**75**	**100**
0.8	32.29	2.712	0.7101	0.6776	0.6355	0.6397	x
1	31.67	3.326	0.9168	0.8451	0.8402	0.7825	x
1.2	31.08	3.917	0.6336	0.5642	0.5663	0.5660	x
	u'_{rms} = 0.82 m/s, 75-90 µm $NaHCO_3$-methane-air premixed flame						
	Air	Methane	Dust Concentration (g/m^3)				
ϕ_g	**lpm**	**lpm**	**25**	**50**	**60**	**75**	**100**
0.8	36.9	3.1	0.7955	0.7469	0.7822	0.6754	x
1	36.2	3.801	0.9218	0.8561	0.8594	0.8057	x
1.2	35.52	4.476	0.6350	0.6148	0.5885	0.5877	x

8.5 Standard deviation of turbulent burning velocity measurements

Table 8.6: Standard deviation of turbulent burning velocity measurements for methane-air-coal premixed flames.

Standard deviation in m/s							
	u'_{rms} = 0.65 m/s, 75-90 µm coal-methane-air premixed flame						
	Air	Methane	Dust Concentration (g/m^3)				No Dust
ϕ_g	**lpm**	**lpm**	**25**	**50**	**60**	**75**	**0**
0.8	27.68	2.325	0.0629	0.0710	0.0743	0.0713	0.0394
1	27.15	2.851	0.0793	0.0816	0.0851	0.0885	0.0596
1.2	26.64	3.357	0.0868	0.0917	0.0763	0.0737	0.0507
	u'_{rms} = 0.72 m/s, 75-90 µm coal-methane-air premixed flame						
	Air	Methane	Dust Concentration (g/m^3)				No Dust

ϕ_g	lpm	lpm	25	50	60	75	0
0.8	32.29	2.712	0.0569	0.0747	0.0680	x	0.0495
1	31.67	3.326	0.0750	0.0855	0.0786	x	0.0722
1.2	31.08	3.917	0.0723	0.0562	0.0671	x	0.0614
	u'_{rms} = 0.88 m/s, 75-90 µm coal-methane-air premixed flame						
	Air	Methane	Dust Concentration (g/m^3)				No Dust
ϕ_g	**lpm**	**lpm**	**25**	**50**	**60**	**75**	**0**
0.8	36.9	3.1	0.0673	0.0677	0.0624	x	0.0637
1	36.2	3.801	0.1111	0.0889	0.0779	x	0.0866
1.2	35.52	4.476	0.0607	0.0804	0.0957	x	0.0575

Table 8.7: Standard deviation of turbulent burning velocity measurements for methane-air-sand premixed flames

Standard deviation in m/s								
	u'_{rms} = 0.65 m/s, 75-90 µm sand-methane-air premixed flame							
	Air	Methane	Dust Concentration (g/m^3)					
ϕ_g	**lpm**	**lpm**	**25**	**50**	**60**	**75**	**100**	**125**
0.8	27.68	2.325	0.0789	0.0598	0.0732	0.0598	0.0810	0.0741
1	27.15	2.851	0.0715	0.1037	0.0841	0.0672	0.0624	0.0879
1.2	26.64	3.357	0.0686	0.0477	0.0447	0.0493	0.0652	0.0405
	u'_{rms} = 0.72 m/s, 75-90 µm sand-methane-air premixed flame							
	Air	Methane	Dust Concentration (g/m^3)					
ϕ_g	**lpm**	**lpm**	**25**	**50**	**60**	**75**	**100**	**125**
0.8	32.29	2.712	0.0477	0.0746	0.0710	0.0783	0.0453	0.0723
1	31.67	3.326	0.0921	0.0990	0.1062	0.0729	0.0568	0.0749
1.2	31.08	3.917	0.0541	0.0560	0.0566	0.0491	0.0542	0.0422
	u'_{rms} = 0.88 m/s, 75-90 µm sand-methane-air premixed flame							
	Air	Methane	Dust Concentration (g/m^3)					
ϕ_g	**lpm**	**lpm**	**25**	**50**	**60**	**75**	**100**	**125**
0.8	36.9	3.1	0.0718	0.0687	0.0693	0.0684	0.0600	0.0689
1	36.2	3.801	0.0791	0.0975	0.0862	0.0920	0.0643	0.1117
1.2	35.52	4.476	0.0480	0.0207	0.0333	0.0539	0.0189	0.0224

Table 8.8: Standard deviation of turbulent burning velocity measurements for methane-air-$NaHCO_3$ premixed flames.

Standard deviation in m/s							
	u'_{rms} = 0.65 m/s, 75-90 µm $NaHCO_3$-methane-air premixed flame						
	Air	Methane	Dust Concentration (g/m^3)				
ϕ_g	**lpm**	**lpm**	**25**	**50**	**60**	**75**	**100**
0.8	27.68	2.325	0.0546	0.0516	0.0611	0.0442	x
1	27.15	2.851	0.0723	0.0765	0.0410	0.0681	x
1.2	26.64	3.357	0.0521	0.0422	0.0144	x	x
	u'_{rms} = 0.72 m/s, 75-90 µm $NaHCO_3$-methane-air premixed flame						
	Air	Methane	Dust Concentration (g/m^3)				
ϕ_g	**lpm**	**lpm**	**25**	**50**	**60**	**75**	**100**
0.8	32.29	2.712	0.0730	0.0455	0.0564	0.0666	x
1	31.67	3.326	0.0960	0.0665	0.0468	0.0468	x
1.2	31.08	3.917	0.0514	0.0212	0.0257	0.0068	x
	u'_{rms} = 0.82 m/s, 75-90 µm $NaHCO_3$-methane-air premixed flame						
	Air	Methane	Dust Concentration (g/m^3)				
ϕ_g	**lpm**	**lpm**	**25**	**50**	**60**	**75**	**100**
0.8	36.9	3.1	0.0525	0.0643	0.0672	0.0534	x
1	36.2	3.801	0.0750	0.0708	0.0697	0.0639	x
1.2	35.52	4.476	0.0244	0.0235	0.0049	0.0043	x

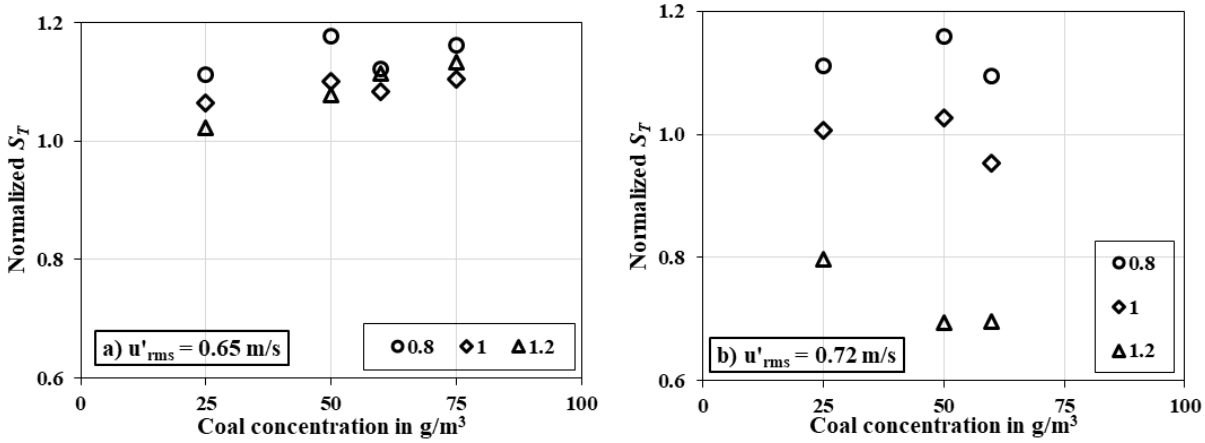

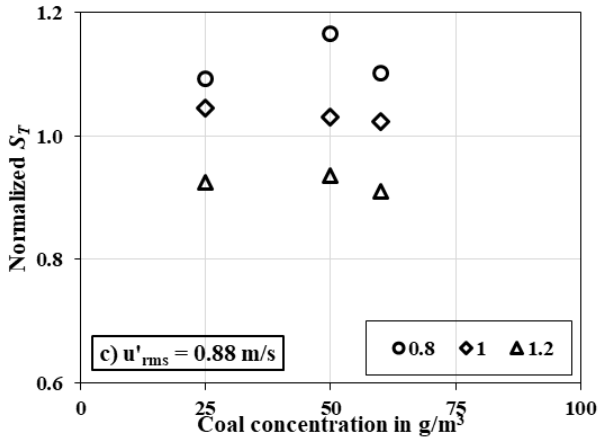

Figure 8.5: Normalized turbulent burning velocity of coal-methane-air premixed flame.

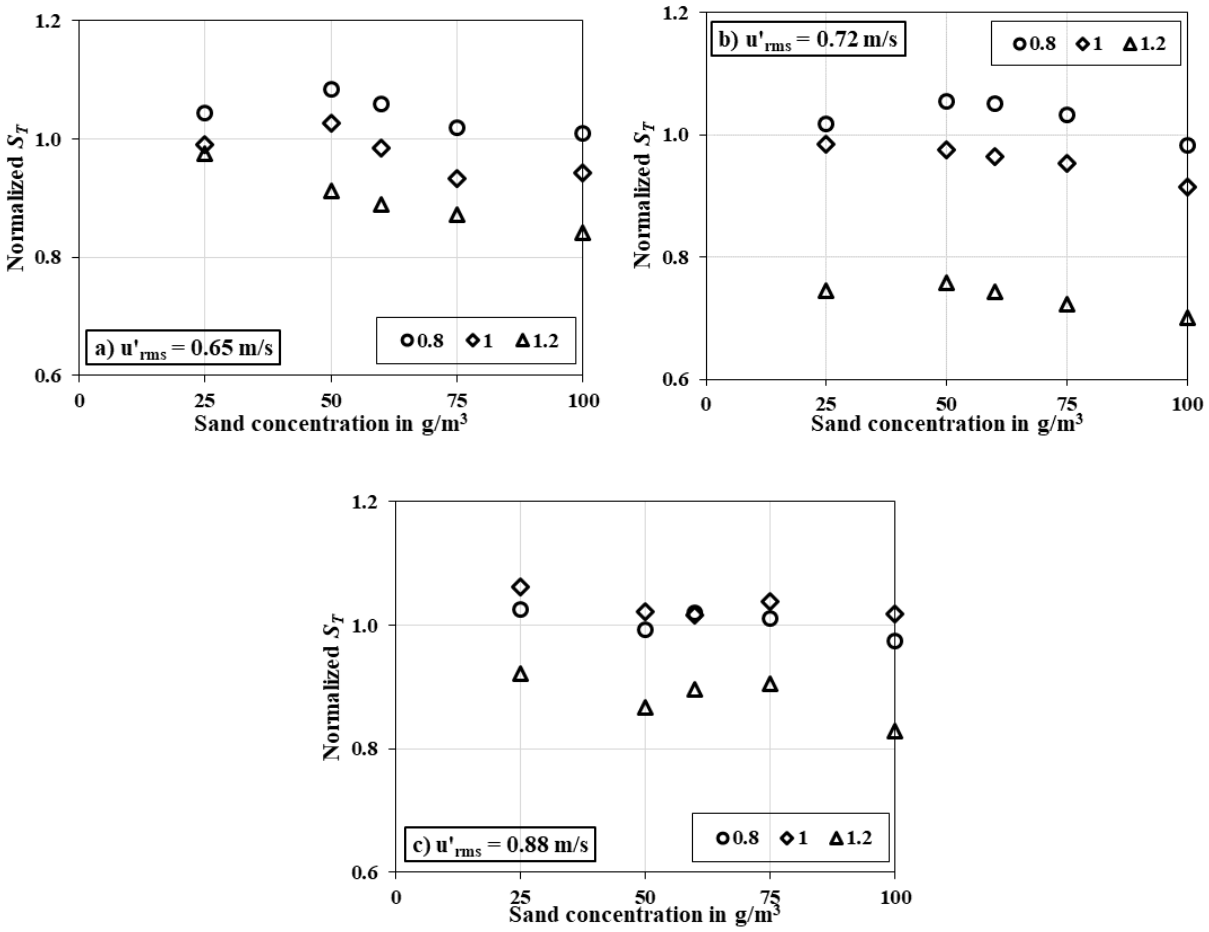

Figure 8.6: Normalized turbulent burning velocity of sand-methane-air premixed flame.

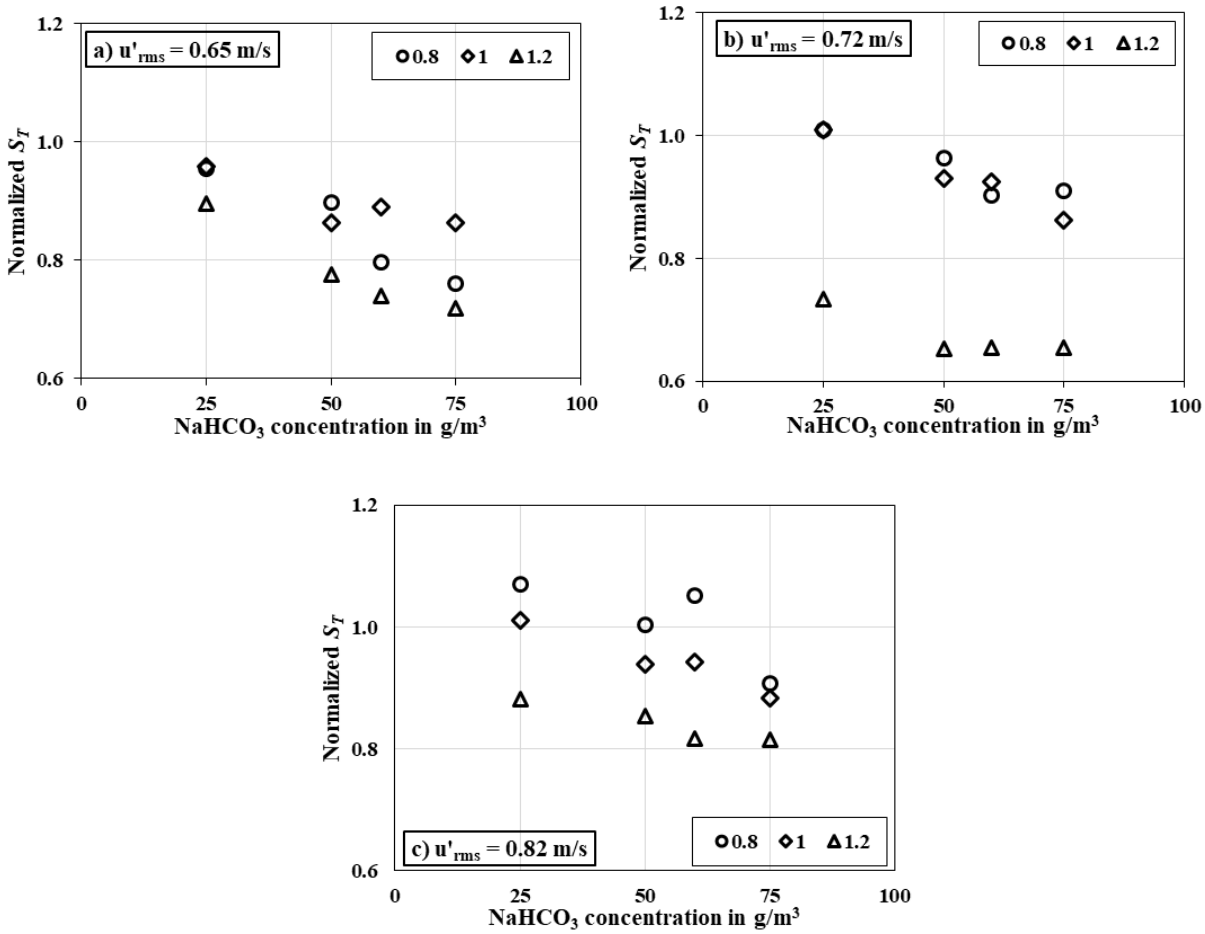

Figure 8.7: Normalized turbulent burning velocity of $NaHCO_3$-methane-air premixed flame.

8.6 Radiative heat flux

Table 8.9: Radiative heat flux measured for methane-air-coal premixed turbulent flames.

Radiative heat flux measurements in kW/m^2							
	u'_{rms} = 0.65 m/s, 75-90 µm coal-methane-air premixed flame						
	Air	Methane	Dust Concentration (g/m^3)				No Dust
ϕ_g	**lpm**	**lpm**	**25**	**50**	**60**	**75**	**0**
0.8	27.68	2.325	6.148	8.369	8.323	9.280	5.290
1	27.15	2.851	8.225	10.461	11.124	12.089	7.200
1.2	26.64	3.357	7.695	9.678	9.956	10.679	6.926
	u'_{rms} = 0.72 m/s, 75-90 µm coal-methane-air premixed flame						
	Air	Methane	Dust Concentration (g/m^3)				No Dust

ϕ_g	lpm	lpm	25	50	60	75	0
0.8	32.29	2.712	6.137	7.717	8.199	x	4.205
1	31.67	3.326	8.413	10.456	11.308	x	5.966
1.2	31.08	3.917	7.275	9.550	9.712	x	5.524
	u'_{rms} = 0.88 m/s, 75-90 µm coal-methane-air premixed flame						
	Air	Methane	Dust Concentration (g/m^3)				No Dust
ϕ_g	**lpm**	**lpm**	**25**	**50**	**60**	**75**	**0**
0.8	36.9	3.1	5.834	7.827	8.269	x	4.003
1	36.2	3.801	8.237	10.426	11.318	x	5.818
1.2	35.52	4.476	7.389	8.874	9.272	x	5.523

Table 8.10: Radiative heat flux measured for methane-air-sand premixed turbulent flames.

Radiative heat flux measurements in kW/m^2								
	u'_{rms} = 0.65 m/s, 75-90 µm sand-methane-air premixed flame							
	Air	Methane	Dust Concentration (g/m^3)					
ϕ_g	**lpm**	**lpm**	**25**	**50**	**60**	**75**	**100**	**125**
0.8	27.68	2.325	4.421	4.350	4.257	4.407	4.231	4.168
1	27.15	2.851	5.703	5.669	5.681	5.683	5.595	5.518
1.2	26.64	3.357	5.477	5.470	5.399	5.367	5.367	5.303
	u'_{rms} = 0.72 m/s, 75-90 µm sand-methane-air premixed flame							
	Air	Methane	Dust Concentration (g/m^3)					
ϕ_g	**lpm**	**lpm**	**25**	**50**	**60**	**75**	**100**	**125**
0.8	32.29	2.712	4.154	4.094	4.053	4.123	4.019	4.052
1	31.67	3.326	5.567	5.638	5.542	5.578	5.566	5.518
1.2	31.08	3.917	5.393	5.342	5.313	5.312	5.305	5.201
	u'_{rms} = 0.88 m/s, 75-90 µm sand-methane-air premixed flame							
	Air	Methane	Dust Concentration (g/m^3)					
ϕ_g	**lpm**	**lpm**	**25**	**50**	**60**	**75**	**100**	**125**
0.8	36.9	3.1	3.882	3.796	3.876	3.788	3.760	3.684
1	36.2	3.801	5.592	5.610	5.698	5.583	5.613	5.587
1.2	35.52	4.476	5.140	5.112	5.084	4.977	5.079	4.933

Table 8.11: Radiative heat flux measured for methane-air-$NaHCO_3$ premixed turbulent flames.

Radiative heat flux measurements in kW/m^2							
	u'_{rms} = 0.65 m/s, 75-90 µm $NaHCO_3$-methane-air premixed flame						
	Air	Methane	Dust Concentration (g/m^3)				
ϕ_g	**lpm**	**lpm**	**25**	**50**	**60**	**75**	**100**
0.8	27.68	2.325	4.243	4.009	3.705	3.286	2.523
1	27.15	2.851	5.650	5.554	5.486	5.608	5.327
1.2	26.64	3.357	5.173	4.984	4.934	4.722	4.218
	u'_{rms} = 0.72 m/s, 75-90 µm $NaHCO_3$-methane-air premixed flame						
	Air	Methane	Dust Concentration (g/m^3)				
ϕ_g	**lpm**	**lpm**	**25**	**50**	**60**	**75**	**100**
0.8	32.29	2.712	4.021	3.614	3.796	3.778	x
1	31.67	3.326	5.783	5.380	5.559	5.573	x
1.2	31.08	3.917	5.036	4.876	5.004	4.888	x
	u'_{rms} = 0.82 m/s, 75-90 µm $NaHCO_3$-methane-air premixed flame						
	Air	Methane	Dust Concentration (g/m^3)				
ϕ_g	**lpm**	**lpm**	**25**	**50**	**60**	**75**	**100**
0.8	36.9	3.1	4.574	4.406	4.223	3.901	x
1	36.2	3.801	5.840	5.706	5.756	5.680	x
1.2	35.52	4.476	5.198	5.095	4.882	4.741	x

8.7 Standard deviation of radiative heat flux measurements

Table 8.12: Standard deviation of radiative heat flux measurements for methane-air-coal premixed turbulent flames.

Standard deviation in kW/m^2							
	u'_{rms} = 0.65 m/s, 75-90 µm coal-methane-air premixed flame						
	Air	Methane	Dust Concentration (g/m^3)				No Dust
ϕ_g	**lpm**	**lpm**	**25**	**50**	**60**	**75**	**0**
0.8	27.68	2.325	0.7736	0.7742	0.7424	0.8169	1.0546
1	27.15	2.851	0.7631	0.6660	0.6641	0.8257	0.8494
1.2	26.64	3.357	0.6930	0.6676	0.5951	0.6032	0.9396
	u'_{rms} = 0.72 m/s, 75-90 µm coal-methane-air premixed flame						
	Air	Methane	Dust Concentration (g/m^3)				No Dust

ϕ_g	**lpm**	**lpm**	**25**	**50**	**60**	**75**	**0**
0.8	32.29	2.712	0.7818	0.6283	0.7692	x	0.8125
1	31.67	3.326	0.7897	0.5857	0.7003	x	0.7822
1.2	31.08	3.917	0.6725	0.6791	0.6101	x	0.6514
	u'_{rms} = 0.88 m/s, 75-90 µm coal-methane-air premixed flame						
	Air	Methane	Dust Concentration (g/m^3)				No Dust
ϕ_g	**lpm**	**lpm**	**25**	**50**	**60**	**75**	**0**
0.8	36.9	3.1	0.7649	0.7237	0.7529	x	0.8458
1	36.2	3.801	0.7694	0.7072	0.6978	x	0.7394
1.2	35.52	4.476	0.6332	0.8059	0.7492	x	0.7595

Table 8.13: Standard deviation of radiative heat flux measurements for methane-air-sand premixed turbulent flames.

Standard deviation in kW/m^2						
	u'_{rms} = 0.65 m/s, 75-90 µm sand-methane-air premixed flame					
	Air	Methane	Dust Concentration (g/m^3)			
ϕ_g	**lpm**	**lpm**	**25**	**50**	**60**	**75**
0.8	27.68	2.325	0.8545	0.8438	0.8537	0.8595
1	27.15	2.851	0.7605	0.7334	0.8659	0.7791
1.2	26.64	3.357	0.6662	0.6686	0.7686	0.7155
	u'_{rms} = 0.72 m/s, 75-90 µm sand-methane-air premixed flame					
	Air	Methane	Dust Concentration (g/m^3)			
ϕ_g	**lpm**	**lpm**	**25**	**50**	**60**	**75**
0.8	32.29	2.712	0.8344	0.8428	0.7902	0.8611
1	31.67	3.326	0.7199	0.7588	0.6746	0.7326
1.2	31.08	3.917	0.6929	0.6539	0.6603	0.6835
	u'_{rms} = 0.88 m/s, 75-90 µm sand-methane-air premixed flame					
	Air	Methane	Dust Concentration (g/m^3)			
ϕ_g	**lpm**	**lpm**	**25**	**50**	**60**	**75**
0.8	36.9	3.1	0.8922	0.8363	0.8720	0.7981
1	36.2	3.801	0.6811	0.6610	0.7620	0.7469
1.2	35.52	4.476	0.6115	0.6350	0.6579	0.6425

Table 8.14: Standard deviation of radiative heat flux measurements for methane-air-$NaHCO_3$ premixed turbulent flames.

Standard deviation in kW/m^2							
	u'_{rms} = 0.65 m/s, 75-90 µm $NaHCO_3$-methane-air premixed flame						
	Air	Methane	Dust Concentration (g/m^3)				
ϕ_g	**lpm**	**lpm**	**25**	**50**	**60**	**75**	**100**
0.8	27.68	2.325	0.7851	0.7877	0.8256	0.8776	0.8738
1	27.15	2.851	0.6641	0.6786	0.6990	0.6984	0.6464
1.2	26.64	3.357	0.5919	0.6443	0.6089	0.6911	0.8013
	u'_{rms} = 0.72 m/s, 75-90 µm $NaHCO_3$-methane-air premixed flame						
	Air	Methane	Dust Concentration (g/m^3)				
ϕ_g	**lpm**	**lpm**	**25**	**50**	**60**	**75**	**100**
0.8	32.29	2.712	0.8833	0.8397	0.8495	0.8709	x
1	31.67	3.326	0.7768	0.6705	0.6662	0.6815	x
1.2	31.08	3.917	0.6510	0.6494	0.6112	0.6205	x
	u'_{rms} = 0.82 m/s, 75-90 µm $NaHCO_3$-methane-air premixed flame						
	Air	Methane	Dust Concentration (g/m^3)				
ϕ_g	**lpm**	**lpm**	**25**	**50**	**60**	**75**	**100**
0.8	36.9	3.1	0.7160	0.8635	0.8462	0.8563	x
1	36.2	3.801	0.7235	0.6968	0.7046	0.7631	x
1.2	35.52	4.476	0.6629	0.6691	0.6334	0.6644	x

8.8 Additional photos

Figure 8.8: Dust sieve shaker

VITA

Sreenivasan Ranganathan
Born: Coimbatore, India.

Education

Doctor of Philosophy in Fire Protection Engineering, Mar 2018, Worcester Polytechnic Institute (WPI), USA.
Master of Science in Fire Protection Engineering, Feb 2016, Worcester Polytechnic Institute (WPI), USA.
Master of Science in Mechanical Engineering (Thermal Eng.), Dec 2011, Indian Institute of Technology (IIT) Madras, India.
Bachelor of Technology in Mechanical Engineering, Jun 2008, N. S. S. College of Engineering, University of Calicut**,** India.

Appointments

Research Project Manager, Fire Protection Research Foundation (FPRF), National Fire Protection Association (NFPA).	**Oct 2015-Present**
Research Co-op, Fire Protection Research Foundation (FPRF), National Fire Protection Association (NFPA).	**Jan 2015-Oct 2015**
Teaching Assistant (Graduate level), Dept. of Fire Protection Engineering, WPI.	**Aug 2013-May 2014**
Research Assistant, Combustion lab, Dept. of Fire Protection Engineering, WPI.	**Jan 2012–Dec 2014**
Teaching Assistant (Graduate & Under-graduate level), Dept. of Mechanical Engineering, IIT Madras.	**Jan 2010–May 2011**
Research Assistant, Thermodynamics and Combustion Engineering lab, Dept. of Mechanical Engineering, IIT Madras.	**Jul 2009–Dec 2011**
Project Associate, Industrial Consultancy and Sponsored Research (ICSR), IIT Madras.	**Sept 2008–Jun 2009**

PUBLICATIONS

Journal Publications

1. **S. Ranganathan**, D. Petrow, S. R. Rockwell and A. S. Rangwala, *"Turbulent burning velocity of methane–air–dust premixed flames"*, Combustion and Flame, 188, 2018, pp. 367-375. (DOI)
2. **S. Ranganathan**, S. R. Rockwell, D. Petrow, R. Zalosh and A. S. Rangwala, *"Radiative fraction of dust entrained turbulent premixed flames"*, Journal of Loss Prevention in the Process Industries, 51, 2018, pp. 65-71. (DOI)
3. **S. Ranganathan**, M. Lee and A. S. Rangwala, *"Influence of the Inert Particles on the Burning Velocity of Laminar Methane-Air Premixed Flames"*, Journal of Loss Prevention in the Process Industries, 35, 2015, pp. 46-51. (DOI)
4. M. Lee, **S. Ranganathan** and A. S. Rangwala, *"Influence of the Reactant Temperature on Particle Entrained Laminar Methane-Air Premixed Flames",* Proceedings of the Combustion Institute, 35 (1), 2015, pp. 729-736. (DOI)
5. **S. Ranganathan**, V. Raghavan and T. Sundararajan, "*An investigation of Flame Zones and Burning Velocities of Laminar Unconfined Methane-Oxygen Premixed Flames"*, Combustion Theory and Modelling, 16 (2), 2012, pp. 199-219. (DOI)
6. S. Arun, S. Raghuram, **S. Ranganathan** and V. Raghavan, *"Effect Of Hydrogen Addition In The Co-Flow Of A Methane Diffusion Flame In Reducing Nitric Oxide Emissions"*, International Journal of Hydrogen Energy, 37 (24), 2012, pp. 19198-19209. (DOI)
7. **S. Ranganathan,** S. K. Koli and V. Raghavan**, "**Experimental Study of Effects of Coflow Air and Partial Premixing on Liquid Petroleum Gas Flames", ISRN Thermodynamics, vol. 2012, Article ID 202715, 6 pages, 2012. (DOI)

8. K. A. Francis, **S. Ranganathan** and V. Raghavan, "*Investigation of structures and reaction zones of methane-hydrogen laminar jet diffusion flames",* International Journal of Hydrogen Energy, 36, 2011, pp. 11183-11194. (DOI)
9. S. Deshpande, **S. Ranganathan** and V. Raghavan, "*A Numerical Study of Structures of Laminar Opposed Flow Premixed Methane-Hydrogen-Air Flames at Low Strain Rate"*, Computational Thermal Sciences, 3 (5), 2011, pp. 359-373. (DOI)
10. **S. Ranganathan**, V. Raghavan and T. Sundararajan, "*Numerical Investigation of Burning and Emission Characteristics of Laminar Methane Diffusion Flames in Preheated Oxidizer"*, International Journal on Energy for a Clean Environment, 11, 2010, pp. 145-161. (DOI)

Conference & Workshop Proceedings

11. **S. Ranganathan**, D. Petrow, S. Rockwell, A. S. Rangwala, *"Experimental Investigation of Laminar Premixed Methane-Air Flame Extinction with Sand and Sodium Bicarbonate Particles"*, Proceedings of 10th U. S. National Combustion Meeting, April 2017.
12. **S. Ranganathan**, "*HAZMAT Incident Commander Workshop"*, Fire Protection Research Foundation Proceedings, Dec 2016. (DOI)
13. S. A. Srinivas, M. R. Arjun, S. Koushik, **S. Ranganathan**, K. Pitchandi and V Raghavan, *"Characterization of Biomass Fuels"*, Proceedings of the 21st National and 10th International ISHMT ASME Heat and Mass transfer conference, IIT Madras, ISHMT_IND_09_016, Dec 2011.
14. R. Manikanda Kumaran, **S. Ranganathan**, S. Ganesan and T. Sundararajan, "*Simulation Of Regenerative Cooling System Performance For Large Expansion Ratio Rocket Motors"*, Proceedings of the 20th National and 9th International ISHMT ASME Heat and Mass transfer conference, IIT Bombay, Jan 2010, pp. 1663-1670.

Technical Reports

15. S. Gillis and **S. Ranganathan**, *"Variables Associated with the Classification of Ammonium Nitrate - A Literature Review"*, Fire Protection Research Foundation Report, March 2017. (DOI)
16. **S. Ranganathan**, *"Fire Based Mobile Integrated Healthcare and Community Paramedicine (MIH & CP) – Data and Resources"*, Fire Protection Research Foundation Report, May 2016. (DOI)
17. **S. Ranganathan** and S. Gillis, *"Oven, Furnace and Dryer Explosion Incidents"*, Fire Protection Research Foundation Report, April 2016. (DOI)
18. **S. Ranganathan** and M. Yin, *"Automotive Fire Apparatus Tire Replacement"*, Fire Protection Research Foundation Report, March 2015. (DOI)
19. **S. Ranganathan** and M. Yin, *"Water Based Fire Protection System Tagging Review"*, Fire Protection Research Foundation Report, April 2015. (DOI)

Presentations

20. **S. Ranganathan** and R. Gallagher, "Oven, furnace and dryer explosion", NFPA Annual Conference and Expo, Las Vegas, June 2016.
21. **S. Ranganathan**, M. Lee and A. S. Rangwala, "Interaction of Dust Particle with Laminar Premixed Flame", NFPA Annual Conference and Expo, Chicago, June 2015 (poster presentation).
22. **S. Ranganathan**, M. Lee, V. Akkerman and A. S. Rangwala, "Characteristics of Coal Dust Entrained Laminar Premixed Hybrid Flames", The Graduate Research Innovation Exchange (GRIE) poster presentation, April 2015, WPI.
23. **S. Ranganathan,** B. E. Elias, and A. S. Rangwala, "*Image Analysis Techniques for Particle Air Flames-A Review"*, 29th International Pittsburgh Coal Conference, Pittsburgh, PA, Oct 15-18, 2012.